Strål
säkerhets
myndigheten
Swedish Radiation Safety Authority

Authors: Steve J. Benbow
Richard Metcalfe
Jenny Burrow

Technical Note

2015:49

Independent Modelling of Engineered Barrier Evolution and Coupled THMC: Canister Corrosion Calculations in SR-Site

Report number: 2015:49 ISSN: 2000-0456
Available at www.stralsakerhetsmyndigheten.se

SSM:s perspektiv

Bakgrund

Strålsäkerhetsmyndigheten (SSM) granskar Svensk Kärnbränslehantering AB:s (SKB) ansökningar enligt lagen (1984:3) om kärnteknisk verksamhet om uppförande, innehav och drift av ett slutförvar för använt kärnbränsle och av en inkapslingsanläggning. Som en del i granskningen ger SSM konsulter uppdrag för att inhämta information i avgränsade frågor. I SSM:s Technical note-serie rapporteras resultaten från dessa konsultuppdrag.

Projektets syfte

Projektet syftar till att granska olika beräkningsfall för korrosion av kopparkapseln som rapporterats i SKB TR-10-66 och som sammanfattas i SKB TR-11-01. Arbetet omfattar en analys av beräkningsfall relaterade till korrosionshastigheten för intakt buffert, delvis eroderad buffert och för advektiva förhållanden i bufferten. Målsättningen är att reproducera alla eller delar av SKB: s korrosionsberäkningsfall. Tillämpningen av SKB: s bufferterosionsmodell för att uppskatta erosionstider som används i korrosionsberäkningarna undersöks med hjälp av hydrologiska simuleringsresultat. Därutöver är syftet att specificera och analysera kompletterande beräkningsfall för att utforska effekten av olika konceptuella eller data osäkerheter som identifierats vid granskningen av SKB modelleringsarbete.

Författarens sammanfattning

Föremål för denna rapport är olika beräkningsfall för korrosion av kopparkapseln som rapporteras i SKB TR-10-66 och som sammanfattas i SKB TR-11-01. Den här rapporten

- presenterar en oberoende granskning av beräkningsfall som definieras av SKB för att bedöma korrosion av kopparkapslarna som ska placeras i förvaret
- beskriver beräkningar som syftar till att återskapa delar av SKB:s korrosionsberäkningsfall
- tillämpar SKB: s modell för erosion av bentonitbufferten för att uppskatta erosionstiden som tillämpas i korrosionsberäkningarna
- specificerar och analyser ytterligare beräkningsfall för att utforska inver kan av konceptuella och data osäkerheter som identifierats vid granskningen av SKB modelleringsarbete
- försöker att självständigt implementera den detaljerade erosionsmodellen som presenteras i SKB TR-10-64 och som ligger till grund för det förenklade erosionsmodellen som används i beräkningarna i SKB TR-10-66
- försöker att verifiera resultaten av antalet eroderade och fallerade deponeringspositioner i SKB:s probabilistiska analys som presenteras i SKB TR-11-01 figur 12-4 och SKB TR-10-50 tabell 4-3.

SKB: s erosions- och korrosionsanalys innefattar en bedömning av osäkerheterna i DFN-modellen pga. valt samband mellan sprickstorlek och transmissivitet och även förekomsten av andra flödesvägar (t.ex. sprängskadeszon och utrymme i deponeringstunneltaket pga. otillräcklig återfyllnad). Resultaten av dessa DFN-modeller har tillämpats i oberoende erosionsberäkningar och god överensstämmelse med SKB: s motsvarande resultat har erhållits. Den beräknade tiden som krävs för korrosion av kopparytterhöljet skiljer sig något från dem som rapporteras i SKB TR-10-66 på grund av ett fel i den antagna erosionsvolymen i SKB:s beräkningar, som har rapporterats i SKB dok ID 1396663. När samma misstag införs i den oberoende modellen återskapas SKB: s resultat för antalet fallerade kapslar. Effekten av felet är att öka mängden korrosion och resultaten som presenteras i SKB TR-10-66 kan anses vara pessimistiska ur detta perspektiv. Betydelsen av sovringskriterier för deponeringspositioner (s.k. EFPC-kriteriet) framhävs av resultaten.

Modeller baserade på hydrogeologiska resultat från oberoende DFN-modeller (Geier, 2015) leder till ett liknande antal eroderade positioner när de är konfigurerade på samma sätt som SKB: s semi-korrelerade DFN modell Detta ger förtroende till de resultat som presenteras av SKB.

Oberoende analys och modellering tyder på att det möjligt att erhålla ett betydligt större antal eroderade deponeringshål jämfört med de resultat som presenteras av SKB, om alternativa antaganden görs i DFN-modellen när det gäller förhållandet mellan sprickapertur och transmissivitet. Framförallt Hjernes modell för förhållandet mellan sprickapertur och transmissivitet eller en alternativ skalning av sprickfrekvenser i deponeringshålen i DFN-modellen leder till ett större antal eroderade deponeringspositioner. Detta tyder på att bufferten skulle kunna vara mindre robust i förvarsmiljön än vad som framgår av SKB: s resultat. Om dessa alternativa relationer och skalningar är rimliga, skulle resultaten möjligtvis kunna ifrågasätta SKB:s säkerhetsfunktion att bufferten ska begränsa advektiva förhållanden i deponeringshålet och minska mikrobiell aktivitet. Men ökningen av antalet eroderade deponeringspositioner leder dock inte till en lika kraftig ökning av antalet fallerade (eroderade + korroderade) positioner, utan endast ca 50 procent fler kapslar fallerar inom en miljon år.

De probabilistiska erosionsberäkningarna i SKB TR-10-66 grundar sig i en förenklad erosionsmodell som är baserad på ett log-lineärt förhållande mellan graden av erosion och flödet av grundvatten. Förhållandet passas till resultaten från en mer detaljerad mekanistisk erosionsmodell, vilket beskrivs i SKB TR-10-64. En implementering av den detaljerade modellen kan återskapa sambandet mellan graden av erosion och grundvattenhastigheten, men inte dess exakta parameteresering. Den oberoende modellen visar sig ge en bättre passning till data som rapporterats i SKB TR-09-35. I rapporten ges mer information om den mekanistiska erosionsmodellen och det kan konstateras att det föreligger en inkonsekvens mellan erosionshastigheterna som redovisas i SKB TR-10- 66 och SKB TR-09-35. Resultaten från den oberoende modellen tyder också på att erosionshastigheterna vid långsamma grundvattenhastigheter (<0,1

m /år) kan vara underskattade av den förenklade erosionsmodellen jämfört med resultaten från den detaljerade modellen. Mer arbete skulle krävas för att avgöra konsekvenserna av denna observation.

Projektinformation
Kontaktperson på SSM: Bo Strömberg
Diarienummer ramavtal: SSM2011-3395
Diarienummer avrop: SSM2014-2074
Aktivitetsnummer: 3030012-4092

SSM perspective

Background

The Swedish Radiation Safety Authority (SSM) reviews the Swedish Nuclear Fuel Company's (SKB) applications under the Act on Nuclear Activities (SFS 1984:3) for the construction and operation of a repository for spent nuclear fuel and for an encapsulation facility. As part of the review, SSM commissions consultants to carry out work in order to obtain information on specific issues. The results from the consultants' tasks are reported in SSM's Technical Note series.

Objective

This assignment concerns copper canister corrosion calculation cases reported and summarized in SKB TR-11-01 and SKB TR-10-66. The work includes analysis of calculation cases related to corrosion rate assessment for conditions of intact buffer, partially eroded buffer, and for advective conditions in the buffer. The objective of this project is to reproduce all or a sub-set of SKB's corrosion calculation cases. If requested by SSM, the application of SKB's buffer erosion model to estimate the "erosion time" used in the corrosion calculations shall also be explored using hydrological simulation results. The supplier shall also specify and analyse a second set of additional calculation cases to explore the influence of various conceptual or data uncertainties identified during the review of the SKB modelling work.

Summary by the authors

The present contribution concerns copper canister corrosion calculation cases reported in SKB TR-10-66 ("Corrosion calculations report for the safety assessment SR-Site") and summarized in SKB TR-11-01 (SR-Site main report). The present report:

- presents an independent review of the calculation cases that were designed by SKB to assess corrosion of the copper SF canisters to be emplaced in the repository;
- describes calculations designed to reproduce a sub-set of SKB's corrosion calculation cases;
- applies SKB's model for the erosion of the bentonite buffer that will be emplaced around the copper canisters, to estimate the "erosion time" used in the corrosion calculations;
- specifies and analyses additional calculation cases to explore the influence of conceptual and data uncertainties identified during the review of the SKB modelling work;
- attempts to independently implement the detailed erosion model, presented in TR-10-64, which is the basis for the simplified power law erosion model that is used in the calculations in TR-10-66; and
- attempts to verify results of numbers of eroded and failed locations in SKB's probabilistic analysis presented in TR 11 01 Figure 12 4 and TR 10 50 Table 4 3 respectively.

SKB's erosion and corrosion analysis includes a consideration of the uncertainties in the DFN model relating to the effect of the fracture size – transmissivity relationship and also considered the presence of other hydrogeological features (such as EDZ and crown space) in the model. The results of these DFN models were used in independent erosion calculations and good agreement was found with SKB's corresponding results. The times required for corrosion of the copper overpack that were calculated differed slightly to those reported in TR-10-66 due to a mistake in the assumed volume for erosion in the SKB calculations, which was subsequently reported in SKB Public Memo 1396663. When the same mistake was imposed on the independent model SKB's results for the numbers of failed canisters are reproduced. (The effect of the mistake is to increase the amount of corrosion and so the results presented in TR-10-66 can be considered pessimistic from this perspective.) The importance of the EFPC rejection criteria was highlighted in the results.

Models based on independently implemented DFN models (Geier, 2015) lead to similar numbers of eroded locations when configured similarly to SKB's semi-correlated DFN, which lends confidence to the primary results presented by SKB.

Independent analysis and modelling suggests that, compared with the results presented by SKB, it is possible to obtain significantly greater numbers of eroded deposition holes by taking reasonable alternative modelling assumptions in the DFN model and in the aperture – transmissivity relationship. In particular the Hjerne aperture-transmissivity model and/or the fracture frequency scaling by fracture area in the DFN leads to greater numbers of eroded locations. This suggests that the buffer could potentially be less robust in the repository environment than implied by SKB's results. Hence, if these alternative relationships and scalings are plausible, the results possibly question SKB's safety function regarding the role of the buffer in limiting advective conditions in the deposition hole and reducing microbial activity. However, the increase in the number of eroded locations is not reflected strongly in the increase in the number of failed (eroded + corroded) locations, with only around 50 percent more locations being failed within one million years.

The probabilistic erosion calculations in TR-10-66 are founded upon a simplified erosion model based on a power law relationship between the rate of erosion and the groundwater flow rate. The power law is fitted to output data from a more detailed mechanistic erosion model, which is documented in TR-10-64. An independent attempt to re-implement the detailed model was able to establish the power law relationship between the rate of erosion and the groundwater velocity, but not its precise parameterisation. The independent model was found to provide a better fit to data reported in the supporting report TR-09-35, which provides more details for the mechanistic erosion model, and highlighted an apparent inconsistency between the erosion rates that are reported in TR-10-66 and TR-09-35. The results of the independent model also sug-

gest that the erosion rates at slow groundwater velocities (<0.1 m/y) may be under-predicted by the simplified power law model when compared to the results of the detailed models. More work would be required to determine the implication of this observation.

Project information
Contact person at SSM: Bo Strömberg

Strål
säkerhets
myndigheten
Swedish Radiation Safety Authority

Authors: Steve J. Benbow, Richard Metcalfe, Jenny Burrow
Quintessa Ltd, Henley-on-Thames, UK

Technical Note 88

2015:49

Independent Modelling of Engineered Barrier Evolution and Coupled THMC: Canister Corrosion Calculations in SR-Site

Date: December 2015
Report number: 2015:49 **ISSN:** 2000-0456
Available at www.stralsakerhetsmyndigheten.se

This report was commissioned by the Swedish Radiation Safety Authority (SSM). The conclusions and viewpoints presented in the report are those of the author(s) and do not necessarily coincide with those of SSM.

Contents

1 Introduction

This report is a contribution to the Strålsäkerhetsmyndigheten's (SSM's) Main Review Phase of the SR-Site safety assessment, which has been undertaken by Svensk Kärnbränslehantering AB (SKB). This safety assessment was undertaken to support SKB's licence application to construct and operate a final repository for spent nuclear fuel at Forsmark in the municipality of Östhammar, Sweden.

The present contribution concerns copper canister corrosion calculation cases reported in SKB TR-10-66 ("Corrosion calculations report for the safety assessment SR-Site") and summarized in SKB TR-11-01 (SR-Site main report). The objectives of the work are to:

- undertake and independent assessment of SKB's calculation cases that were designed to assess copper canister corrosion, in order to:
  - develop an understanding of SKB's calculations;
  - identify any questions that should be addressed to SKB concerning these calculations;
- reproduce a sub-set of SKB's corrosion calculation cases;
- apply SKB's buffer erosion model to estimate the "erosion time" used in the corrosion calculations; and
- specify and analyse additional calculation cases to explore the influence of conceptual and data uncertainties identified during the review of the SKB modelling work.

The work includes analyses of timescales required for erosion of the buffer and general corrosion of the copper canister under advective conditions in the deposition hole. Account is taken of the different hydrogeological Discrete Fracture Network (DFN) variants that have been analysed by SKB. Deterministic sensitivity analyses are undertaken related to buffer loss representation, sulphide concentrations and corrosion geometry.

In Section 2, independent analysis and modelling is presented relating to the erosion and corrosion calculations presented in TR-10-66. Sections 2.1 - 2.7 provide an overview of the erosion calculations and a comparison of independent erosion calculations with SKB's calculations for a range of realisations of SKB's DFN models. Alternative conceptual models for the aperture – transmissivity relationship that is assumed in the DFN model are considered that are shown to lead to more eroded locations in general. Sections 2.8 - 2.10 provide an overview of the corrosion model, and present results from the independent modelling on failure timescales (combined erosion and corrosion timescales) for the suite of SKB's DFN models.

In Section 3, independent erosion calculations based on independent DFN model outputs by Geier (2014) are presented. The results are compared to those obtained by SKB where comparable DFN models exist, and also includes other conceptual modelling alternatives that were not considered by SKB (alternative aperture – transmissivity relationships) and alternative fracture size distribution models.
The conclusions of the independent modelling are summarised in Section 4 and some potential questions for SKB that arise from the work are listed in Section 5.

Appendix A and Appendix B list the DFN model output files produced by SKB and by Geier (2014) that have been used in the analysis and Appendix C provides details of the Perl scripts that were developed to perform the calculations.

Appendix D describes an attempt to implement SKB's detailed mechanistic erosion model, which is the basis for the simplified power law erosion model that is used in the performance assessment calculations.

Appendix E presents an independent attempt to reproduce results of numbers of eroded and failed locations in SKB's probabilistic analysis presented in TR-11-01 Figure 12-4 and TR-10-50 Table 4-3 respectively.

2 Understanding and Checking SKB's Erosion and Corrosion Calculations

2.1 Summary of Erosion Model in TR-10-66

SKB's model of buffer erosion is summarised in TR-10-66, Section 4.3.1. Some supplemental information on how velocity data for use in the erosion model is obtained from the DFN calculations is provided in TR-10-66, Section 4.3.2. It is stated that:

$$R_{Erosion} = A_{ero}\delta v^{0.41} \qquad \text{(TR-10-66, Eqn. 4-20)} \qquad (2\text{-}1)$$

where δ is the fracture aperture, v is the water velocity and the constant $A_{ero} = 27.2$ when the velocity is given in m/y and the buffer erosion rate is given in kg/y.

SKB derived this equation by calculating erosion rates as a function of water velocity using a numerical model, which is described in TR-10-35 and TR-10-64. The above equation was then fitted to the model outputs.

Appendix D gives details of an independent attempt to reproduce the underlying numerical model in TR-10-64, where it is shown that the power law form of (2-1) with a power of 0.41 can be reproduced by an independent model. However the constant $A_{ero} = 27.2$ can only be obtained by fitting to SKB's data. The value of A_{ero} that arises naturally in the independent model is an order of magnitude smaller.

In TR-10-66 it is not stated whether the groundwater velocity, v, that is used in (2-1) is the 'background' water velocity in the fracture intersecting the deposition hole, or whether it is the faster groundwater velocity close to the buffer where the flow pathway is perturbed around the buffer. However, TR-10-64 (p46) states that the modelled erosion rates, upon which the fit (2-1) are based, use water velocities in fractures that are 'far away' from the deposition hole.

In TR-10-66, Section 4.3.2 it is noted that the Darcy flux reported by the DFN models is derived from the volumetric flows that are calculated by the DFN models by assuming that the volumetric flow is over an area with cross section A_{Darcy}, where:

$$A_{Darcy} = 2r_h h_{can}. \qquad (2\text{-}2)$$

Here, r_h (m) is the radius of the deposition hole and h_{can} (m) is the height of the waste canister (which is taken to be 5 m). It is noted that equation (3-8) in report R-09-20 would appear to suggest that the correct cross sectional area is $w_C\sqrt{a_f}$, where w_C is the deposition hole height (taken to be 5 m) and a_f is the area of the fracture plane intersecting the deposition hole.

2.2 Summary of Provided Spreadsheet Erosion Calculations

Erosion rate calculations, which calculate $R_{Erosion}$ according to (2-1, 2-2) for all deposition holes in the hydrogeological base case model, are provided in the spreadsheet file:

SSM2011-2426-130 1396328 - hydrogeological_base_case_r0_velocity.XLS
Outputs from SKB's base case DFN model are given in the worksheet 'fs_Q1_2000_pline_merged.ptb'. A summary of the column headings used in the worksheet is given in R-09-20. The outputs relevant to the erosion model are given in columns U0, TRAPP, FPC and EFPC, whose corresponding columns in the worksheet are described in R-09-20 (p138) as follows (text in italics in square brackets has been added for clarification):

$\boldsymbol{U0}$	Initial equivalent flux (m/y) for Q1 ($\boldsymbol{U_{r1}}$ in equation (3-8) [*of R-09-20*]) and Q2 ($\boldsymbol{U_{r2}}$ in equation (3-10)). For Q3 this is just the initial Darcy flux (m/y) and U_R should be used for radionuclide transport. *[Here, Q1, Q2 and Q3 are pathways for radionuclides to leave a canister. In the case of Q1, radionuclides travel by diffusion into the mobile water in fractures surrounding the deposition hole, while in Q2, the radionuclides travel by diffusion into mobile water in the EDZ. In Q3 radionuclides leave a canister and diffuse into a tunnel-intersecting fracture in which advection occurs.]*
$\boldsymbol{TRAPP}$	Initial transport aperture (m) in the first fracture *[encountered by a radionuclide after leaving the canister]* for Q1 or Q2, or the porosity for Q3.
$\boldsymbol{FPC}$	Whether or not the path is associated with a deposition hole that would be excluded if the FPC[1] (Section 3.2.7 [*of R-09-20*]) were applied: 0 = would not be excluded; 1 = excluded due to background fracture; 2 = excluded due to deformation zone fracture.
$\boldsymbol{EFPC}$	The largest number of adjacent deposition holes (including this deposition hole) fully intersected by a fracture that fully intersects this deposition hole. A value of 5 or greater means that the hole would be excluded if the EFPC[2] (Section 3.2.7 [*of R-09-20*]) were applied.

The 'Full Perimeter Criteria' (FPC) and 'Extended Full Perimeter Criteria' (EFPC) are SKB's criteria for acceptance or rejection of deposition holes and can be described as:

[1] Full Perimeter Criterion: a deposition hole is excluded if it is intersected by the hypothetical
extension of a fracture that intersects the full perimeter of the corresponding deposition tunnel.

[2] Extended Full Perimeter Criterion: – a deposition hole is excluded if its full perimeter is
intersected by a fracture that also intersects the full perimeter of four or more neighbouring
deposition holes in the same deposition tunnel.

- Full Perimeter Criteria (FPC) - a deposition hole is excluded if it is intersected by the hypothetical extension of a fracture that intersects the full perimeter of the corresponding deposition tunnel.
- Extended Full Perimeter Criteria (EFPC) - a deposition hole is excluded if its full perimeter is intersected by a fracture that also intersects the full perimeter of four or more neighbouring deposition holes in the same deposition tunnel.

(More details are given in TR-10-21.)

The erosion calculations are relevant only to the Q1 pathway, so the $U0$ and $TRAPP$ data is considered in that sense, thus $U0$ is assumed to be an equivalent flux and $TRAPP$ is the fracture aperture.

The calculation of the erosion rate is presented in the 'velocities' worksheet. First the aperture δ is calculated as:

$$\delta = \begin{cases} TRAPP & FPC < 2 \\ 0 & \text{otherwise} \end{cases}$$

[It is not clear why deposition holes that would be excluded due to background fractures ($\mathrm{FPC} = 1$) are included in the calculation, but it would appear conservative to include them since this could only lead to a larger number of eroded locations.]

The groundwater velocity, v, that is used in the erosion calculation is then calculated as

$$v = \begin{cases} U0 \times 5/\delta & \delta \neq 0 \\ 0 & \text{otherwise} \end{cases} \quad (2\text{-}3)$$

where δ is the fracture aperture.

The scaling of the Darcy flux by $5/\delta$ to obtain the groundwater velocity can be understood as follows. The volumetric flux Q_f (m^3/y) is obtained from $U0$ by applying the scaling (2-2),

$$Q_f = 2r_h h_{can} U0.$$

The groundwater velocity is then obtained by dividing the volumetric flux by the appropriate cross section area. Since the water is flowing in the fracture it is clear that one of the lengths defining the cross section is the fracture aperture, δ. If the other length in the other dimension forming the area is L (m), then the groundwater velocity is given by

$$v = \frac{Q_f}{\delta L} = \frac{2r_h h_{can}}{\delta L} U0.$$

The height of the canister is approximately 5m (TR-10-66 quotes the canister height to be 4.835m on p11). Thus setting $h_{can} = 5\mathrm{m}$ gives

$$v = \frac{Q_f}{\delta L} = \frac{5}{\delta}\frac{2r_h}{L} U0. \quad (2\text{-}4)$$

Comparing (2-4) with the rule for calculating v used in the spreadsheet (2-3), we see that (2-4) matches the rule if $L = 2r_h$, i.e. L is the deposition hole diameter.

Given the groundwater velocity in the fracture (calculated as in (2-3)), TR-10-66 states that the erosion rate can be calculated according to (2-1). This is calculated in the spreadsheet in the 'R_Erosion' column of the velocities worksheet. The units of the inputs to the model (i.e. δ and v) are correct. Since v, calculated by (3), is zero for fractures with $FPC = 2$, the calculated erosion rates are only non-zero when $FPC = 0$ or 1. [Again, it is not clear why fractures with FPC $= 1$ are included in the calculation.]

Equation (2-1) is presented in TR-10-64 (Section 5.1). Figure 1 shows the fit of equation (2-1) to the source data in TR-10-64, Figure 5-3. The fit to the data is very good, although it is important to note that the source data is actually the predicted erosion rate from a more detailed numerical model rather than being experimentally measured data. Also shown is the erosion data from another model presented in Figure 9-6 of TR-09-35 (the data shown corresponds to the 1.75 m hole diameter case).

The models appear similar from the descriptions that are provided in the two reports, with the same assumed fracture aperture (1mm) and buffer diameter (1.75m). Furthermore the results given in Table 5-1 of TR-10-64 and Table 9-2 of TR-09-35 are identical and agree with the data plotted in Figure 5-3 of TR-10-64. Therefore, the reason for the order of magnitude difference in the results plotted in Figure 5-3 of TR-10-64 and those for the 1.75 m hole diameter in Figure 9-6 of TR-09-35 is not clear. It is noted however that the attempt to independently implement the detailed numerical model, described in Appendix D, results in erosion rates that provide a very good fit to the data points from TR-09-35, Figure 9-6 (See Appendix D, Figure 15).

The model (2-1) is conservative in the sense that it fits the model predicting the greater amount of erosion. However the modelling in Appendix D suggests that it may underestimate the erosion rate for slow flows (<0.1 m/y) when compared to the detailed model. The effect of this in the probabilistic analysis is that the majority of the deposition holes experiencing slow flow rates could undergo more erosion than is predicted by equation (2-1).

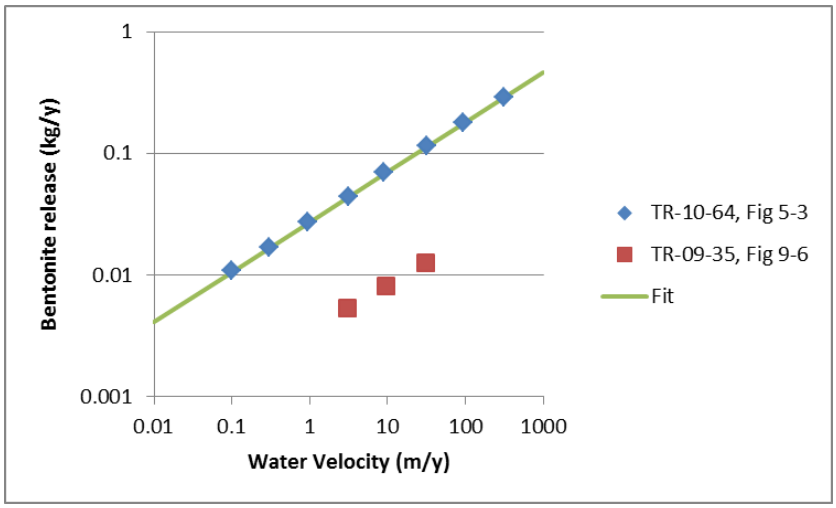

Figure 1: Fit of the erosion model (2-1) to erosion rates predicted by models in TR-10-64 and TR-09-35.

2.3 Independent Erosion Calculations – Base Case

The erosion calculations presented in TR-10-66 (described in Sections 2.1, 2.2) have been re-implemented in new worksheets that have been added to the provided spreadsheet. The new worksheets only use as input the DFN output data from SKB's base case DFN model provided in the fs_Q1_2000_pline_merged.ptb worksheet.

If a 5m canister height is assumed in the calculations (which, as noted in Section 2.2, is the deposition hole height h_{hole} assumed in the ECPM approximation in the DFN model), then an exact match to the erosion rates that were originally provided is obtained. The calculated erosion rates for all deposition holes are shown in Figure 2.

The maximum calculated erosion rate is 0.194 kg/y for deposition hole 2043, which has $FPC = 1$ (which indicates a deposition hole that would be excluded due to the extension of a fracture that intersects the full perimeter of the deposition tunnel also intersecting the deposition hole). The largest erosion rate in a deposition hole that would not be excluded due to background fractures is 0.053 kg/y, for deposition hole 1978.

Figure 3 shows the percentage of deposition holes that achieve erosion below a given rate. Approximately 92% of the deposition holes achieve erosion rates of <1 g/y, 99.3% achieve <10 g/y, and only one deposition hole experiences >100 g/y.

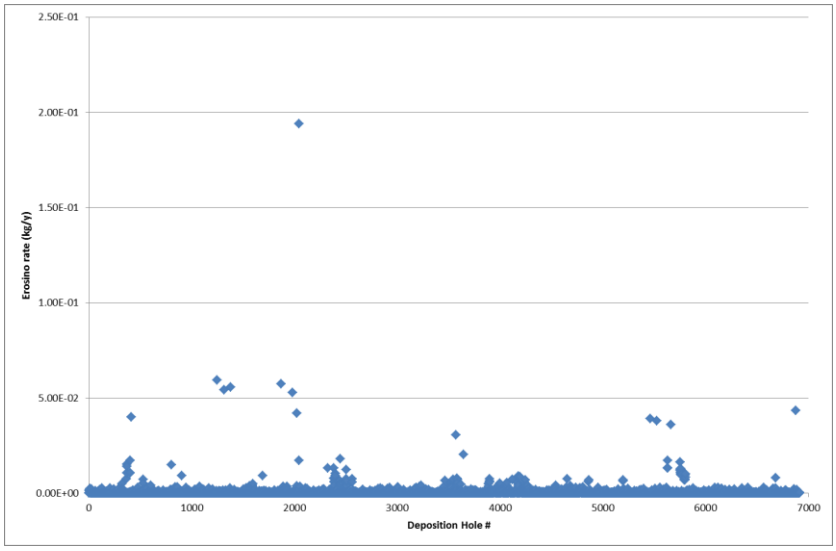

Figure 2: Erosion rates (kg/y) obtained in independent calculations. (Results are identical to those provided in the spreadsheet.) The maximum erosion rate is 0.194 kg/y for deposition hole 2043.

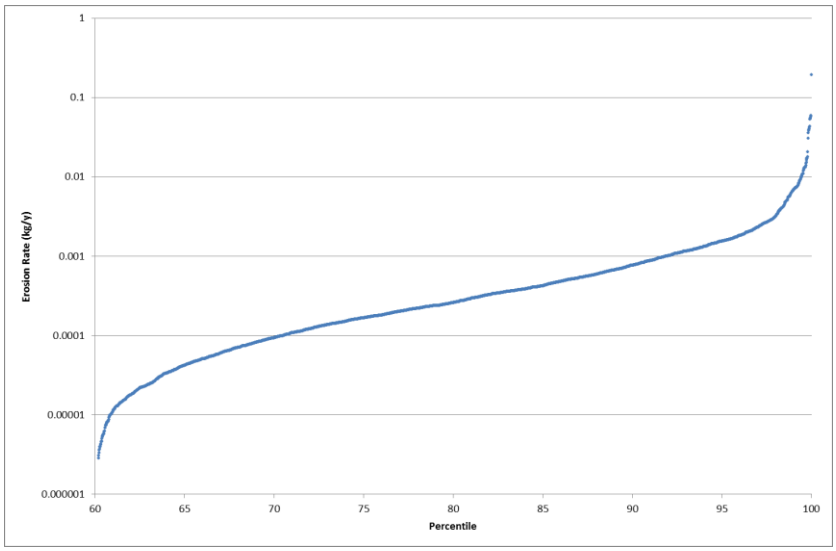

Figure 3: Erosion rates (kg/y) obtained in independent calculations, plotted as percentile of deposition holes that achieve erosion below a given rate.

2.4 Alternative Transmissivity Models– Background

The base case DFN assumes that transmissivity is related to the fracture aperture as

$$\delta_{base} = 0.5T^{0.5}. \qquad (2\text{-}5)$$

An alternative relationship was proposed by Hjerne et al. (R-09-28),

$$\delta_{alt} = 0.28T^{0.3}. \quad (2\text{-}6)$$

This relationship was derived from a compilation of tracer test data from multiple sites in Sweden (Studsvik, Stripa, Finnsjön, Äspö, Forsmark and Laxemar). The fit of the model to the flow path measurement dataset is shown in Figure 4. The relationship $\delta = 0.275T^{0.297}$ (which is close to 2-6 and has an R^2 error of 0.57) was obtained by excluding two data points (referred to as HLX28). This data was felt to be more uncertain since the pump tests at Laxemar from which it was obtained were performed by pumping in a different feature from the one in which the tracer injection took place. A similar fit to another subset of the data (R-09-28, Figure 6-10) obtains $\delta = 0.281T^{0.295}$, with an R^2 error of 0.44 and in another fit (R-09-28, Figure 6-16) where only the subset of fractures where apparent storativity is available $\delta = 0.282T^{0.310}$ is obtained, with an R^2 error of 0.35. When the full dataset was used, the best fit was found to be $\delta = 0.33T^{0.31}$.

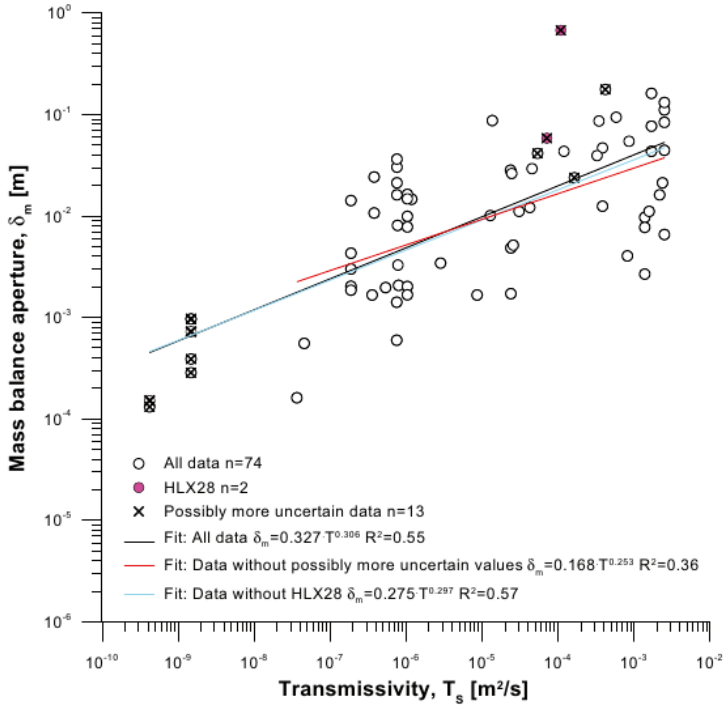

Figure 4: Model fit of mass balance aperture vs. transmissivity for flow path measurements from multiple sites, using the relationship $\boldsymbol{\delta = \alpha T^{\beta}}$ (from R-09-28, Figure 6-5).

The fit derived in R-09-28 is for the 'mass balance aperture', which is defined to be the aperture measure that, when combined with appropriate geometrical assumptions leads to a volume that is equal to the mean residence time in the fracture multiplied by the flow rate. R-09-28 explains that of the various measures of aperture that are available, the mass balance aperture has 'rather good support in the data' compared to the alternative aperture measures.

The aperture-transmissivity model (2-6) will be referred to in this report as the 'Hjerne model'. TR-10-66, p25 states that (2-6) is

'dismissed as being unrealistic for the quantification of buffer erosion (TR-10-52)',

however TR-10-52, p335 states that

'the derived mass balance aperture relationship presented by (SKB-R-09-28) should yield apertures on the larger side and is therefore considered appropriate for use as a bounding variant in SR-Site in particle tracking calculations.'.

The argument for the model (2-6) being an upper bound is presented in R-09-22, where it is suggested that since tracer tests are typically performed in fractures that are known to have preferential properties for tracer transport, and also that site-specific electrical resistivity measurements tend to give smaller apertures. However R-09-22 states that electrical resistivity measurements tend to give larger apertures than the SR-Site model (2-5), so by the same argument it could equally be assumed that the SR-Site model is towards a lower bound.

In both (2-5, 2-6), the constants are such that when the aperture is measured in m, the transmissivity is measured in m^2/s. It is noted that for a given transmissivity,

$$\delta_{alt} \cong 0.42\ \delta_{base}^{0.6}, \qquad (2\text{-}7)$$

i.e. that $\delta_{alt} > \delta_{base}$ for apertures of interest ($\delta_{alt} > \delta_{base}$ when $\delta_{base} < 0.117$ m) and so the apertures predicted by 2-6 will be larger than the corresponding ones from the SR-Site model. This would tend to give rise to slower calculated groundwater velocities in the fracture, given the same Darcy velocity, but increases the area of the buffer exposed to erosion.

2.5 Alternative Transmissivity Models - Erosion Results, Base Case

SKB's semi-correlated base case DFN results are provided (in the worksheet 'fs_Q1_2000_pline_merged.ptb'). Whether the provided calculation results can be used to infer the impact upon erosion predictions using the alternative model depends upon how the porosity and/or transmissivity inputs are used in the DFN:

- If the base case DFN is conditioned on measured or calculated transmissivity data, then (2-6) can be used together with the DFN calculated Darcy flux to infer corresponding fracture apertures and groundwater velocities in the fracture based on the Hjerne model (2-6).
- If the base case DFN is conditioned on measured or calculated fracture aperture data, then (2-6) should be used to compute alternative transmissivity inputs to the DFN model, which should then be rerun to calculated corresponding Darcy fluxes.

The description in R-09-20, Section 3.1.3 (para 2) suggests that it is the former that is true (and that the transmissivity data is calculated rather than

measured), and that the equivalent hydraulic conductivity of the ECPM block is determined by calculating the response of the 'mini-DFN' in each ECPM block to linear head gradients in each of the coordinate axis directions to form an anisotropic hydraulic conductivity tensor.

Therefore, it is possible to estimate the effect of the alternative porosity-transmissivity model (2-6) on the rate of erosion by using (2-1), with the fracture aperture $\delta = \delta_{alt}$ inferred from the DFN output 'TRAPP' according to (2-6), and the velocity v calculated from the Darcy velocity output 'U0' of the DFN as described in Section 2.2, but again with $\delta = \delta_{alt}$. To be clear, the steps to follow to calculate the erosion rate under the alterative porosity-transmissivity assumption are:

- Calculate T from the TRAPP (δ_{base}) output of the DFN using (2-5)
- Calculate δ_{alt} using (2-6)
- Calculate the groundwater velocity v_{alt} from the U0 output of the DFN using (2-3) or (2-4) with $\delta = \delta_{\text{alt}}$
- Calculate the erosion rate $R_{\text{erosion,alt}}$ using (2-1) with $v = v_{\text{alt}}$ and $\delta = \delta_{\text{alt}}$

(Equation (2-7) could be used in place of the first two steps.)

Erosion rates based on the Hjerne model (2-6) are provided by SKB in the 'velocities_hjerne' worksheet. The erosion rates based on (2-6) that were independently calculated are different to those supplied. It appears that the difference is caused due to the third step above being missed so that $v = v_{base}$ is used in the final step. This would appear to be an error and results in a faster groundwater flow rate being used in SKB's erosion calculation, which therefore increases the calculated rate of erosion.

The calculated erosion rates are shown in Figure 5 as percentiles of deposition holes achieving erosion below specified rates. Also plotted are the rates of erosion when the base porosity-transmissivity assumption (2-5) is used and the seemingly erroneous rates calculated by SKB in the 'velocities_hjerne' worksheet, which attempts to use (2-6).

The data is summarised in Table 1. With the alternative relationship (2-6), 15 deposition holes experience erosion greater than 0.1 kg/y (compared to one when (2-5) is used) and 446 (7% of) deposition holes experience erosion greater than 0.01 kg/y (compared to 36 when (2-5) is used).

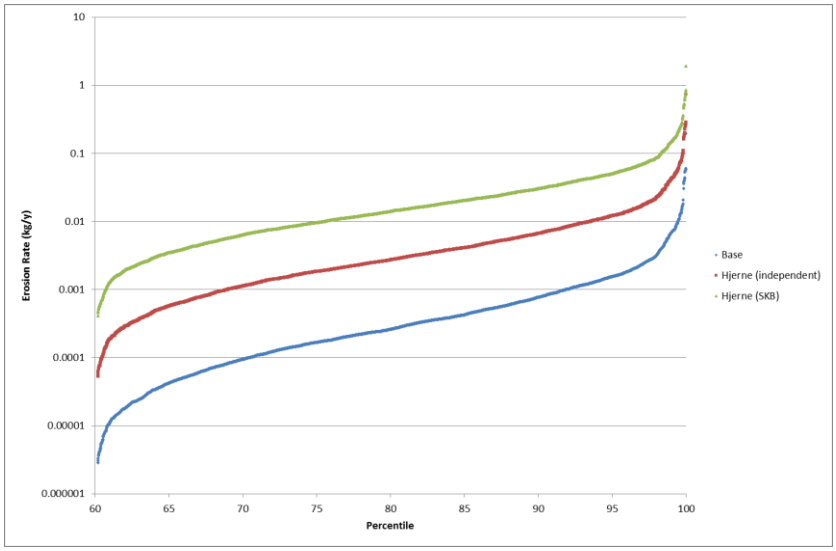

Figure 5: Erosion rates (kg/y) for the different porosity-transmissivity models: blue -base ($\boldsymbol{\delta = 0.5T^{0.5}}$); red - alternative ($\boldsymbol{\delta = 0.28T^{0.3}}$), obtained in independent calculations; green - alternative ($\boldsymbol{\delta = 0.28T^{0.3}}$), obtained by SKB. Erosion rates are plotted as percentile of deposition holes that achieve erosion below a given rate.

Table 1: Percentage of deposition holes that achieve erosion below a given rate for the base ($\boldsymbol{\delta = 0.5T^{0.5}}$) and alternative ($\boldsymbol{\delta = 0.28T^{0.3}}$) porosity-transmissivity models.

	Percentage of deposition holes that achieve erosion below given rate	
	Base model $\boldsymbol{\delta_{base} = 0.5T^{0.5}}$	Alternative (Hjerne) model $\boldsymbol{\delta_{alt} = 0.28T^{0.3}}$
$< \boldsymbol{1e^{-5}}$ kg/y	61	-
$< \boldsymbol{1e^{-4}}$ kg/y	70	60
$< \boldsymbol{1e^{-3}}$ kg/y	92	69
$< \boldsymbol{1e^{-2}}$ kg/y	99.3	93
$< \boldsymbol{1e^{-1}}$ kg/y	99.9 (all but one)	99.8 (15 above 0.1 kg/y)

2.6 Establishment of Advective Conditions in the Deposition Hole – Base Case

The erosion rates calculated in Sections 2.3 and 2.5 can be used to determine the number of deposition holes that experience advective conditions (for the first time) during each glacial cycle by determining the time taken to erode a volume sufficient for advection to take place. TR-10-66 suggests the approximation

$$V_{zone} = \frac{h_{zone}\pi(r_h^2 - r_{can}^2)}{2}$$

to determine the volume of the eroded zone, V_{zone}. The approximation assumes a uniform thickness of eroded buffer, h_{zone}, and that only the 'upstream' side of the buffer must be eroded. SKB's suggested value is

$h_{zone} = d_{buf}$ (the buffer thickness), which assumes that the thickness of the eroded area is the same in the horizontal and vertical directions. The mass of buffer that must be eroded before advective conditions occur adjacent to the canister surface is then $M_{adv} = V_{zone}\rho_{buf}$, where ρ_{buf} (kg/m^3) is the saturated buffer density. The values of the relevant input parameters are given in Table 2 and result in an eroded volume $V_{zone} = 0.27$ m^3 and an eroded mass $M_{adv} = 531$ kg. This derivation assumes that no re-homogenisation of the buffer takes place to close the eroded gap, and therefore 531 kg can be taken to be a pessimistic value. In TR-10-66, SKB assume a base case mass of eroded buffer to be 1,200 kg and vary the amount between 600 kg and 2,400 kg in their sensitivity analysis, but the reasoning for these values (or a corresponding reference) is not presented in TR-10-66. The value appears to derive from discussion in TR-11-01 (p387) in which modelling is referred to that demonstrated that even when two entire bentonite rings (with a dry mass of 2,400 kg) are omitted from the buffer, the buffer is able to re-homogenise and almost maintain the minimum dry density in the buffer (1,000 kg/m^3). The value of 1,200 kg therefore corresponds to a 'half annulus'.

Table 2: Properties used in erosion time calculations.

Property	Value	Source / Notes
$\boldsymbol{r_{can}}$	0.525 m	TR-10-66, p11
$\boldsymbol{d_{buf}}$	0.35 m	TR-10-66, p22 (and the assumption $\boldsymbol{h_{zone} = d_{buf}}$ is made, consistent with TR-10-66)
$\boldsymbol{r_h}$	0.875 m	(Inferred from $\boldsymbol{r_{can}}$ and $\boldsymbol{d_{buf}}$)
$\boldsymbol{\rho_{buf}}$	1971 kg/m^3	Assumes dry density of 1571 kg/m3 (TR-10-66, p31) and a porosity of 0.4 (TR-10-66, p27).

Deposition holes that would be excluded on the basis of the FPC ($FPC < 1$) or the $EFPC$ ($EFPC < 5$) are excluded from the erosion timescale calculations, consistent with the calculations presented in TR-10-66, Section 5.3.5 (but in contrast to the analysis in Section 2.2-2.3, in which depositions with $FPC = 1$ were included in the analysis).

The number of deposition holes experiencing advective conditions adjacent to the canister (for the first time) during each glaciation is shown in Table 3 for the base and alternative porosity-transmissivity relationships. Also shown are the same results when the eroded mass required for advection, M_{adv}, is set to 1,200 kg (the 'base case' value – TR-10-66, p40).

The same results are also shown in Figure 6 ($M_{adv} = 1{,}200$ kg) and Figure 7 ($M_{adv} = 531$ kg). The calculations assume a glacial period of length 120,000 y, with dilute water assumed to be flowing at repository depths for 25% of the glacial cycle period, consistent with the assumptions made in TR-10-66 (p37).

It is clear that a significantly greater number of deposition holes experience advective conditions when the alternative porosity-transmissivity model (2-6) is used. For example, during the first five glacial periods 294 locations experience advective conditions when the Hjerne model is assumed, compared to 10 for the 'base' model. When the required eroded mass M_{adv} is set to 531 kg, the 'profile' of the number of deposition holes that become

advective in each glacial period is different (Figure 7). In this case there is a big increase in the early glacial cycles, with the number of new deposition holes becoming advective falling off thereafter. Effectively, since the required eroded mass is more than halved, deposition holes that would have required one or two glacial periods, and some that would have required three glaciations, become advective during the first glacial period, and so on.

Table 3: Number of deposition holes experiencing advective conditions for the first time during each glacial cycle for the base and alternative (Hjerne) porosity-transmissivity models assuming $\boldsymbol{M_{adv} = 1,200}$ kg and $\boldsymbol{M_{adv} = 531}$ kg.

Glacial cycle	Case when $M_{adv} = 1{,}200$ kg.		Case when $M_{adv} = 531$ kg.	
	Base model $\delta_{base} = 0.5T^{0.5}$	Alternative (Hjerne) model $\delta_{alt} = 0.28T^{0.3}$	Base model $\delta_{base} = 0.5T^{0.5}$	Alternative (Hjerne) model $\delta_{alt} = 0.28T^{0.3}$
1	3	15	3	66
2	0	34	6	192
3	1	74	8	183
4	3	82	7	166
5	3	89	10	152
6	5	85	11	124
7	3	74	18	94
8	3	83	19	88
9	3	68	20	77
10	4	67	20	89

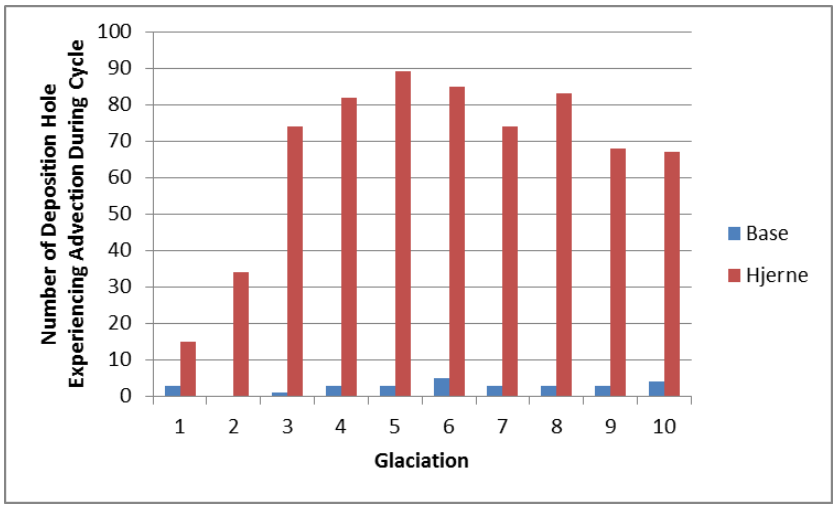

Figure 6: Number of deposition holes experiencing advective conditions for the first time during each glacial cycle for the base and alternative (Hjerne) porosity-transmissivity models assuming $\boldsymbol{M_{adv} = 1,200}$ kg (see Table 3).

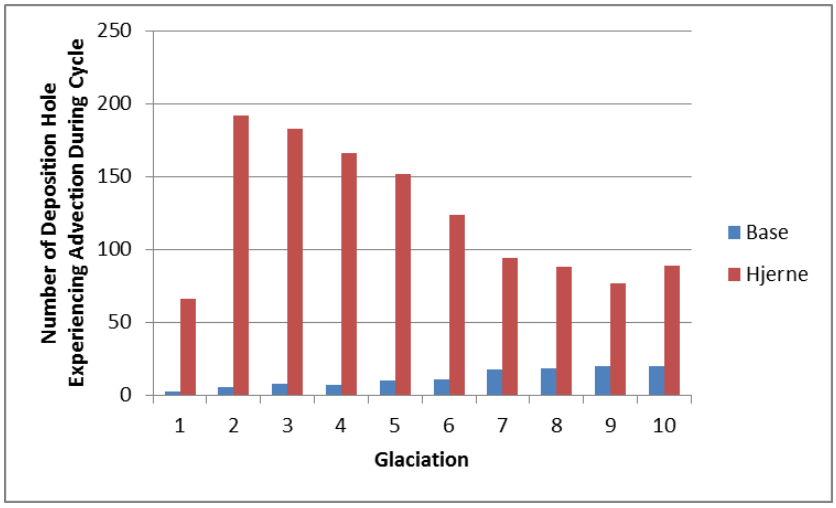

Figure 7: Number of deposition holes experiencing advective conditions for the first time during each glacial cycle for the base and alternative (Hjerne) porosity-transmissivity models assuming $\boldsymbol{M_{adv}} = \mathbf{531}$ kg (see Table 3).

2.7 Establishment of Advective Conditions in the Deposition Hole – Other SKB DFN Realisations

The analysis presented in Section 2.6 determined the time required for erosion to establish advective conditions in the deposition holes in the base case DFN model. A selection of other DFN cases has also been provided, and is described in Appendix A. In all, there are 25 sets of results in total. The cases comprise:

- (#2) Ten alternative realisations of the base case;
- (#3) Four realisations of the correlated size-transmissivity case;
- (#4) Four realisations of the truncated, uncorrelated size-transmissivity case;
- (#5) Two realisations with different EDZ transmissivities;
- (#6) A variant with no EDZ;
- (#7) Three realisations with possible deformation zones included; and
- (#8) A tunnel variant with crown space.

(Model numbers #n in parenthesis correspond to the axis labels in Figure 8 and Figure 9, which will be discussed later. The base case DFN model is referred to as #1.)

Two additional cases were also provided in the file merged/100610_fs_top25_Q123_2000_pline10_merged_ptb.zip, which correspond to 'Multiple particles per start point from 25% highest U0 locations in hydro base case at 2000 AD'. The precise background to these cases is not known, so these cases are reported separately since they lead to much greater numbers of eroded deposition holes.

Since there are several sets of results, the analysis is performed using a script (described in Appendix C) rather than implementing the calculations in several spreadsheets.

The number of deposition holes experiencing advective conditions for the first time during the first five glacial cycles for each of the above cases is shown in Table 4 for both the base and Hjerne aperture-transmissivity relationships. The corresponding results for the base case (from Table 3) are also shown.

The correlated and uncorrelated size-transmissivity cases and the base case (in which a semi-correlated model is assumed) lead to similar numbers of advective deposition holes after the first glaciation (2, 1.5 and 1.7 respectively) for the base aperture-transmissivity model. However the uncorrelated model leads to significantly more advective deposition holes in subsequent glaciations (averaging 15.75, 29.5, 39.5 and 43.5 respectively for the second, third fourth and fifth glaciations) compared to the correlated model (8.25, 9.25, 8.5 and 6.25 respectively) and base case (1.2, 0.9, 1.8 and 2 respectively).

The use of the Hjerne aperture-transmissivity model leads to significantly more advective deposition holes, especially in the uncorrelated and correlated models, with an average of 46.75, 86.25, 118.25, 113.5 and 118.25 over the first five glaciations in the case of the correlated size-transmissivity relationship and 158.5, 343.5, 289.5, 232.25 and 117.5 in the uncorrelated size-transmissivity case.

The other cases that were considered (the EDZ variants and the tunnel with crown space model) each lead to similar numbers of advective deposition holes as the base case.

Over the first 8 glacial periods (corresponding to a total evolution of 960,000 y) the average of the total number of advective positions for the Hjerne realisations of the base case is 537 holes. This number agrees quite well with the 575 positions quoted by SKB for the pessimistic fracture aperture case in Figure 12-3 of TR-11-01.

The analogous results when the amount of buffer required to be eroded before advection can begin is assumed to be 531 kg are shown in Table 5. In this case the correlated and uncorrelated size-transmissivity cases lead to more advective deposition holes in all glacial periods (not just the second period onwards, as was the case when the eroded mass was 1,200 kg). The correlated model gives 13.5, 18, 19.3, 21, 23,25 and the uncorrelated model gives 23.8, 87.25, 105, 106, 105 newly advective deposition holes in the first five glacial periods, compared to the base case giving 3, 3.6, 6.6, 8.2, 12.4. Again, the other cases that were considered (the EDZ variants and the tunnel with crown space model) each lead to similar numbers of advective deposition holes as the base case.

The results for the 1,200 and 531 kg eroded masses are shown graphically in the bar charts in Figure 8 and Figure 9 respectively, which show the number of deposition holes becoming advective in each of the first five glacial periods for each of the models, assuming both the base and Hjerne aperture-transmissivity relationships.

The results for the DFN model corresponding to the 25% highest U0 locations in the hydrogeological base case are shown in Table 5 for both the 1,200 and 531 kg of eroded buffer cases. These cases result in far greater numbers of deposition holes becoming advective in the first glacial period (~2,000 deposition holes for both the base and Hjerne models). It would therefore appear that these cases represent a different form of output that is maybe not compatible with this analysis.

Appendix E presents an independent attempt to reproduce results of numbers of eroded locations in SKB's probabilistic analysis that are presented in TR-11-01 Figure 12-4.

Table 4: Number of deposition holes experiencing advective conditions for the first time during each glacial cycle for the base and alternative (Hjerne) porosity-transmissivity models assuming $\boldsymbol{M_{adv} = 1,200}$ kg.

	Base Aperture-Transmissivity Glaciation number					Hjerne Aperture-Transmissivity Glaciation number				
	1	2	3	4	5	1	2	3	4	5
#1 Base case										
fs_Q1_2000_pline_merged.xls	3	0	1	3	3	15	34	74	82	90
#2 Ten alternative realisations of the base case										
fs_r1_Q1_2000_pline_merged.xls	2	1	1	3	4	16	38	63	95	84
fs_r3_Q1_2000_pline_merged.xls	2	3	0	0	1	9	50	76	74	83
fs_r4_Q1_2000_pline_merged.xls	0	0	0	1	1	11	36	88	105	93
fs_r5_Q1_2000_pline_merged.xls	0	1	0	1	2	6	55	70	72	94
fs_r6_Q1_2000_pline_merged.xls	0	1	0	1	1	8	41	75	91	89
fs_r7_Q1_2000_pline_merged.xls	2	3	5	2	5	23	37	76	86	72
fs_r8_Q1_2000_pline_merged.xls	1	1	1	1	0	4	23	53	90	73
fs_r9_Q1_2000_pline_merged.xls	5	1	0	3	2	19	35	62	92	73
fs_r10_Q1_2000_pline_merged.xls	0	0	1	3	2	6	41	82	77	88
fs_r12_Q1_2000_pline_merged.xls	5	1	1	3	2	15	32	67	88	79
Average	1.7	1.2	0.9	1.8	2	11.7	38.8	71.2	87	82.8
#3 Four realisations of the correlated size-transmissivity case										
fs_corr_Q1_2000_pline_merged.xls	4	6	2	9	2	34	88	129	108	105

	Base Aperture-Transmissivity Glaciation number					Hjerne Aperture-Transmissivity Glaciation number				
	1	2	3	4	5	1	2	3	4	5
fs_r2_corr_Q1_2000_pline_merged.xls	2	4	3	3	6	29	101	118	116	124
fs_r4_corr_Q1_2000_pline_merged.xls	0	14	26	10	7	73	86	134	135	130
fs_r5_corr_Q1_2000_pline_merged.xls	2	9	6	12	10	51	70	92	95	114
Average	2	8.25	9.25	8.5	6.25	46.75	86.25	118.25	113.5	118.25

Table 4 (continued)

	Base Aperture-Transmissivity Glaciation number					Hjerne Aperture-Transmissivity Glaciation number				
	1	2	3	4	5	1	2	3	4	5
#4 Four realisations of the truncated, uncorrelated size-transmissivity case										
fs_uncorr_truncHCD_Q1_2000_pline_merged.xls	1	17	30	47	40	166	327	276	200	172
fs_r2_uncorr_truncHCD_Q1_2000_pline_merged.xls	1	12	23	30	39	134	322	280	236	180
fs_r3_uncorr_truncHCD_Q1_2000_pline_merged.xls	4	19	34	38	48	172	379	278	235	166
fs_r5_uncorr_truncHCD_Q1_2000_pline_merged.xls	0	15	31	43	47	162	346	324	258	192
Average	1.5	15.75	29.5	39.5	43.5	158.5	343.5	289.5	232.25	177.5
#5 Two realisations with different EDZ transmissivity										
fs_maxedz_6_Q1_2000_pline_merged.xls	3	1	4	8	4	24	41	87	83	88
fs_maxedz_7_Q1_2000_pline_merged.xls	3	0	1	4	4	17	40	79	89	101
Average	3	0.5	2.5	6	4	20.5	40.5	83	86	94.5
#7 Three realisations with possible deformation zones included										
fs_pdzr1_Q1_2000_pline_merged.xls	2	1	1	3	4	16	36	74	96	92
fs_pdzr2_Q1_2000_pline_merged.xls	5	1	2	2	2	16	34	65	93	79
fs_pdzr3_Q1_2000_pline_merged.xls	2	3	0	0	1	9	52	74	87	73
Average	3	1.67	1	1.67	2.33	13.67	40.67	71	92	81.33
#6 No EDZ case										
fs_noedz_Q1_2000_pline_merged.xls	2	1	1	3	3	14	20	34	45	54
#8 Tunnel variant with crown space										

fs_crown_Q1_2000_pline_merged.xls	3	0	1	4	5	22	37	63	79	95

Table 5: Number of deposition holes experiencing advective conditions for the first time during each glacial cycle for the base and alternative (Hjerne) porosity-transmissivity models assuming $\boldsymbol{M_{adv} = 531}$ kg.

	Base Aperture-Transmissivity Glaciation number					Hjerne Aperture-Transmissivity Glaciation number				
	1	2	3	4	5	1	2	3	4	5
#1 Base case (two identical cases, one with extra TRAPP output)										
fs_Q1_2000_pline_merged.xls	3	6	8	7	10	66	192	183	166	152
#2 Ten alternative realisations of the base case										
fs_r1_Q1_2000_pline_merged.xls	3	6	9	11	12	67	189	201	163	160
fs_r3_Q1_2000_pline_merged.xls	5	0	3	10	23	84	171	172	168	164
fs_r4_Q1_2000_pline_merged.xls	0	2	11	7	14	68	228	197	163	140
fs_r5_Q1_2000_pline_merged.xls	1	3	5	10	15	83	160	196	180	146
fs_r6_Q1_2000_pline_merged.xls	1	2	8	3	12	70	190	192	179	154
fs_r7_Q1_2000_pline_merged.xls	5	8	13	8	12	79	185	165	168	166
fs_r8_Q1_2000_pline_merged.xls	3	1	0	5	5	38	177	206	146	167
fs_r9_Q1_2000_pline_merged.xls	6	4	7	9	8	68	186	174	168	147
fs_r10_Q1_2000_pline_merged.xls	0	6	5	8	12	67	181	204	190	153
fs_r12_Q1_2000_pline_merged.xls	6	4	5	11	11	60	184	173	148	132

	Base Aperture-Transmissivity Glaciation number					Hjerne Aperture-Transmissivity Glaciation number				
	1	2	3	4	5	1	2	3	4	5
Average	3	3.6	6.6	8.2	12.4	68.4	185.1	188	167.3	152.9
#3 Four realisations of the correlated size-transmissivity case										
fs_corr_Q1_2000_pline_merged.xls	11	11	16	24	23	163	249	295	318	269
fs_r2_corr_Q1_2000_pline_merged.xls	8	7	21	24	26	163	259	351	309	289
fs_r4_corr_Q1_2000_pline_merged.xls	20	35	16	23	26	186	313	327	335	238
fs_r5_corr_Q1_2000_pline_merged.xls	15	19	24	13	18	147	221	292	300	254
Average	13.5	18	19.3	21	23.25	164.8	260.5	316.25	315.5	262.5

Table 5 (continued)

	Base Aperture-Transmissivity Glaciation number					Hjerne Aperture-Transmissivity Glaciation number				
	1	2	3	4	5	1	2	3	4	5
#4 Four realisations of the truncated, uncorrelated size-transmissivity case										
fs_uncorr_truncHCD_Q1_2000_pline_merged.xls	24	99	109	94	99	571	486	317	210	129
fs_r2_uncorr_truncHCD_Q1_2000_pline_merged.xls	19	67	99	102	93	534	538	283	209	110
fs_r3_uncorr_truncHCD_Q1_2000_pline_merged.xls	28	94	107	113	122	630	535	292	197	127
fs_r5_uncorr_truncHCD_Q1_2000_pline_merged.xls	24	89	106	116	106	593	599	296	176	113
Average	23.8	87.25	105	106	105	582	539.5	297	198	119.75

	Base Aperture-Transmissivity Glaciation number					Hjerne Aperture-Transmissivity Glaciation number				
	1	2	3	4	5	1	2	3	4	5
#5 Two realisations with different EDZ transmissivities										
fs_maxedz_6_Q1_2000_pline_merged.xls	4	14	7	9	8	83	204	172	169	142
fs_maxedz_7_Q1_2000_pline_merged.xls	4	5	12	7	8	76	195	186	167	140
Average	4	9.5	9.5	8	8	79.5	199.5	179	168	141
#7 Three realisations with possible deformation zones included										
fs_pdzr1_Q1_2000_pline_merged.xls	3	6	10	8	12	71	195	200	164	156
fs_pdzr2_Q1_2000_pline_merged.xls	6	4	6	10	14	64	191	172	149	140
fs_pdzr3_Q1_2000_pline_merged.xls	5	0	4	7	25	84	176	171	172	160
Average	4.67	3.33	6.67	8.33	17.00	73.00	187.33	181	161.67	152.00
#6 No EDZ case										
fs_noedz_Q1_2000_pline_merged.xls	3	6	6	5	8	46	98	104	105	81
#8 Tunnel variant with crown space										
fs_crown_Q1_2000_pline_merged.xls	3	8	12	16	12	76	175	203	168	136

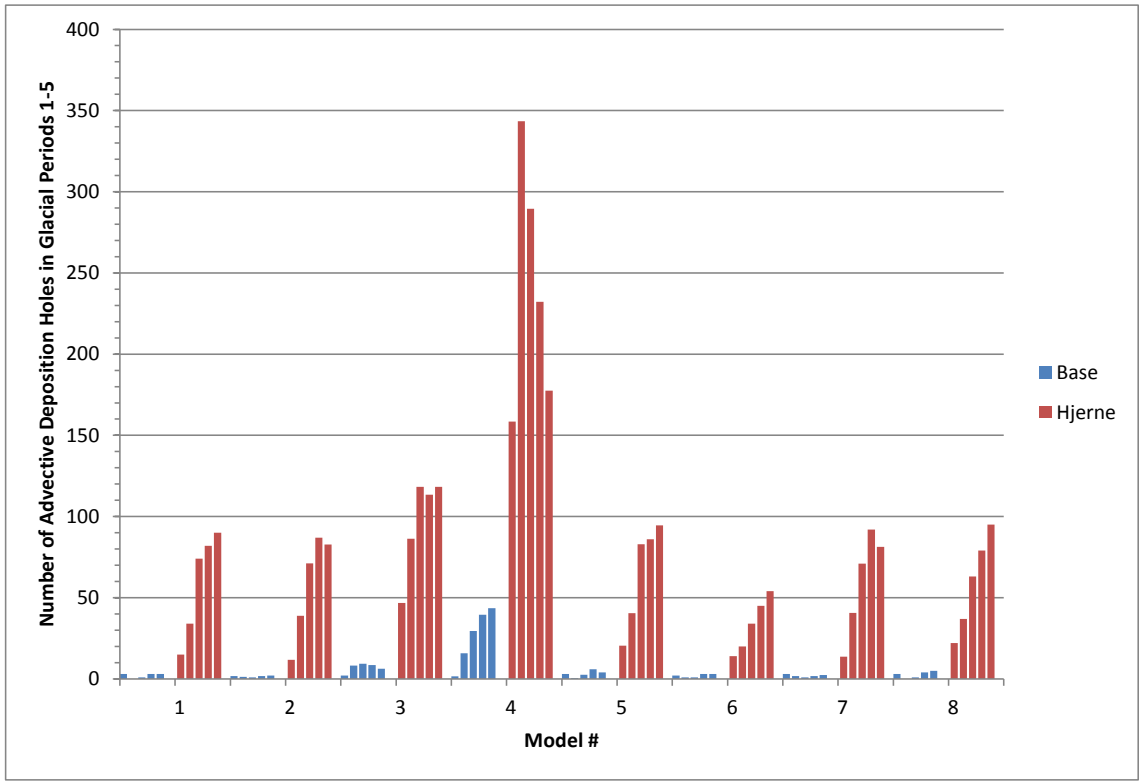

Figure 8: Number of deposition holes experiencing advective conditions for the first time during each glacial cycle for the base and alternative (Hjerne) porosity-transmissivity models assuming $\boldsymbol{M_{adv} = 1,200}$ kg. Summarises data shown in Table 4 – see the introduction to Section 2.7 for a description of the model numbers (x axis label). The groups of five same coloured bars shows the number of deposition holes in the first five glacial periods.

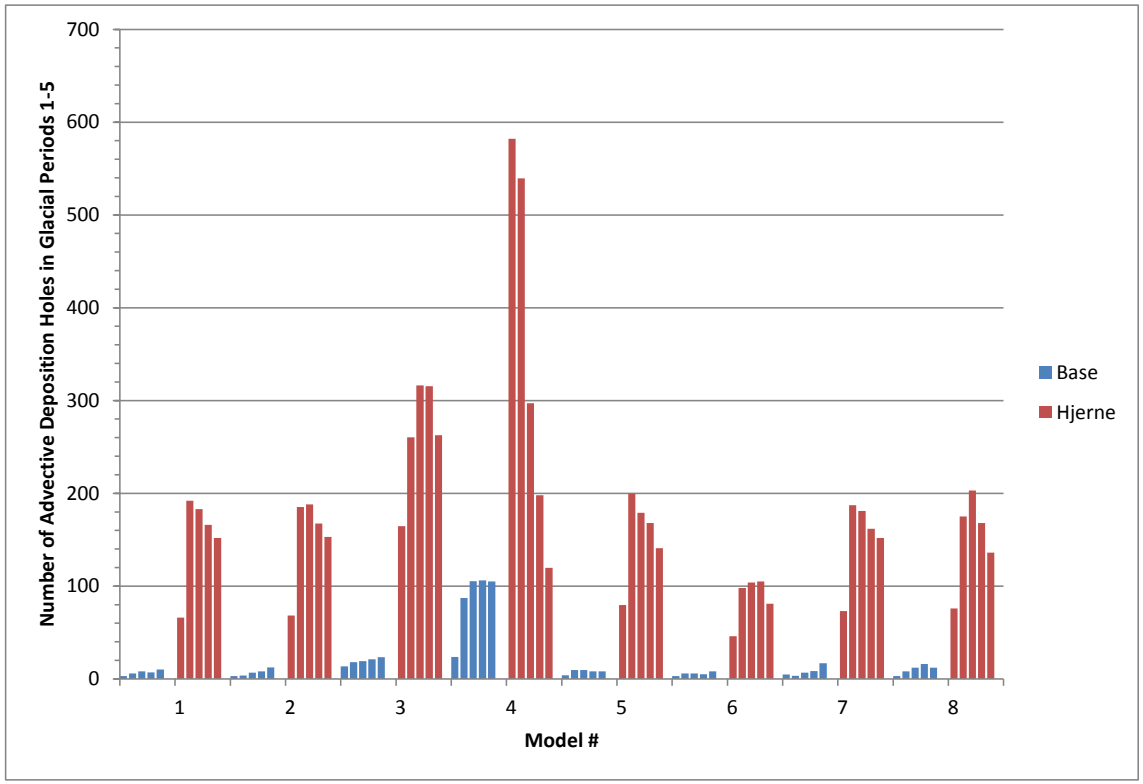

Figure 9: Number of deposition holes experiencing advective conditions for the first time during each glacial cycle for the base and alternative (Hjerne) porosity-transmissivity models assuming $\boldsymbol{M_{adv} = 531}$ kg. Summarises data shown in Table 5 – see the introduction to Section 2.7 for a description of the model numbers (x axis label). The groups of five same coloured bars shows the number of deposition holes in the first five glacial periods.

Table 6: Number of deposition holes experiencing advective conditions for the first time during each glacial cycle for the base and alternative (Hjerne) porosity-transmissivity models assuming $\boldsymbol{M_{adv} = 1,200}$ and $\boldsymbol{M_{adv} = 500}$ kg in the DFN case corresponding to the 25% highest U0 locations in hydrogeological base case.

	Base Aperture-Transmissivity Glaciation number					Hjerne Aperture-Transmissivity Glaciation number				
	1	2	3	4	5	1	2	3	4	5
$M_{adv} = 1{,}200$ kg										
fs_top25_Q1_2000_pline10_merged.xls	30	0	10	70	60	230	420	990	1180	1140
fs_top25_Q1_2000_pline_merged.xls	3	0	1	3	3	15	34	74	82	90
$M_{adv} = 531$ kg										
fs_top25_Q1_2000_pline10_merged.xls	30	130	110	80	130	890	2590	2150	1840	1680
fs_top25_Q1_2000_pline_merged.xls	3	6	8	7	10	66	192	183	166	152

2.8 Summary of Corrosion Model for Advective Conditions in TR-10-66

SKB's corrosion model for advective conditions is summarised in TR-10-66, Section 4.3.2. The rate of corrosion depends upon the equivalent flow rate of corrodants to the canister surface, Q_{eq} (m^3/y) which is given by TR-10-66, eq (4-22/23),

$$Q_{eq} = \begin{cases} q_{eb} & q_{eb} \le q_{\lim}, \\ 1.13 \frac{\sqrt{q_{eb} D_w V_{zone}}}{d_{buf}} & q_{eb} > q_{\lim}. \end{cases} \quad (2\text{-}8)$$

Here, q_{eb} (m^3/y) is the "water flux through the part of the fracture that intersects the deposition hole", D_w (m^2/s) is the diffusion coefficient of the corrodant solute in water, V_{zone} (m^3) is the volume of buffer that has been eroded, d_{buf} (m) is the buffer thickness and the constant 1.13 is more accurately given by $2/\sqrt{\pi}$. The flux $q_{\lim}$ defines a "high flow rate".

No value for $q_{\lim}$ is given in TR-10-66, but the appendix of TR-10-42 provides a derivation based on an analytical solution to an advection-diffusion problem. The geometry assumed in the analysis is shown in Figure 10.

In the setting of Figure 10, $q_{\lim}$ is determined to be the limiting (slow) flow rate into the deposition hole at which the solute is able to diffuse across the eroded buffer to establish a mean concentration of solute in the eroded buffer, c_{mean}, that is equal to the concentration of the solute at the bottom boundary, c_0 (i.e. the concentration is uniform and equal to c_0 across the eroded buffer). Q_{eq} is related to q_{eb} by

$$Q_{eq} c_0 = q_{eb} c_{mean} \quad (2\text{-}9)$$

and, for small residence times t_{res} (y) in the buffer (i.e. for fast flow rates), c_{mean} and c_0 are related approximately as (Bird et al., 2002)

$$\frac{c_{mean}}{c_0} = \frac{2}{\sqrt{\pi}} \frac{\sqrt{D_w t_{res}}}{d_{buffer}}. \quad (2\text{-}10)$$

The approximation becomes invalid for residence times above a sufficiently long residence time $t_{\lim}$, since the physical constraint $c_{mean} \le c_0$ must always be satisfied.

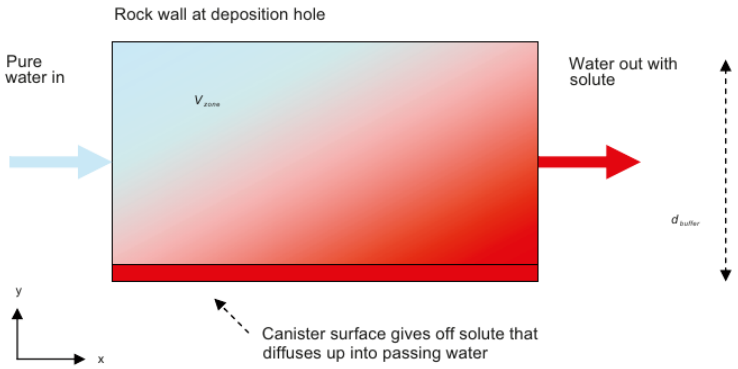

Figure 10: Geometry assumed in the analysis presented in the appendix of TR-10-42 (reproduced from TR-10-42, Fig A1).

[The approximation $t_{res} = V_{zone}/q_{eb}$ is made in the analysis, which assumes that the inflowing water is 'perfectly mixed' around the eroded buffer. This is a valid assumption within the simplified 2-D geometry of Figure 10, but when the aperture of the intersecting fracture is much smaller than the height of the eroded buffer section, h_{zone} (Section 2.6), it would seem possible that $t_{res} < V_{zone}/q_{eb}$ on average for the solute particles, so it is not clear that the approximation is a good one in the 3-D eroded geometry.]

Using the approximation $t_{res} = V_{zone}/q_{eb}$, a limiting water flux corresponding to $t_{\lim}$ can be denoted $q_{\lim}$, for which the approximation (2-10) becomes invalid when $q_{eb} < q_{\lim}$. The value of $q_{\lim}$ can be found, by setting $c_{mean} = c_0$ in (2-10),

$$q_{\lim} = \frac{4}{\pi}\frac{D_w V_{zone}}{d_{buffer}^2}. \qquad (2\text{-}11)$$

Rearranging (2-9) and (2-10) allows the case $q_{eb} > q_{\lim}$ in (2-8) to be obtained. The limit $c_{mean} = c_0$ is equivalent to the condition $Q_{eq} = q_{eb}$ (from (2-9)) and therefore the flux limit $q_{\lim}$ can also be considered to be the flux at which Q_{eq} and q_{eb} become equal. For flows with $q_{eb} \leq q_{\lim}$, it will be the case that $c_{mean} = c_0$, and therefore in this flow regime $Q_{eq} = q_{eb}$ by (2-9).

It is noted that in the context of a corroding solute travelling to the canister surface it is assumed that $c_0 = 0$ (i.e. all sulphide is consumed in corrosion reactions at the canister surface), and therefore the analysis of TR-10-42 would seem to break down since it suggests that there is a limiting flux $q_{\lim}$ (which is greater than zero by (2-11)) at which the mean sulphide concentration across the eroded buffer would be zero, but this can never be the case for a solute that is arriving from the inflowing boundary of Figure 10. Therefore it would seem that the part of this analysis related to $q_{\lim}$ is not necessarily applicable to the corrosion case (and is only relevant for models of solute release form the canister surface). In this case, a conservative assumption would be to assume that $Q_{eq} = q_{eb}$ always, i.e. that the equivalent flux is directly equal to the water flux, meaning that all incoming solute is consumed in the corrosion reaction.

The water flux q_{eb} into the eroded deposition hole is found by scaling the Darcy flux calculated in SKB's DFN models by

$$q_{eb} = f_{conc} 2 r_h h_{can} U0. \quad (2\text{-}12)$$

Here f_{conc} is a flow concentration factor accounting for the focussing of flows into the eroded void. The area scaling $2r_h h_{can}$ was explained in Section 2.2. Given q_{eb}, Q_{eq} can be calculated by (2-8) and then the rate of corrosion v_{corr} (m/y) caused by the mass transport of corrodant is given by TR-10-66, equation (4-25)

$$v_{corr} = Q_{eq}[\mathrm{HS}^-] \frac{f_{HS} M_{Cu}}{\rho_{Cu}} \frac{1}{A_{corr}} \quad (2\text{-}13)$$

where $[\mathrm{HS}^-]$ (mol/m^3) is the concentration of sulphide in the groundwater, $f_{HS} = 2$ is a stoichiometric factor relating the number of moles of copper consumed in the corrosion reaction per mole of sulphide, M_{Cu} (kg/mol) and ρ_{Cu} (kg/m^3) are the molar weight and density of copper respectively, and A_{corr} (m^2) is the area over which corrosion is assumed to occur (i.e. the copper surface area exposed by corrosion).

The only terms in the analysis so far unaccounted for are the geometric factors V_{zone} and A_{corr}, which both depend on the assumptions made regarding the geometry of the eroded volume.

In the absence of a detailed model for the development of the eroded void volume, SKB assume that the by the time that the surface of the canister is exposed, the void has a rectangular cross-section and that only the upstream half of the buffer is eroded. Therefore when the eroded volume reaches the canister surface,

$$V_{zone} = \frac{h_{zone}\, \pi (r_h^2 - r_{can}^2)}{2}, \quad (2\text{-}14)$$

where h_{zone} (m) is the height of the eroded void. SKB assume that the eroded depth is equal to this height, so that $h_{zone} = d_{buf}$, and acknowledge that this assumption is 'a bit crude'.

In SKB (2011), SKB note that equation (2-14) was implemented erroneously in the calculations performed in TR-10-66 and that the trailing divide by 2 was omitted from the calculation, so that

$$V_{zone} = h_{zone}\, \pi (r_h^2 - r_{can}^2)$$

was used. The consequence of the error is that that value of q_{lim} is twice as large as intended, by (2-11), which affects the 'switch' in equation (2-8) that is used to determine Q_{eq}. This results in more locations satisfying $q_{eb} \leq q_{\mathrm{lim}}$ (in which case $Q_{eq} = q_{eb}$ is assumed) and for those locations for which it is still true that $q_{eb} > q_{\mathrm{lim}}$, the resulting value of Q_{eq} is a factor of $\sqrt{2}$ too large.

In both cases a value of Q_{eq} is obtained that is larger than if (2-14) had been implemented correctly, and by (2-13) this results in a larger corrosion rate than intended. The mistake therefore leads to a pessimistic estimate of the corrosion rate compared to the intended calculation.

From (2-13) it is clear that a larger exposed area will lead to smaller depths of corrosion. Following the assumed rectangular eroded volume, SKB assume that the height of the exposed area h_{corr} (m) is equal to h_{zone} ($= d_{buf}$). Given h_{zone}, A_{corr} is given by

$$A_{corr} = \pi r_{can} h_{corr} \quad (2\text{-}15)$$

(since only the upstream half of the deposition hole is assumed to be eroded).

SKB also present a more conservative approach to determine h_{corr} (m), in which it is assumed that prior to the rectangular void cross section (discussed above) develops by growing the void as a semi-circular cross section, until the copper surface is reached. Then erosion is assumed to halt as soon as a band of the canister surface is exposed whose height h_{corr} (m) is given by

$$h_{corr} = \frac{\pi d_{Cu}}{2} \quad (2\text{-}16)$$

where d_{Cu} (m) is the copper thickness. The height is obtained by equating a hypothetical rectangular cross-sectional corrosion area $h_{corr} d_{Cu}$ to a hypothetical semi-circular cross-sectional corrosion area $\pi d_{Cu}^2/2$. The semi-circular corrosion cross-section in the copper that is assumed is almost certainly not realistic (it would imply that rates of corrosion are somehow proportional to the rate at which the canister surface area is exposed by erosion), but is nevertheless clearly a conservative assumption, since it is unlikely that erosion would halt after exposing such a small fraction of the surface area in precisely the way that is assumed. Results presented in Figure 5-9 of TR-10-66 suggest that the assumption of this more pessimistic corrosion geometry increases the mean number of failed canisters in 10^6 year by a factor of ~5 (to 0.557) compared to the semi-correlated base case.

2.9 Independent Corrosion Calculations – Base Case

SKB's corrosion model, described in Section 2.8, has been implemented in an independent spreadsheet model. A set of parameters for the model has been chosen to correspond to the set of parameters chosen by SKB to produce the results in TR-10-66, Table 5-4. The parameter values are listed in Table 7, together with the values of the derived quantities V_{zone}, q_{lim}, and A_{corr}.

Table 7: Parameters in the corrosion calculations.

Parameter	Value	Units	Notes
$\boldsymbol{r_{can}}$	0.525	m	TR-10-66, p11 states 4.835m, but 5m appears to have been used in calculations
$\boldsymbol{d_{buffer}}$	0.35	m	TR-10-66, p49
$\boldsymbol{r_h}$	0.875	m	$(\boldsymbol{r_{can} + d_{buffer}})$
$\boldsymbol{h_{zone}}$	0.35	m	TR-10-66, p49 $(= \boldsymbol{d_{buffer}})$
$\boldsymbol{h_{corr}}$	0.35	m	TR-10-66, p21 (corresponds to rectangular CSA, although alternative assumptions are presented)
$\boldsymbol{D_w}$	$\boldsymbol{10^{-9}}$	m^2/s	TR-10-66, p49
$\boldsymbol{f_{conc}}$	2	-	TR-10-66, p49
$\boldsymbol{f_{HS}}$	2	-	TR-10-66, p49
$\boldsymbol{M_{Cu}}$	63.55	g/mol	TR-10-66, p50
$\boldsymbol{\rho_{Cu}}$	8,920	kg/m^3	TR-10-66, p50
$\boldsymbol{d_{Cu}}$	0.047	m	TR-10-66, p37 (Conservative value: 5cm starting thickness minus initial corrosion)
$[HS^-]$	$\boldsymbol{1.2 \times 10^{-4}}$	mol/kg	TR-10-66, p24 (Maximum assumed value)

Derived quantities

$\boldsymbol{V_{zone}}$	0.269	m^3	Calculated (2-14)
$\boldsymbol{q}_{\text{lim}}$	0.088	m^3/y	Calculated (2-11)
$\boldsymbol{A_{corr}}$	0.577	m^2	Calculated (2-15)

Equivalent flow rates (Q_{eq}) and timescales for corrosion (d_{Cu}/v_{corr}) were calculated for selected deposition holes listed in TR-10-66, Table 5-4 for groundwater sulphide concentrations of $[HS^-] = 1.2 \times 10^{-4}$ mol/kg (the maximum sulphide concentration considered in TR-10-66). These correspond to the two deposition holes with the shortest overall failure time (erosion time + corrosion time), as determined by SKB. Calculations were performed with V_{zone} given by (2-14) and with V_{zone} calculated using the erroneous formula (SKB, 2011) (see the discussion in Section 2.8). The results are shown alongside the corresponding results from TR-10-66 in Table 8.

The independently calculated flow rates are slower than those presented in TR-10-66, leading to longer timescales for corrosion, with a discrepancy of 20-25% in the calculated corrosion times. This is expected, since as noted in Section 2.7, the erroneous form for V_{zone} that was used in TR-10-66 results in faster rates of corrosion. With V_{zone} implemented in the erroneous form in the independent model, the calculated flow rates agree to the 3 s.f. that are given in TR-10-66, and corrosion timescales are within 0.1% of those presented in TR-10-66.

The same calculations were rerun assuming the smaller corrosion area given by (2-16), giving $h_{corr} = 7.38$ cm. The results in this case are shown in Table 9. As

expected the timescales for corrosion are reduced to approximately 21% of the previous value (since 0.0738/0.35=0.21). As noted in Section 2.8, equation (2-16) appears to represent a conservative choice. However it would seem unlikely that the erosion process would lead to a precisely rectangular cross-section and that some 'tapering' towards the canister surface might be expected as the buffer swells to attempt to close the void. If this is the case, then the timescale for erosion may lie between the two computed timescales (for an erosion 'height' at the deposition hole wall of d_{buf}).

Table 8: Independently calculated flow rate ($\boldsymbol{Q_{eq}}$) and corrosion times for selected boreholes in the base case when $[HS^-] = \mathbf{1.2 \times 10^{-4}}$. Rates and timings were calculated for $\boldsymbol{q}_{\text{lim}}$ calculated according to (2-11) and for $\boldsymbol{q}_{\text{lim}}$ set to a large value (so that $\boldsymbol{Q_{eq}} = \boldsymbol{q_{eb}}$ always).

Dep. hole ID in DFN hydro model	SKB (TR-10-66)		Independent Model		Independent Model (with erroneous V_{zone} formula)	
	Flow rate (m^3/y) (Q_{eq})	Corrosion time (y) (d_{Cu}/v_{corr}))	Flow rate (m^3/y) (Q_{eq})	Corrosion time (y) (d_{Cu}/v_{corr}))	Flow rate (m^3/y) (Q_{eq})	Corrosion time (y) (d_{Cu}/v_{corr}))
1978	0.144	109,967	0.113	140,362	0.144	110,025
411	0.161	98,482	0.119	132,830	0.161	98,535

Table 9: Independently calculated flow rate ($\boldsymbol{Q_{eq}}$) and corrosion times for selected boreholes in the base case when $[HS^-] = \mathbf{1.2 \times 10^{-4}}$ when the more conservative corrosion area given by (2-16) is used. Rates and timings were calculated for $\boldsymbol{q}_{\text{lim}}$ calculated according to (2-11) and for $\boldsymbol{q}_{\text{lim}}$ set to a large value (so that $\boldsymbol{Q_{eq} = q_{eb}}$ always).

Dep. hole ID in DFN hydro model	SKB (TR-10-66)		Independent Model with h_{corr} determined by (2-16)		Independent Model with h_{corr} determined by (2-16) (with erroneous V_{zone} formula)	
	Flow rate (m^3/y) (Q_{eq})	Corrosion time (y) (d_{Cu}/v_{corr}))	Flow rate (m^3/y) (Q_{eq})	Corrosion time (y) (d_{Cu}/v_{corr}))	Flow rate (m^3/y) (Q_{eq})	Corrosion time (y) (d_{Cu}/v_{corr}))
1978	Not reported	Not reported	0.113	29,607	0.144	23,208
411	Not reported	Not reported	0.119	28,018	0.161	20,784

The distribution of corrosion rates from the independent model in the case that $[HS^-] = 10^{-5}$ mol/kg (with all other input parameters as in Table 7) is shown in Figure 11. This lower concentration of HS^- is stated in TR-10-66 to be the lower bound of the range of in-situ HS^- concentrations in groundwater at Forsmark. The results appear to agree well with the corresponding data from TR-10-66 Fig 5-6. In this case only one deposition hole has a potential[3] corrosion rate greater than 4.7×10^{-2} μm/y, which is the rate required to achieve complete corrosion of the 47 mm copper thickness in 10^6 y (if the q_{lim} switch is omitted from (2-8) then four deposition holes exceed the rate).

Figure 12 shows the similar plot when $[HS^-] = 1.2 \times 10^{-4}$ mol/kg. In this case 42 deposition holes have potential corrosion rates that exceed 47 mm in 10^6 y, and 3 of these deposition holes have potential rates that exceed 47 mm in 10^5 y. When the q_{lim} switch is omitted from (2-8) these numbers become 42 and 6 respectively.

SKB do not appear to quote the precise numbers of canisters whose potential corrosion rates would exceed the rate needed for complete corrosion of the 47 mm of copper and instead quote the deposition holes whose failure time, when taking in to account both the erosion and corrosion timescales would lead to complete corrosion in less than 10^6 y, so it is not possible to directly compare the above values with those calculated by SKB. Independently calculated timescales for combined erosion and corrosion are presented in Section 2.10 for the suite of realisations of SKB's DFN models that were introduced in Section 2.7.

[3] It is a potential rate, because no account has been taken in this analysis of whether the flow conditions in the deposition hole would give rise to sufficient erosion for advective conditions to be established.

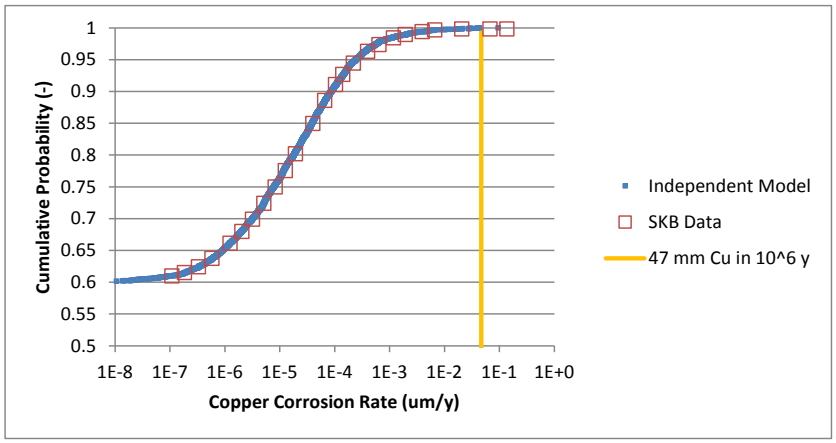

Figure 11: Distribution of corrosion rates in the case that $[HS^-] = \mathbf{10^{-5}}$ mol/kg, with all other parameters as in Table 7. Comparison of SKB data (from TR-10-66, Fig 5-6) and independent model.

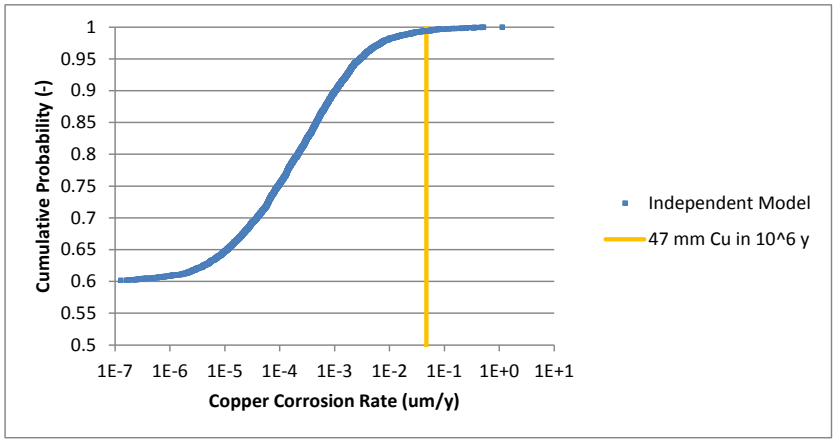

Figure 12: Distribution of corrosion rates in the case that $[HS^-] = \mathbf{1.2 \times 10^{-4}}$ mol/kg, with all other parameters as in Table 7.

The above range of HS^- concentrations is consistent with the range given in SKB report TR-10-39, which describes the variations in sulphide contents of groundwaters from Forsmark. This report states that almost all Forsmark groundwaters have HS^- concentrations of $<1.3 \times 10^{-5}$ mol/kg, but notes that it cannot be ruled out that for some deposition locations, the groundwater may have HS- concentrations as high as 1.2×10^{-4} mol/kg.

In TR-10-39 SKB recognize that at any given location the concentrations of HS^- will vary within groundwaters throughout a glacial cycle, and that consequently the spatial distribution of HS^- concentrations will also vary. However, it is argued that under temperate conditions like those of the present, the supply of reductants to the groundwater system (CH_4, H_2, organic matter) will be near a maximum. Hence, SO_4 reduction in the groundwater system would cause present HS^- concentrations to be at least as high as in any other part of a climatic cycle. These arguments were used to justify the validity of using present concentrations of HS^- conservatively in corrosion calculations. This approach is reasonable. However, TR-10-39 also notes that at depths > 600 m the HS- concentrations systematically increase, which was attributed to a decrease in Fe^{2+} concentrations with depth. At shallower depths, the

Fe^{2+} concentrations were considered high enough to cause precipitation of amorphous Fe(II)-monosulphides, the solubility of which was interpreted to constrain maximum HS^- concentrations. These observations, combined with the relatively few groundwater samples from below the target the repository volume, as noted by Bath (2012), raises the questions as to whether it might be possible for future upwelling of deeper water to lead to more elevated HS^- concentrations at any given locality.

Bath (2012) also pointed out that relatively little is known about the porewater compositions in the rock matrix; analysed groundwater samples are obtained exclusively from flowing fractures. Given that deposition holes will be located at some distance from significant fractures, the water that will eventually resaturate the buffer buffer could originate in fractures with very low transmissivity. Such water could have a composition intermediate between fracture water and pore water. Again, the question arises as to whether the HS^- concentration in the porewater could be higher than in the flowing fracture water in a particular part of the repository volume. Nevertheless, there is no reason to suppose overall that the range of HS^- concentrations in the porewater would differ from the range of HS^- concentrations in the groundwater across the repository volume.

Bath (2012) considered that SKB has not sufficiently justified the discounting of certain high HS^- concentrations. However, this discounting would not seem to result in the maximum copper canister corrosion being underestimated by the corrosion calculations since they use a maximum HS^- concentration of 1.2×10^{-4} mol/kg that is near the maximum of all reported groundwater values (including those believed to have been perturbed by down-borehole processes) (e.g. Figure 4-1 of TR-10-39). Nevertheless, further assessment of these uncertainties to establish their implications for the corrosion calculations, and notably to establish more firmly the degree of conservatism in the model assumptions, would be beneficial. SKB considered that some high HS^- concentrations reflect analytical errors, on the basis that they are supersaturated with respect to FeS. Such supersaturation would imply that measured ferrous Fe and / or sulphide concentrations are anomalously high, because it is considered that FeS would precipitate rapidly in the event that it becomes supersaturated. Following such precipitation Fe^{2+} and HS^- concentrations would be buffered by this phase. However, page 46 of TR-10-39 states that "Actual precipitation of FeS(am) has not been possible to demonstrated".

2.10 Independent Corrosion Calculations – Other SKB DFN Realisations

Rates of corrosion and canister failure times have been computed in all deposition holes for the additional DFN models and realisations discussed in Section 2.7. Again the analysis is performed using a script (described in Appendix C). Failure times are computed by adding the time taken for corrosion in the deposition hole (Section 2.9) to the time for erosion in each deposition hole (as calculated in Section 2.7, which accounts for the fraction of each glacial period for which dilute waters are assumed to penetrate to repository depth). Failure times have been calculated assuming both the base aperture-transmissivity relationship and assuming the Hjerne model.

The corrosion results presented in this section use the correct form for the V_{zone} term (equation 2-14) which, as was discussed in Section 2.9, results in more conservative

estimates of the rate of corrosion compared to the erroneous form that was used in SKB's calculations in TR-10-66.

The results of the calculation applied to the base case are shown in Table 10 and Table 11 for the base and Hjerne aperture-transmissivity models respectively. The tables list those deposition holes for which the combined erosion and corrosion timescales are less than 10^6 y and can be compared with Table 5-4 of TR-10-66. For the base model, the same deposition holes as those listed in Table 5-4 of TR-10-66 are identified. The results are the same as those shown in Table 8 in Section 2.9 when Q_{eq} is given by (2-8) and q_{lim} is given by (2-11).

When the Hjerne aperture-transmissivity model is used, one additional deposition hole (#2395) is found to fail in less than 10^6 y. Figure 13 shows the importance of the EFPC rejection criteria in reducing the number of canisters that could potentially erode and corrode in less than 10^6 y. In the top graph, which shows the time for erosion plotted against the time for corrosion for all canister positions regardless of EFPC rejection, 46 positions are found to lie within the contour delimiting failure within 10^6 y, whereas when the EFPC is applied, only the 5 positions listed in Table 11 fall inside the 10^6 y timescale.

Table 10: **Erosion, corrosion and failure times for deposition holes with failure times < 10^6 y for the base case DFN model with base aperture-transmissivity model. (c.f.** Table 11 **which shows the analogous results for the Hjerne aperture-transmissivity model.)**

DFN hole ID	Qeq (m^3/y)	$q_{eq} > q_{lim}$	Erosion time (y)	Sulphide conc. (mol/kg)	Corrosion time (y)	Failure time (y)
1978	0.113	Y	90,745	0.00012	140,371	231,116
411	0.119	Y	119,686	0.00012	132,845	252,532
6875	0.084	N	110,653	0.00012	188,508	299,161
401	0.026	N	278,942	0.00012	608,540	887,482

Table 11: **Erosion, corrosion and failure times for deposition holes with failure times < 10^6 y for the base case DFN model with Hjerne aperture-transmissivity model. (c.f.** Table 10 **which shows the analogous results for the base aperture-transmissivity model.)**

DFN hole ID	Qeq (m^3/y)	$q_{eq} > q_{lim}$	Erosion time (y)	Sulphide conc. (mol/kg)	Corrosion time (y)	Failure time (y)
411	0.119	Y	24,233	0.00012	132,845	157,079
1978	0.113	Y	20,899	0.00012	140,371	161,270
6875	0.084	N	25,713	0.00012	188,508	214,221
401	0.026	N	54,270	0.00012	608,540	662,809
2395	0.017	N	79,034	0.00012	912,197	991,231

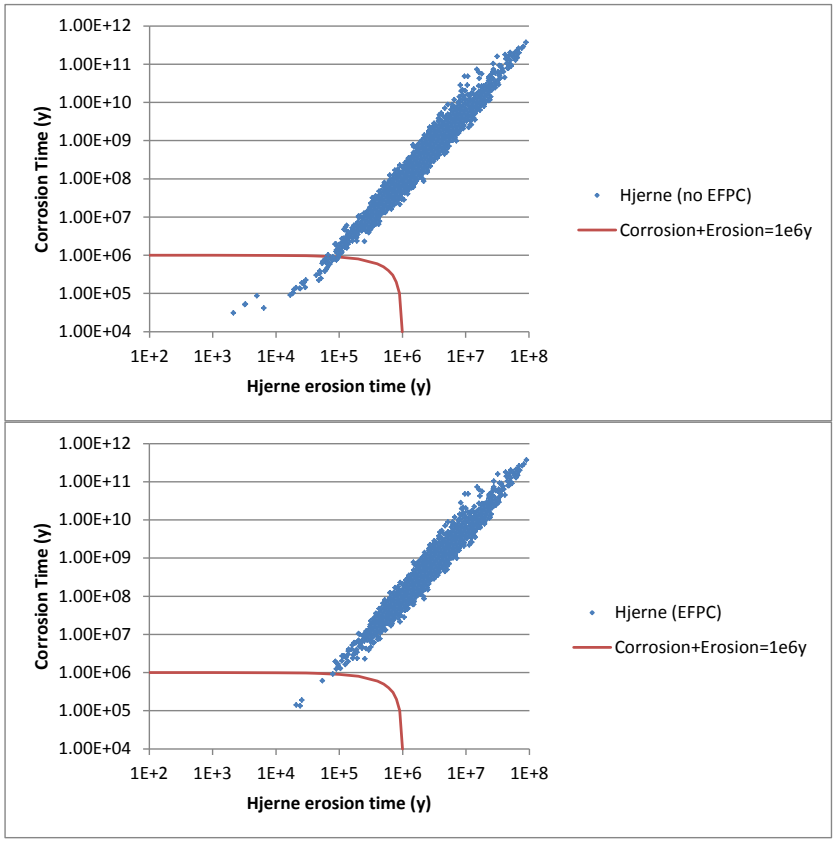

Figure 13: Time taken for erosion of 1,200 kg of buffer (accounting for glacial dilute water fraction) calculated using the Hjerne aperture-transmissivity model vs. time required for corrosion when $[HS^-] = \mathbf{1.2 \times 10^{-4}}$ mol/kg for the base case DFN model. Top: no borehole rejection due to EFPC; Bottom: with borehole rejection for EFPC. The solid line shows the contour where the combined erosion and corrosion time is equal to 10^6 y.

The number of failed locations in all the available realisations of the SKB DFN is shown in Table 12 for the case when HS^- concentrations are assumed to be 1.2×10^{-4} mol/kg in the fracture porewater in all deposition holes. Results are presented for both the base and Hjerne aperture-transmissivity models. The Hjerne model leads to roughly 50% more failed locations in most of the cases that are considered.

Appendix E presents an independent attempt to reproduce results of numbers of failed locations in SKB's probabilistic analysis that are presented in TR-10-50 Table 4-3.

SKB perform a similar analysis (for the base aperture-transmissivity model) but assume that the sulphide concentration at each location is randomly distributed. The corresponding CDF is shown in TR-10-66, Figure 4-4. They therefore arrive at much lower mean numbers of failed locations than calculated here, due to the 'requirement' that sulphide must be present at the maximal concentration in order for any locations to fully corrode within 10^6 y. SKB's results are shown in TR-10-66, Figures 5-7 and 5-8 (which includes one set of results assuming the Hjerne model; referred to as the 'pessimistic fracture aperture' case).

Although the independently calculated numbers of failed locations is greater than that calculated by SKB, the ratio of failed locations in the correlated and uncorrelated DFN models to the base case is approximately the same in both analyses, which suggests that the models are consistent. The correlated and uncorrelated DFN models lead to around 6 or 7 times as many failed locations as the semi-correlated base case.

Whilst it is improbable that all deposition holes will experience sulphide concentrations at the maximal value, the results in Table 12 usefully illustrate the dependence of SKB's results upon the sulphide concentration probability distribution that is assumed.

Microbial activity is a potentially significant process that might affect aqueous HS^- concentrations and hence Cu corrosion rates. TR-10-39 reports that SO_4-reducing bacteria have been found in deep groundwaters from Forsmark, Laxemar and Äspö (quoting SKB reports R-08-85, R-08-109 and P-10-18; Rosdahl et al. 2010). However, it is also noted that SO_4 contents of groundwaters are much higher (generally more than an order of magnitude higher) than the HS^- contents. Therefore it is unlikely that variations in SO_4 concentrations due to reduction could be distinguished from variations due to other processes, principally mixing between groundwater components with difference SO_2 contents. Nevertheless, TR-10-39 presents stable S-isotopic evidence for microbially mediated SO_4 reduction; $\delta^{34}S$ values exceed the marine values of +21‰ CDT.

The most significant reactions would be microbially mediated reduction of SO_4 in the groundwater, thereby increasing the concentration of HS^-. This process requires the presence of a reductant, the main candidates being:

- H_2 produced by corrosion of Cu.
- Dissolved Organic Carbon (DOC);
- CH_4 of deep origin.

As pointed out in TR-10-39, copper corrosion can be described by the reaction:

$$2Cu(s) + HS^- + H^+ \leftrightarrow Cu_2S(s) + H_2(aq)$$

However, in the presence of sulphate-reducing bacteria (SRB), the hydrogen produced could reduce SO_4 in the porewater to produce additional sulphide, giving the overall reaction:

$2Cu(s) + 0.25\ SO_4^{2-} + 0.75\ HS^- + 1.25\ H^+ \rightarrow Cu_2S(s) + H_2O(l)$

This reaction is not taken into account in equation 2-13, which uses only the reported HS^- concentration in the water. An implication is that, at least in this sense, the corrosion treatment is not conservative. However, this reaction would only occur at the canister surface following erosion of the buffer, since prior to this time significant microbial activity is not expected to occur. Furthermore, even if all produced H_2 were to participate in SO_4^{2-} reduction and all the resulting HS^- were to react with the copper, there would only be a 25% increase in the amount of corrosion. Although it is unclear what proportion of the H_2 produced by corrosion would in fact be used by SRB to produce HS^- and hence enhance corrosion in comparison to that expected in the absence of H_2, it does seem likely that the overall impact would be small.

The reliability of SKB's results will depend greatly on whether the sulphide concentration CDF (TR-10-66, Figure 4-4) genuinely represents the distribution of groundwaters at Forsmark. Both analyses ignore any possible time-dependence in the porewater composition at each location, except insofar as the fraction of the time during which dilute waters are assumed to be present at repository depths is taken into account.

Table 12: Number of failed locations (eroded+corroded) in the first 10^6 y assuming $\boldsymbol{M_{adv}} = \mathbf{1,200}$ kg and $[HS^-] = \mathbf{1.2 \times 10^{-4}}$ for all realisations of the SKB DFN.

	Number of failed locations (eroded+corroded) in <1e6 y	
	Base	Hjerne
#1 Base case (two identical cases, one with extra TRAPP output)		
fs_Q1_2000_pline_merged.xls	4	5
#2 Ten alternative realisations of the base case		
fs_r1_Q1_2000_pline_merged.xls	4	5
fs_r3_Q1_2000_pline_merged.xls	5	6
fs_r4_Q1_2000_pline_merged.xls	1	3
fs_r5_Q1_2000_pline_merged.xls	1	1
fs_r6_Q1_2000_pline_merged.xls	2	3
fs_r7_Q1_2000_pline_merged.xls	7	11
fs_r8_Q1_2000_pline_merged.xls	3	3
fs_r9_Q1_2000_pline_merged.xls	5	10
fs_r10_Q1_2000_pline_merged.xls	1	4
fs_r12_Q1_2000_pline_merged.xls	6	9
Average	3.5	5.5
#3 Four realisations of the correlated size-transmissivity case		
fs_corr_Q1_2000_pline_merged.xls	14	20
fs_r2_corr_Q1_2000_pline_merged.xls	10	14
fs_r4_corr_Q1_2000_pline_merged.xls	42	58
fs_r5_corr_Q1_2000_pline_merged.xls	19	30
Average	21.25	30.25
#4 Four realisations of the truncated, uncorrelated size-transmissivity case		
fs_uncorr_truncHCD_Q1_2000_pline_merged.xls	29	48
fs_r2_uncorr_truncHCD_Q1_2000_pline_merged.xls	22	40
fs_r3_uncorr_truncHCD_Q1_2000_pline_merged.xls	28	40
fs_r5_uncorr_truncHCD_Q1_2000_pline_merged.xls	23	39
Average	25.5	41.75
#5 Two realisations with different EDZ transmissivities		
fs_maxedz_6_Q1_2000_pline_merged.xls	9	15
fs_maxedz_7_Q1_2000_pline_merged.xls	4	6
Average	6.5	10.5
#7 Three realisations with possible deformation zones included		
fs_pdzr1_Q1_2000_pline_merged.xls	4	5
fs_pdzr2_Q1_2000_pline_merged.xls	7	9
fs_pdzr3_Q1_2000_pline_merged.xls	5	6
Average	5.33	6.67

	Number of failed locations (eroded+corroded) in <1e6 y	
	Base	Hjerne
#6 No EDZ case		
fs_noedz_Q1_2000_pline_merged.xls	4	4
#8 Tunnel variant with crown space		
fs_crown_Q1_2000_pline_merged.xls	4	9

3 Independent DFN Calculations

3.1 Onset of Advective Conditions from Multiple Realisations for the Base Fracture Size Distribution Models

Calculations have been performed to determine the time of onset of advective conditions for multiple realisations of an independent DFN model constructed along similar lines to SKB's hydro DFN CONNECTFLOW models. The modelling is summarised in Geier (2015) and tends to predict slightly faster velocities than SKB's CONNECTFLOW models due to the adoption of more conservative assumptions. A collection of 16 Excel files[4] have been provided; each file containing the results of calculations from 10 DFN realisations in separate worksheets. Each of the 16 files has different assumptions for:

- Fracture size – transmissivity relationship: correlated, uncorrelated, semi-correlated;
- Fracture aperture – transmissivity relationship: base case, cubic, Hjerne, or stochastic
- Fracture frequency option: length or area;
- Random seed: 1 or 2.

The DFN model uses the same assumptions SKB's base Geo-DFN model. Results from independent DFN simulations using the alternative OSM-TFM and TCM fracture size distribution models (see TR-08-05) are discussed in Section 3.2. The fracture size – transmissivity models that are assumed are the same as those considered by SKB (Section 2.7). The base case and Hjerne fracture aperture – transmissivity models are the same as those described in Section 2 (given by equations 2-5 and 2-6 respectively). The cubic fracture aperture – transmissivity model assumes

$$\delta = \sqrt[3]{\frac{12\mu_w}{\rho_w g}} T^{1/3},$$

and the stochastic model assumes

$$\delta = 0.5 T^{0.5} 10^{0.5N(0,1)}.$$

[4] The list of files is provided in Appendix B

Here δ (m) is the fracture aperture, T (m^2/s) is the fracture transmissivity, μ_w (Pa s) and ρ_w (kg/m^3) are the dynamic viscosity and density of water, g (m/s^2) is the acceleration due to gravity and $N(0,1)$ is the standard normal distribution (so that the stochastic model is equal to the base case model with a half order of magnitude standard deviation).

The output data in the Excel files has been produced with the program 'parameter_estimation.awk v. 2014-08-29' (Geier, 2015) and is formatted differently to SKB's spreadsheets that were described in sections (2.2-2.6). The key data fields in the file for the purposes of the erosion analysis are:

- Tun / Pos – the tunnel / position of the deposition hole;
- u_0 (m/y) – the groundwater velocity in the fracture intersecting the deposition hole (in contrast to the earlier sections (2.2-2.6), where U_0 was the equivalent flux);
- b (m) – the fracture aperture (m).

Data is only provided in each worksheet for a subset of the deposition holes, with different numbers of deposition holes included in the data for each realisation (presumably corresponding to deposition holes that are intersected by fractures). Equation (2-1) can be used directly with the u_0 and b data to obtain the erosion rate in each deposition hole and the number of glacial cycles that are required before advective conditions can be established. As in Section 2.6, the calculations assume a glacial period of length 120,000 y, with dilute water assumed to be flowing at repository depths for 25% of the glacial cycle period, consistent with the assumptions made in TR-10-66 (p37). The mass of buffer M_{adv} that must be lost before advective conditions occur is set to 1,200 kg (although as noted in Section 2.6, a lower bound figure of $M_{adv} = 531$ kg could be assumed).

Since there are 160 individual sets of results, the analysis is performed using a script (described in Appendix C) rather than implementing the calculations in a spreadsheet.

The results are summarised in Table 13, Table 14 and Table 15, which describe the parameterisation used in the individual flow models and show the average, minimum and maximum number of deposition holes respectively in which advective conditions are established in each glacial period, over the 10 realisations per set of assumptions.

It is clear that the Hjerne aperture-transmissivity assumption (2-6) leads to significantly more deposition holes in which advective conditions are established, with up to 137 deposition holes eroded during the first glacial period when the fracture frequency is parameterised by area in the semi-correlated case and up to 423 deposition holes affected in the similar uncorrelated case.

In general it seems that parameterising the fracture frequency by area leads to around an order of magnitude more affected holes per glaciation than when it is parameterised by length.

The erosion results from the independent and SKB DFN models for the base case and Hjerne aperture-transmissivity models are compared in Table 16 (by combining analogous results from Table 13 and Table 4). With the exception of the uncorrelated Hjerne model, the results from all of the cases are broadly comparable for the first glaciation, typically differing by only one or two eroded deposition

holes. Over the first five glaciations the SKB DFN leads to significantly more eroded locations overall, except for the semi-correlated base case aperture-transmissivity model (the SKB base case) where the independent model predicts two more eroded locations.

The correlated DFN with the base case aperture-transmissivity relationship is an exception to the above. The independent DFN version predicts no eroded deposition holes in the first five glaciations (thirteen glaciations are required before the first eroded location is seen) whereas the SKB model predicts 34.25 eroded locations over the same period. The independent results look unrealistic for this case, and are understood to be due to the rigid coupling between the sizes of successive fractures in the series model (Geier, 2015), which causes sequential long and then short fractures to have an overall small transmissivity.

Table 13: Average number of deposition holes experiencing advective conditions for the first time during each glacial cycle, averaged over 10 realisations. Cases that give rise to more advective depositions holes after one glaciation than SKB's semi-correlated base case (which gives rise to 3 cases – Section 2.6) are shown in bold.

Size relationship	Aperture relationship	Scaling	Seed	Glacial cycle				
				1	2	3	4	5
Correlated	Base case	Length	1	0	0	0	0	0
Correlated	Base case	Area	1	0	0	0	0	0
Semi-Correlated	Base case	Length	1	0.5	2.1	2.4	1.7	2.8
Semi-Correlated	Base case	Area	1	4.1	14.9	19.4	22.8	23.8
Semi-Correlated	Base case	Length	2	0.5	1.5	2.1	1.9	2.9
Semi-Correlated	Base case	Area	2	8.1	15.6	21.5	22.7	27.7
Semi-Correlated	Cubic	Length	1	0.3	0.3	1.5	1.6	1.6
Semi-Correlated	Cubic	Area	1	1.1	4.8	9.3	12.3	14.4
Semi-Correlated	Hjerne	Length	1	14.3	21.4	21.6	23.7	16.7
Semi-Correlated	Hjerne	Area	1	120.7	217	224.1	193.3	177.5
Semi-Correlated	Stochastic	Length	1	0.1	1	0.8	1	1.1
Semi-Correlated	Stochastic	Area	1	10.6	23	25.8	28.4	31.9
Uncorrelated	Base case	Length	1	3.6	5.8	6.8	7.6	5.9
Uncorrelated	Base case	Area	1	28.1	59.5	64	65.5	71.7
Uncorrelated	Hjerne	Length	1	39.7	49.7	35.6	27.2	21.5
Uncorrelated	Hjerne	Area	1	379.3	441.5	337.1	227	170

Table 14: Minimum number of deposition holes experiencing advective conditions for the first time during each glacial cycle, from 10 realisations.

Size relationship	Aperture relationship	Scaling	Seed	Glacial cycle				
				1	2	3	4	5
Correlated	Base case	Length	1	0	0	0	0	0
Correlated	Base case	Area	1	0	0	0	0	0
Semi-Correlated	Base case	Length	1	0	1	1	0	1
Semi-Correlated	Base case	Area	1	1	9	9	17	18
Semi-Correlated	Base case	Length	2	0	0	0	0	1
Semi-Correlated	Base case	Area	2	5	6	16	17	17
Semi-Correlated	Cubic	Length	1	0	0	0	0	0
Semi-Correlated	Cubic	Area	1	0	3	4	9	8
Semi-Correlated	Hjerne	Length	1	9	16	13	18	10
Semi-Correlated	Hjerne	Area	1	104	191	202	182	148
Semi-Correlated	Stochastic	Length	1	0	0	0	0	0
Semi-Correlated	Stochastic	Area	1	6	18	19	20	21
Uncorrelated	Base case	Length	1	1	2	3	3	3
Uncorrelated	Base case	Area	1	22	50	53	50	59
Uncorrelated	Hjerne	Length	1	34	45	26	19	18
Uncorrelated	Hjerne	Area	1	341	408	307	200	155

Table 15: Maximum number of deposition holes experiencing advective conditions for the first time during each glacial cycle, from 10 realisations.

Size relationship	Aperture relationship	Scaling	Seed	Glacial cycle				
				1	2	3	4	5
Correlated	Base case	Length	1	0	0	0	0	0
Correlated	Base case	Area	1	0	0	0	0	0
Semi-Correlated	Base case	Length	1	1	4	4	3	5
Semi-Correlated	Base case	Area	1	7	20	25	30	30
Semi-Correlated	Base case	Length	2	2	3	3	4	5
Semi-Correlated	Base case	Area	2	12	21	26	29	36
Semi-Correlated	Cubic	Length	1	1	2	3	3	3
Semi-Correlated	Cubic	Area	1	3	6	15	18	20
Semi-Correlated	Hjerne	Length	1	18	25	29	30	25
Semi-Correlated	Hjerne	Area	1	137	240	238	206	194
Semi-Correlated	Stochastic	Length	1	1	2	2	3	3
Semi-Correlated	Stochastic	Area	1	14	27	30	35	39
Uncorrelated	Base case	Length	1	8	10	12	11	8
Uncorrelated	Base case	Area	1	34	70	72	78	91
Uncorrelated	Hjerne	Length	1	45	55	50	42	27
Uncorrelated	Hjerne	Area	1	423	470	361	248	180

Table 16: Comparison of number of locations expected to experience advective conditions for the first time in each of the first five glaciations from the independent and SKB DFN models. (i.e. comparison of results in Table 13 and Table 4).

Size relationship	Aperture relationship	Scaling	Indep / SKB	Glacial cycle					
				1	2	3	4	5	Total
Correlated	Base case	Length	Indep.	0	0	0	0	0	0
			SKB	2	8.25	9.25	8.5	6.25	34.25
Semi-Correlated	Base case	Length	Indep.	0.5	2.1	2.4	1.7	2.8	9.5
			SKB	1.7	1.2	0.9	1.8	2	7.6
Semi-Correlated	Hjerne	Length	Indep.	14.3	21.4	21.6	23.7	16.7	97.7
			SKB	11.7	38.8	71.2	87	82.8	291.5
Uncorrelated	Base case	Length	Indep.	3.6	5.8	6.8	7.6	5.9	29.7
			SKB	1.5	15.75	29.5	39.5	43.5	129.75
Uncorrelated	Hjerne	Length	Indep.	39.7	49.7	35.6	27.2	21.5	173.7
			SKB	158.5	343.5	289.5	232.25	177.5	1201.25

3.2 Onset of Advective Conditions for Alternative Fracture Size Distribution Models

An additional set of erosion calculations has been performed using a second set of independent DFN calculations (Geier, 2015), which are based on SKB's alternative fracture size distribution models: the Tectonic Continuum Model (TCM) and the Outcrop Scale Model with Tectonic Fault Model (OSM-TFM). The background to these is described in SKB TR-08-05, p162-165. The data from the DFN simulations is provided in 8 Excel files[5]; each file containing the results of calculations from 10 DFN realisations in separate worksheets. Each of the 8 files has different assumptions for:

- Fracture distribution model: OSM-TFM or TCM;
- Fracture size - transmissivity relationship: uncorrelated or semi-correlated;
- Fracture aperture - transmissivity relationship: Äspö or Hjerne; and
- Fracture frequency option: length or area.

The erosion analysis for these cases was performed using the script described in Appendix C. The results are summarised in Table 17, Table 18 and Table 19, which show the average, minimum and maximum number of deposition holes respectively in which advective conditions are established in each glacial period, over the 10 realisations per set of assumptions. No corresponding SKB files are available for comparison.

Since the Hjerne aperture-transmissivity model is only considered together with the uncorrelated size-transmissivity relationship and the base case model is only considered together with the semi-correlated size-transmissivity relationship no direct comparison regarding the effect of the aperture-transmissivity model can be drawn from this set of simulations.

Comparing the results for the OSM-TFM and TCM fracture distribution models, for all combinations of parameters the OSM-TFM model leads to more deposition holes with advective conditions established earlier, except for the combination of the uncorrelated Hjerne model with fracture frequency parameterised by area, when the TCM model leads to earlier onset of advective conditions. The results agree with the general result from Section 3.1 that parameterising the fracture frequency by area tends to lead to around an order of magnitude more affected holes per glaciation than when it is parameterised by length.

The results are shown against those for the base fracture distribution model (which was considered in Section 3.1) in Table 20, where the average number of deposition holes experiencing advective conditions after the first glacial cycle is compared. The base, OSM-TFM and TCM fracture distribution models each lead to the maximum number of deposition holes for different combinations of the model parameters. Therefore it is not possible to state that one model leads to worse predicted performance than another. The largest difference between the predicted number of deposition holes is for the uncorrelated Hjerne model with fracture frequency parameterised by area, where the OSM-TFM and TCM models lead to

[5] The list of files is provided in Appendix B

significantly more advective deposition holes (around twice as many) but for the other parameter choices the relative differences between the models is smaller.

Table 17: Average number of deposition holes experiencing advective conditions for the first time during each glacial cycle, averaged over 10 realisations, for the alternative fracture distribution models. Cases that give rise to more advective depositions holes after one glaciation than SKB's semi-correlated base case (which gives rise to 3 eroded locations – Section 2.6) are shown in bold.

Fracture distr. model	Size relationship	Aperture relationship	Scaling	Glacial cycle				
				1	2	3	4	5
OSM-TFM	Semi-Correlated	Base case	Length	1.5	1.3	1.6	2.8	3
OSM-TFM	Semi-Correlated	Base case	Area	12.2	25.9	30.9	44.5	49
OSM-TFM	Uncorrelated	Hjerne	Length	44.3	50.5	33.8	23.5	15
OSM-TFM	Uncorrelated	Hjerne	Area	744.5	814.2	575	409.1	306
TCM	Semi-Correlated	Base case	Length	0.4	1.1	0.6	1.2	1.1
TCM	Semi-Correlated	Base case	Area	9.7	23.6	31	43.8	46.3
TCM	Uncorrelated	Hjerne	Length	35.3	46	37.2	27.4	15.7
TCM	Uncorrelated	Hjerne	Area	914.3	1056.2	767.3	563.6	398.8

Table 18: Minimum number of deposition holes experiencing advective conditions for the first time during each glacial cycle, from 10 realisations, for the alternative fracture distribution models.

Fracture distr. model	Size relationship	Aperture relationship	Scaling	Glacial cycle				
				1	2	3	4	5
OSM-TFM	Semi-Correlated	Base case	Length	1	0	0	0	1
OSM-TFM	Semi-Correlated	Base case	Area	9	14	24	38	34
OSM-TFM	Uncorrelated	Hjerne	Length	40	46	26	17	7
OSM-TFM	Uncorrelated	Hjerne	Area	703	772	558	379	264
TCM	Semi-Correlated	Base case	Length	0	0	0	0	0
TCM	Semi-Correlated	Base case	Area	4	13	22	31	38
TCM	Uncorrelated	Hjerne	Length	27	36	27	23	11
TCM	Uncorrelated	Hjerne	Area	874	986	723	537	379

Table 19: Maximum number of deposition holes experiencing advective conditions for the first time during each glacial cycle, from 10 realisations, for the alternative fracture distribution models.

Fracture distr. model	Size relationship	Aperture relationship	Scaling	Glacial cycle				
				1	2	3	4	5
OSM-TFM	Semi-Correlated	Base case	Length	3	3	3	6	5
OSM-TFM	Semi-Correlated	Base case	Area	17	40	39	49	72
OSM-TFM	Uncorrelated	Hjerne	Length	47	54	43	34	24
OSM-TFM	Uncorrelated	Hjerne	Area	822	848	595	441	354
TCM	Semi-Correlated	Base case	Length	2	3	2	3	4
TCM	Semi-Correlated	Base case	Area	13	30	46	52	60
TCM	Uncorrelated	Hjerne	Length	40	55	48	35	20
TCM	Uncorrelated	Hjerne	Area	955	1106	830	604	426

Table 20: Average number of deposition holes experiencing advective conditions for the first time during the first glacial cycle, averaged over 10 realisations, for the base and alternative fracture distribution models. Maximum values in each case are shown in bold.

Size relationship	Aperture relationship	Scaling	Fracture distribution model			
			Base (seed=1)	Base (seed=2)	OSM-TFM	TCM
Semi-Correlated	Base case	Length	1	2	1.5	0.4
Semi-Correlated	Base case	Area	7	12	12.2	9.7
Uncorrelated	Hjerne	Length	45	-	44.3	35.3
Uncorrelated	Hjerne	Area	423	-	744.5	914.3

4 Summary

SKB's report TR-10-66 describes the erosion and corrosion models that form the basis for SKB's corrosion failure analysis in SR-Site. The erosion and corrosion models have been independently reviewed and supporting reports have been consulted in order to develop an understanding of their derivation and implementation in the SR-Site analysis.

The key parameters determining the rate of erosion in the empirical model that is used by SKB (represented by equation 2-1) are the fracture aperture and porewater velocity in the fracture. These quantities are outputs from SKB's DFN model. The fracture aperture is determined by the relationship that is assumed to equate the fracture transmissivity (an input to the DFN model) to the aperture. Having determined the aperture, the fracture porewater velocities can be calculated from the equivalent flux terms calculated by the DFN model. Thus the data forming the input to the erosion calculations is determined by a sequence of models and modelling assumptions, and confidence must be gained in each of these, and an understanding of the related uncertainties must be obtained, in order to have confidence in the final result.

SSM has undertaken extensive review and independent modelling of SKB's hydrogeological DFN modelling (e.g. Geier 2015,2014, 2010), and a large collection of outputs of these models, based on a wide range of modelling assumptions, was made available for use in the independent erosion calculations that were developed.

SKB's erosion and corrosion analysis includes a consideration of the uncertainties in the DFN model relating to the effect of the fracture size – transmissivity relationship and also considered the presence of other hydrogeological features (such as EDZ and crown space) in the model. The results of these DFN models were used in independent erosion calculations (Sections 2.3, 2.6 and 2.7) and good agreement was found with SKB's corresponding results.

SKB's erosion analysis in TR-10-66 focussed primarily on the base aperture-transmissivity relationship, with most sensitivity cases assuming this model. An alternative relationship was proposed by Hjerne et al. (R-09-28) and additional aperture – transmissivity models (cubic and stochastic models) are considered in the independent DFN modelling (Geier, 2015). The effect of each of these alternatives has been tested in the independent modelling (Sections 2.5, 2.6, 2.7, 3.1 and 3.2). Results from one set of calculations to determine the mean number of failed canisters in 10^6 y in which the Hjerne model was used (referred to by SKB as the 'pessimistic fracture aperture scenario') are presented in TR-10-66, Figure 5-8.

A general conclusion of the modelling is that the Hjerne model leads to larger rates of erosion. This is a consequence of the larger fracture aperture that is obtained when the Hjerne model is compared to the base model for a fracture with a given transmissivity. The Hjerne model results in slower fracture porewater velocities, but the linear dependence on fracture aperture in equation (2-1) and the nonlinear dependence on velocity means that the aperture term dominates at the relevant scales. For the SKB semi-correlated base case DFN model the net erosion rates are around an order of magnitude greater when the Hjerne model is assumed.

The increased rates of erosion result in greater numbers of deposition holes that experience advective conditions (Section 2.5), with the semi-correlated base case DFN seeing 15 advective locations during the first glacial period when the Hjerne

model is used (compared to 3 when the 'base' model is assumed) and 294 in total during the first five glaciations (compared to 10 when the 'base' model is assumed). Similar effects were seen for all of the SKB DFN cases (Section 2.7) and the independent DFN models (Sections 3.1 and 3.2).

The independent DFN model was found to lead to similar numbers of eroded locations when configured similarly to the SKB semi-correlated base case, which lends confidence to SKB's base case results. SKB's uncorrelated DFN model leads to greater numbers of eroded locations than the independent DFN (approximately four times as many during the first five glacial cycles) and when the SKB results are modified for the Hjerne aperture – transmissivity relationship the SKB models result in greater numbers of eroded locations (between three and six times for the cases considered). The independent correlated DFN model leads to no eroded locations until the thirteenth glacial cycle, which appears questionable.

The cubic and stochastic aperture-transmissivity models that were also considered in the independent DFN modelling were seen to have less of an effect when calculating rates of erosion, giving rise to similar number of eroded locations as the base aperture-transmissivity model. However the scaling of the fracture frequency by fracture area in the independent modelling was found to significantly increase the number of eroded locations in all cases.

The background to SKB's general corrosion model under advective conditions (equation 2-13) was considered in Section 2.8. The model is based upon an analytical solution to an advection-diffusion problem, which SKB apply to both the transport of corrodants to the canister surface and also the release of radionuclides from the canister. The key controlling parameters in the model are the equivalent flow rate of corrodants, the area over which corrosion is assumed to occur and the sulphide concentration in the groundwater.

The equivalent flow rate of corrodants in the model is related to the volumetric water flux in the fracture (equation 2-8). In particular, this equation includes a 'switch' at a limiting flow rate (q_{lim}) to describe the relative reduction in corrodant transport to the canister surface at higher fracture flow rates. No information is given in TR-10-66 regarding the value of the limiting flow rate, although its derivation can be found in the appendix of TR-10-42, which analyses the problem from the perspective of radionuclide release. The analysis regarding the value of q_{lim} appears to be possibly not appropriate for the case of corrodant transport when the assumption that corrodants are immediately consumed in corrosion reactions is made (so that their concentration is zero on the canister surface).

SKB's corrosion calculations for the semi-correlated base case DFN are reproduced in independent calculations in Section 2.9. In SKB's corresponding analysis a mistake was made in the implementation of the V_{zone} term, which describes the size of the eroded volume. The mistake is documented in SKB (2011). In the independent modelling it was found that a good match with SKB's results is achieved if the same erroneous form for V_{zone} is used. The erroneous form results in greater amounts of corrosion than if the correct form is used, and therefore the mistake does at least result in a pessimistic outcome.) All subsequent independent calculations were performed with the corrected version of V_{zone}.

Consideration of the shape of the eroded volume and the area of the canister surface that are exposed for corrosion are based on simple assumptions rather than on any detailed modelling of evolved eroded geometries. In the base case, SKB make the

simple assumption that the height of the eroded void, which determines the area for corrosion, is equal to the thickness of the buffer. SKB also present a more conservative geometrically-based erosion geometry that is almost certainly not realistic. No results are presented for the specific application of this model to individual realisations of the DFN, but results for mean number of canister failures are presented, where it is shown that the mean number of failures increases by a factor of ~5. The effect of the more conservative geometry on individual realisations is simple to estimate since it results in timescales for corrosion being scaled by around 21% (the ratio of the exposed surface areas in each case) and this was confirmed by the independent model.

The HS^- concentration in the groundwater is a key parameter that controls calculated corrosion rates. In their calculations, SKB sample the presently observed distribution of HS^- concentrations in the groundwater. This approach is reasonable since there are good reasons to believe that the maximum HS^- concentrations under present climatic conditions will not be exceeded during other climatic conditions within a typical glacial cycle. However, there remain some uncertainties concerning SKB's interpretation of HS^- that could usefully be explored in future. Notably, HS^- concentrations seem to increase with depth below about 600 m depth (e.g. Figure 4-1 of TR-10-39), but there are actually few sampling locations beneath the repository volume. In view of this possible trend, and taking into account the uncertainties in the HS^- data, it would be worthwhile to check whether there could indeed be elevated HS^- concentrations beneath the depth of the repository. If it is then judged that elevated HS^- concentrations could be real, it would be beneficial to evaluate the implications for the degree of conservatism in the calculations of Cu canister corrosion in the repository, should there be any future upwelling of deeper, water. Finally, it should be noted that the corrosion calculations seem to have used only HS^- concentrations in the groundwater and neglected the possibility that SRB could use corrosion-generated H_2 to reduce SO_4 adjacent to the canister. While it is likely that this effect is small, it would be beneficial to confirm this to be the case.

Canister failure times (timescales for erosion + corrosion) were calculated in Section 2.10 for the suite of SKB DFN model outputs. The independent model predicted the same failed locations as the SKB model when the sulphide concentration was taken to be at its maximum value in all fractures, although precise timescales for failure were slightly different due to the question regarding the implementation of the q_{lim} parameter. Assuming the Hjerne aperture – transmissivity model in the semi-correlated base case DFN resulted in only one additional canister failure within 10^6 y. The importance of the EFPC rejection criteria was highlighted in the results.

Across the full suite of DFN models, the Hjerne model was found to lead to approximately 50% more failed locations than for the base aperture – transmissivity model in 10^6 y when the maximal sulphide concentration was applied at all locations. In their analysis, SKB assume that the sulphide concentration at each location is randomly distributed and obtain smaller numbers of failed locations, which highlights the importance of the sulphide concentration distribution in obtaining the results and so its reliability should be carefully considered.

The overall conclusion of the independent analysis and modelling is that it would appear that it is possible to obtain significantly greater numbers of eroded deposition holes by taking reasonable alternative modelling assumptions in the DFN model and in the aperture – transmissivity relationship. In particular, the Hjerne model and/or the fracture frequency scaling by fracture area leads greater numbers of eroded locations. SKB already consider this case as the 'pessimistic fracture aperture'

model and present numbers of eroded locations in Figure 12-3 of TR-11-01 and mean numbers of failed locations at 10^6 y in Figure 5-8 of TR-10-66. In the independent modelling presented here, the Hjerne model is considered with a range of SKB DFN modelling variants that were supplied (Section 2.7), as well as with independently calculated DFN models (Section 3.1). The independent modelling suggests that the number of locations that are eroded and become advective in the first glacial period can increase by up to an order of magnitude compared to the SR-Site base case aperture-transmissivity model (from 1.7 to 11.7), and that over five glacial periods the number of locations that are eroded increase from 7.6 to 291.5. Other realisations of the SKB DFN (e.g. the correlated and uncorrelated fracture size-transmissivity case) lead to more dramatic increases. The results based on the independently modelled DFN show similar behaviour.

These results suggest that the buffer could potentially be less robust in the repository environment, and possibly questions SKB's safety function regarding the role of the buffer in limiting advective conditions in the deposition hole and reducing microbial activity if these alternative relationships and scalings are plausible. However, the increase in the number of eroded locations is not reflected strongly in the increase in the number of failed (eroded + corroded) locations, with only around 50% more locations being failed within 10^6 y.

If greater numbers of eroded locations in the repository are genuinely possible, the consequences should be considered from a wider perspective than in this report, where consequences for corrosion are the primary focus. For example, there may be implications for the earthquake shear scenario.

The simplified power law erosion model, represented by equation (2-1), is a key factor in the canister failure calculations. Without erosion, the diffusion-limited corrosion calculations presented by SKB suggest that timescales for corrosion are sufficiently long that canister failure is not possible over the timescales relevant to the assessment. The erosion model (2-1) is a simple empirical fit to the output from a more detailed mechanistic erosion model, rather than experimentally-obtained data.

The underlying conceptual model of the mechanistic erosion model has not been independently reviewed, but an attempt to independently implement the mechanistic model based on the description in TR-10-64, and the supporting reference TR-09-35, is described in Appendix D. This showed that it is possible to reproduce the power law form of equation (2-1) and obtain an identical power for the nonlinear term (0.41) but that it was not possible to obtain the precise parameterisation (in particular the value of the constant term A_{ero}) without fitting the results to SKB's data. The value of A_{ero} that arose naturally in the independent model, and hence the overall erosion rate itself, was an order of magnitude smaller than the value obtained in TR-10-64.

Furthermore, the independent modelling results suggested that the simple fit erosion rate (2-1) might underestimate the erosion rate for slow flows (<0.1 m/y) compared to the detailed model, since the erosion rate (2-1) tends to zero as the groundwater velocity tends to zero whereas the detailed model tends to a non-zero limiting erosion rate determined by the Einstein-Stokes diffusivity. The effect of this in the probabilistic analysis is that the majority of the deposition holes experiencing slow flow rates could undergo more erosion than is predicted by equation (2-1), but the implication of this cannot be quantified without additional modelling, which was beyond the scope of the work reported here.

Some aspects of the detailed model are not explained clearly in the reports. For example there is an apparent inconsistency between Table 9-2 and Figure 9-6 of TR-09-35 (as was discussed in Section 2.2). The independent model (Appendix D) provides a very good fit to the erosion rates in TR-09-35, Figure 9-6, which may suggest that the description of the model and its implementation to obtain the results that are presented in TR-10-64 (and TR-09-35) are possibly not consistent[6].

5 Possible questions for SKB

- Why are deposition holes that would be excluded due to background fractures (FPC $= 1$) included in the erosion calculations in SSM2011-2426-130 1396328 - hydrogeological_base_case_r0_velocity.XLS?
- What are the cases represented in the file merged/100610_fs_top25_Q123_2000_pline10_merged_ptb.zip, which correspond to 'Multiple particles per start point from 25% highest U0 locations in hydro base case at 2000 AD'. These lead to much larger numbers of eroded deposition holes (up to 2,000 eroded locations during the first glacial period) and have been excluded from further analysis in this report, but if they represent genuinely possible scenarios then they should be investigated further.
- What are the wider implications (i.e. other than corrosion) of significantly increased numbers of eroded locations?
- What is the reason for the apparent order of magnitude discrepancy between the erosion rate results in Figure 9-6 of TR-09-35 and those of Figure 5-3 of TR-10-64? (Table 5-1 of TR-10-64 and Table 9-2 of TR-09-35 would both appear to agree with the data plotted in Figure 5-3 of TR-10-64, so the results in Figure 9-6 of TR-09-35 appear to come from a different model. However an independently implemented model appears to better fit Figure 9-6 of TR-09-35.)
- In the modelling presented in TR-10-64, was a constant bentonite particle separation distance h assumed, or was the form $h = h(\phi)$ fromTR-09-35 used? (This latter form is not mentioned in TR-10-64.)
- The simplified erosion rate $R_{Erosion} = A_{ero}\delta v^{0.41}$ tends to zero as the groundwater velocity tends to zero. However the erosion rate in the underlying detailed erosion model would appear not to (bentonite transport into the fracture tends to a non-zero limit determined by the Einstein-Stokes diffusivity). Does the simplified model therefore under-predict the erosion rate for slow flows, when compared to the detailed model? What are the implications of this in terms of the number of eroded locations?

Some additional questions are given in Appendix E relating to the attempt to independently verify results of numbers of eroded and failed locations in SKB's

[6] Equally there may be an error in the independent model, but the presentation of the model in TR-10-64 and TR-09-35 does not make it easy to confirm whether this is the case.

probabilistic analysis that are presented in TR-11-01 Figure 12-4 and TR-10-50 Table 4-3 respectively.

Referenced Reports

SKB Reports

SKB (2011), "Documentation of the code for erosion and corrosion calculations in SR-Site", SKB Public Memo 1396663, November 2011.

TR-10-66: Corrosion calculations report for the safety assessment SR-Site. SKB TR-10-66, Svensk Kärnbränslehantering AB.

TR-10-64: Moreno L, Neretnieks I, Lui L, 2010. Modelling of erosion of bentonite gel by gel/sol flow. SKB TR-10-64, Svensk Kärnbränslehantering AB.

TR-10-52: Data report for the safety assessment SR-Site. SKB TR-10-52, Svensk Kärnbränslehantering AB.

TR-10-42: Neretnieks I, Liu L, Moreno L, 2010. Mass transfer between waste canister and water seeping in rock fractures: Revisiting the Q-equivalent model. SKB TR-10-42, Svensk Kärnbränslehantering AB.

TR-10-39: Tullborg E-L, Smellie J, Nilsson A-Ch, Gimeno MJ, Brüchert V and Molinero J, 2010. SR-Site – sulphide content in the groundwater at Forsmark. SKB TR-10-39, Svensk Kärnbränslehantering AB.

TR-10-21: Munier R, 2010. Full perimeter intersection criteria . Definitions and implementations in SR-Site . SKB TR-10-21, Svensk Kärnbränslehantering AB.

TR-09-35: Neretnieks I, Liu L, Moreno L, 2009. Mechanisms and models for bentonite erosion. SKB TR-09-35, Svensk Kärnbränslehantering AB.

TR-08-05: Site description of Forsmark at completion of the site investigation phase: SDM-Site Forsmark. SKB TR-08-05, Svensk Kärnbränslehantering AB.

R-09-28: Hjerne C, Nordqvist R, Harrström J, 2010. Compilation and analyses of results from cross-hole tracer tests with conservative tracers. SKB R-09-28, Svensk Kärnbränslehantering AB.

R-09-20: Joyce S, Simpson T, Hartley L, Applegate D, Hoek J, Jackson P, Swan D, 2009. Groundwater flow modelling of periods with temperate climate conditions – Forsmark. SKB R-09-20, Svensk Kärnbränslehantering AB.

R-08-109: Hallbeck L, Pedersen K, 2008c. Explorative analysis of microbes, colloids and gases together with microbial modelling. Site description model, SDM-Site Laxemar. SKB R-08-109, Svensk Kärnbränslehantering AB.

R-08-85: Hallbeck L, Pedersen K, 2008. Explorative analysis of microbes, colloids and gases. SDM-Site Forsmark. SKB R-08-85, Svensk Kärnbränslehantering AB.

P-10-18: Rosdahl A, Pedersen K and Wallin B, 2010. Investigation of sulphide in core drilled boreholes KLX06, KAS03 and KAS09 at Laxemar and Äspö. Chemical and microbiological data from four investigated borehole sections. SKB P-10-18, Svensk Kärnbränslehantering AB.

Other reports and papers

Bath AH, 2012. Groundwater chemistry in SKB's safety assessment SR-Site: initial review. SSM Technical Note 12, 2012:32

Bird R B, Stewart W E, Lightfoot E N, 2002. Transport phenomena, 2nd ed. Wiley.

Geier J E, 2015. Assessment of flow-related transport parameters used in the SR-Site safety case. SSM Technical Note 2015:40, Swedish Radiation Safety Authority, Stockholm.

Geier, J., 2014. Independent evaluation of the number of critical canister positions in the KBS-3 repository at Forsmark – Main Review Phase. SSM Technical Note 2014:44, Swedish Radiation Safety Authority, Stockholm.

Geier, J., 2010. Discrete-feature model implementation of SDM-Site Forsmark. SSM Report 2010:05, Swedish Radiation Safety Authority, Stockholm.

Hallbeck L and Pedersen K, 2008. Characterization of microbial processes in deep aquifers of the Fennoscandian Shield. Applied Geochemistry, 23, 1796–1819.

Appendix A: SKB DFN Files

SKB PTB files that were used in the independent analysis in Section 2.7 are listed in Table A-1. The following SKB file names were also listed in the document "PTB files delivered to SKB by Serco for SR-Site Forsmark, Serco, 17 November 2010", but were not included in the set of files that were available for this analysis.

- merged/100628_fs_r3_corr_Q123_2000_pline_merged_ptb.zip
  Realisation 3 of the correlated transmissivity-size relationship at 2000 AD
- merged/100617_fs_r6_corr_Q123_2000_pline_merged_ptb.zip
  Realisation 6 of the correlated transmissivity-size relationship at 2000 AD
- merged/100628_fs_r4_uncorr_truncHCD_Q123_2000_pline_merged_ptb.zip Realisation 4 of the truncated, uncorrelated transmissivity-size relationship at 2000 AD
- merged/100617_fs_r6_uncorr_truncHCD_Q123_2000_pline_merged_ptb.zip Realisation 6 of the truncated, uncorrelated transmissivity-size relationship at 2000 AD

The PTB files are supplied in a text files. They have been imported into Microsoft Excel and re-saved as xls format in order to allow them to be parsed using the script described in Appendix C.

Table A-1: Subset of PTB files delivered to SKB by Serco for SR-Site Forsmark used in the independent analysis

File name	Description	# Realisations / notes
merged/100615_fs_Q123_2000_pline_merged_ptb.zip	Hydro base case at 2000 AD	1 (same case considered in base case analysis)
merged/100610_fs_trapp_Q123_2000_pline_merged_ptb	Hydro base case at 2000 AD with TRAPP column added	1
merged/100610_fs_r1-10_Q123_2000_pline_merged_ptb.zip	10 realisations of the hydro base case at 2000 AD	10
merged/100610_fs_top25_Q123_2000_pline10_merged_ptb.zip	Multiple particles per start point from 25% highest U0 locations in hydro base case at 2000 AD	2
merged/100610_fs_corr_Q123_2000_pline_merged_ptb.zip	Correlated transmissivity-size relationship at 2000 AD	1
merged/100617_fs_r2_corr_Q123_2000_pline_merged_ptb.zip	Realisation 2 of the correlated transmissivity-size relationship at 2000 AD	1

File name	Description	# Realisations / notes
merged/100617_fs_r4_corr_Q123_2000_pline_merged_ptb.zip	Realisation 4 of the correlated transmissivity-size relationship at 2000 AD	1
merged/100628_fs_r5_corr_Q123_2000_pline_merged_ptb.zip	Realisation 5 of the correlated transmissivity-size relationship at 2000 AD	1
merged/100610_fs_uncorr_truncHCD_Q123_2000_pline_merged_ptb.zip	Truncated, uncorrelated transmissivity-size relationship at 2000 AD	1
merged/100617_fs_r2_uncorr_truncHCD_Q123_2000_pline_merged_ptb.zip	Realisation 2 of the truncated, uncorrelated transmissivity-size relationship at 2000 AD	1
merged/100610_fs_r3_uncorr_truncHCD_Q123_2000_pline_merged_ptb.zip	Realisation 3 of the truncated, uncorrelated transmissivity-size relationship at 2000 AD	1
merged/100628_fs_r5_uncorr_truncHCD_Q123_2000_pline_merged_ptb.zip	Realisation 5 of the truncated, uncorrelated transmissivity-size relationship at 2000 AD	1
merged/100610_fs_pdz_Q123_2000_pline_merged_ptb.zip	3 realisations with possible deformation zones included at 2000 AD	3
merged/100610_fs_edz_Q123_2000_pline_merged_ptb.zip	Tunnel variants with different EDZ transmissivities or no EDZ at 2000 AD	3
merged/100610_fs_trapp_noedz_Q123_2000_pline_merged_ptb.zip	The no EDZ case with TRAPP column added at 2000 AD	1
merged/100610_fs_trappdz_noedz_Q123_2000_pline_merged_ptb.zip	The no EDZ case with TRAPP and DZ columns added at 2000 AD	1
merged/100610_fs_crown_Q123_2000_pline_merged_ptb.zip	Tunnel variant with crown space at 2000 AD	1
	Total	31

Appendix B: Independent DFN Files

Excel files used in the analysis in Section 3.1:

- uncoaspo1_gl_20140908.xls
- uncoaspo1a_gl_20140908.xls
- semistoch1_gl_20140909.xls
- semistoch1a_gl_20140908.xls
- semihjerne1_gl_20140909.xls
- semihjerne1a_gl_20140909.xls
- semicubic1_gl_20140909.xls
- semicubic1a_gl_20140909.xls
- semiaspo2_gl_20140909.xls
- semiaspo2a_gl_20140909.xls
- semiaspo1_gl_20140908.xls
- semiaspo1a_gl_20140908.xls
- corraspo1_gl_20140908.xls
- corraspo1a_gl_20140908.xls
- uncohjerne1.xls
- uncohjerne1a.xls

Excel files used in the analysis in Section 3.2

- o3semiaspo1.xls
- o3semiaspo1a.xls
- o3uncohjerne1.xls
- o3uncohjerne1a.xls
- t2semiaspo1.xls
- t2semiaspo1a.xls
- t2uncohjerne1.xls
- t2uncohjerne1a.xls

Appendix C: Scripts

The calculations described in this report use as source data results from DFN models supplied in spreadsheet and CSV files containing output from hundreds of realisations. Rather than implementing the calculations in each spreadsheet, the analysis is performed using a script 'erosion_analsys.pl'. The script is written using the Perl language and uses the Spreadsheet::Read module[7] to parse Microsoft Excel xls files. The script is structured such that a nested outer loop is performed to loop over each xls file and each worksheet within the file. A subroutine 'DoAnalysis()' is called within the nested loops and is passed the data contents for each deposition hole in each realisation, ordered by rows. Some independent analysis was performed using only spreadsheet calculations in order to verify the implementation of the script (e.g. the analysis in Sections 2.6 and 2.9).

The DoAnalysis() subroutine implements the erosion and corrosion model. In the case of erosion it writes a separate CSV output file for each realisation containing the erosion rate for each deposition hole in the realisation worksheet and the number of glacial cycles required to achieve advective conditions. A summary file ('Summary.csv') is also appended with a summary of the results for the realisation, listing the number of deposition holes becoming advective in each glacial period for each realisation. In the case of the corrosion analysis it reports the time for corrosive failure and produces summary tables of the form of Table 10 listing deposition holes with combined corrosion and erosion times less than 10^6 y.

A copy of the DoAnalysis() subroutine implementing the erosion rate calculation (2-1) used in the analysis of the independent DFN simulations in Sections 3.1 and 3.2 is shown below. The routine is reasonably long and is mostly concerned with formatting of the output that is generated. The DoAnalysis() subroutine used in the analysis of the alternative SKB DFN realisations in Section 2.7 is similar.

One unfortunate side-effect of using the Perl 'Spreadsheet::Read' module is that it makes data available 'as displayed' in Excel, rather than making the true value available. This results in a loss of accuracy in the input to the batch calculations, but this difference is only small (and any serious sensitivity to such differences would highlight a major sensitivity in the underlying models). An example of the consequences of this effect is as follows.

The key factor determining the corrosion rate from the SKB output spreadsheets is U_0 (the equivalent flux). For the base case model, hole #1978 has U0=0.008241 m/y. If the corresponding spreadsheet file is opened in Excel, this is displayed as '8.24E-03'.

Table 8 shows the calculated corrosion time calculated directly in Excel. Table 10 shows the corresponding corrosion time calculated in the Perl batch calculations. In the Excel calculation, the calculation is performed with U0=0.00824**1** and the resulting timescale for corrosion is 140,362 y. However in the Perl calculation it is performed with U0=0.00824 (which is equal to the displayed value 8.24E-03) the resulting timescale for corrosion is 140,371 y.

[7] http://search.cpan.org/~hmbrand/Spreadsheet-Read/

If the value of U0 is replaced in the spreadsheet with 0.00824 then the identical value computed by the Perl script is obtained, which verifies that this is indeed the source of the difference.

It is noted that the percentage difference between U0 values 0.008241 and 0.00824 is ~0.012%. The percentage difference between the computed erosion times (140,362 y and 140,370 y) is ~0.006%. This halving of the percentage difference in the computed corrosion times compared to the U0 values is due to the dependence of q_{eb} on the square root of U0.

Although this difference is not ideal, the impact on the computed results is small, and therefore the calculations are felt to be fit for purpose.

The source code is stored in a Git version control system. The version used in the analysis (shown here) has commit ID 211bd2ecf54f98d55cbbf49ca0a9873dd2f76fc8.

```
sub DoAnalysis
{
	my $outputDir           = $_[0];
	my $bookName            = $_[1];
	my $sheetName           = $_[2];
	my $modelDetailsRef     = $_[3];
	my $rowStrucRefArrayRef = $_[4];

	# Parameter values
	my $massToErode   = 1200;              # kg
	my $glacialPeriod = 120000;            # y
	my $fracDilute    = 0.25;              # -

	# Do row-by-row analysis, build up output to write
	my @outputToWrite;
	my @warningsToWrite;
	my %NumErodedInCyle;

	my $nRow = scalar @{$rowStrucRefArrayRef};
	for($iRow=0; $iRow<$nRow; $iRow++)
	{
		$rowStrucRef = @{$rowStrucRefArrayRef}[$iRow];

		# Entries in the hash are dereferenced as
follows:
		my $v     = $rowStrucRef->{u_0};       # m/y
		my $delta = $rowStrucRef->{b};         # m

		# Erosion rate
		my $Rero = 27.2 * $delta * ($v**0.41); # kg/y

		if($Rero == 0.0)
		{
			# Either aperture or vel is zero...
			push(@warningsToWrite, "Zero erosion rate
for Tun/Pos: "
				. $rowStrucRef->{Tun} . "/" .
$rowStrucRef->{Pos});
		}
		else
		{
			# Calculate time until advective
conditions established
```

```
                    my $Tadv     = $massToErode / $Rero;    # y
(eroding time)
                    my $Telapsed = $Tadv / $fracDilute;     # y
(elapsed time)
                    my $NCycles  = ceil($Telapsed /
$glacialPeriod); # -

                    my @output = Csv($rowStrucRef-
>{Tun},$rowStrucRef->{Pos},$Rero,$Tadv,$Telapsed,$NCycles);
                    push(@outputToWrite,\@output);

                    # Build hash
                    if( exists $NumErodedInCyle{$NCycles} )
                    {
                           $NumErodedInCyle{$NCycles}=
$NumErodedInCyle{$NCycles} + 1;
                    }
                    else
                    {
                           $NumErodedInCyle{$NCycles} = 1;
                    }
             }
      }

      # Append glacial cycle count output to first N rows
(N=30 is large, to capture most holes)
      my $NCOUNT = 30;
      my $totalEroded = 0; # to check
      for( my $i=0; $i<$NCOUNT; $i++ )
      {
             if( exists $NumErodedInCyle{$i+1} )
             {
                    my @output = Csv( @{$outputToWrite[$i]}
,"", Csv($i+1,$NumErodedInCyle{$i+1}) );
                    $outputToWrite[$i] = \@output;

                    $totalEroded += $NumErodedInCyle{$i+1};
             }
             else
             {
                    my @output = Csv( @{$outputToWrite[$i]}
,"", Csv($i+1,0) );
                    $outputToWrite[$i] = \@output;
             }
      }
      # Append check val
      my @output = Csv( @{$outputToWrite[$NCOUNT+1]} ,"",
Csv("TOTAL",$totalEroded) );
      $outputToWrite[$NCOUNT+1] = \@output;

      # Initialise output file, write header
      my $fname = $outputDir . "/" . $bookName . "." .
$sheetName . ".csv";
      open(my $fh, '>', $fname) or die "Could not open file
'$fname' $!";

      print $fh Csv("Book:",$bookName) . "\n";
      print $fh Csv("Sheet:",$sheetName) . "\n";
      print $fh "\n";

      print $fh Csv("Size:",     @{$modelDetailsRef}[0]) .
"\n";
      print $fh Csv("Aperture:", @{$modelDetailsRef}[1]) .
"\n";
```

```
	print $fh Csv("Seed:",	@{$modelDetailsRef}[2]) .
"\n";
	print $fh Csv("Scaling:",  @{$modelDetailsRef}[3]) .
"\n";
	print $fh "\n";

	# Warnings
	if( scalar(@warningsToWrite) > 0 )
	{
		print "   " . scalar(@warningsToWrite) . "
warnings\n";
		foreach my $warning (@warningsToWrite)
		{
			print $fh Csv("Warning", $warning) . "\n";
		}
		print $fh "\n";
	}

	# Table - headers
	print $fh Csv("Tun","Pos","Erosion (kg/y)","Reqd Erosion
Time (y)","Elapsed Erosion Time (y)","N Glacial Cycles (-
)","","Cycle","Num Eroded In Cycle") . "\n";

	# Table - values
	foreach my $output (@outputToWrite)
	{
		print $fh Csv( @{$output} ) . "\n";
	}

	close $fh;

	# Append to summary output
	open(my $fsum,'>>',$summaryFile) or die "Could not open
$summaryFile\n";
	if( not $writtenSummaryHeader )
	{
		print $fsum Csv("Size relationship","Aperture
relationship","Scaling","Seed","Realisation");
		for( my $i=0; $i<$NCOUNT; $i++ )
		{
			print $fsum ",Eroded in glaciation " .
($i+1);
		}
		print $fsum "\n";
		$writtenSummaryHeader = 1;
	}
	my $output =
Csv(@{$modelDetailsRef}[0],@{$modelDetailsRef}[1],@{$modelDeta
ilsRef}[3],@{$modelDetailsRef}[2],$sheetName);
	for( my $i=0; $i<$NCOUNT; $i++ )
	{
		if( exists $NumErodedInCyle{$i+1} )
		{
			$output = Csv( $output ,
$NumErodedInCyle{$i+1} );
		}
		else
		{
			$output = Csv( $output , 0 );
		}
	}
	print $fsum $output . "\n";
}
```

Appendix D: Independent Modelling of Erosion

Introduction

The overall timescales for canister failure as a consequence of the erosion of the buffer and subsequent corrosion of the copper overpack, which were calculated by the models described in Section 2 and 3, are very dependent on SKB's model for buffer erosion. As was noted in Section 2.1, the erosion model (2-1) is a simple empirical fit to the output from a more detailed mechanistic erosion model, rather than being a fit to experimentally-obtained data.

This appendix describes a short attempt to independently implement the underlying detailed mechanistic model described in TR-10-64. The main aim of this work is to verify the derivation of the empirical fit, by attempting to reproduce Figure 5-3 of TR-10-64 (re-plotted in Section 2, Figure 1 of this report), and to understand any sensitivities of the underlying mechanistic model that could impact upon the results. It is noted that the underlying conceptual model for buffer erosion that the mechanistic model is based on is not a subject of the review.

Model

As in TR-10-64 a two-dimensional model is used to represent the expansion of the buffer and the diffusion of sodium ions from the buffer, into a fracture intersecting the deposition hole. The model includes the following processes:

- The gel/sol/water fluid flow, represented by the Darcy equation with the viscosity of the fluid in the fracture depending on the smectite volume fraction and the concentration of the sodium ions;
- The expansion of the bentonite into the fracture, described by a dynamic force balance model, which was developed by Liu et al. (2009) and reproduced in TR-10-64;
- The transport of the ions in the pore water, by advection and diffusion, with the diffusion coefficient for the cation depending on the smectite volume fraction.

The model was implemented using the QPAC code (Quintessa, 2013) and solves for the concentration of sodium ions and the volume fraction of bentonite in the fluid. The model geometry is shown in Figure 1. The cylindrical deposition hole has a radius of 0.875 m. The fracture is modelled to an outer radius of 20 m in the cylindrical geometry shown, which is sufficiently large that the background flow is unperturbed at this distance.

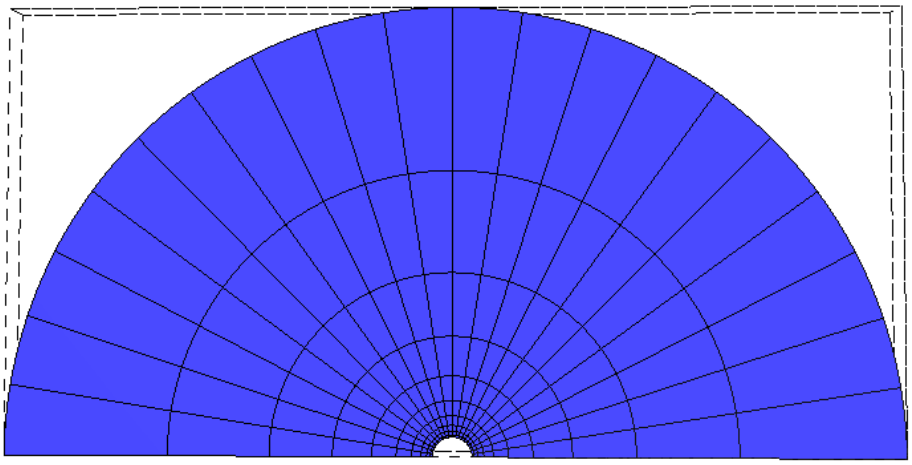

Figure 1: Model geometry.

Darcy Equation

The fluid flow in the fracture is modelled using the Darcy equation. The viscosity of the gel is very strongly dependent on the volume fraction of bentonite in it (TR-10-64, section 2.4), and the hydraulic conductivity was modified to account for this.

The standard equation for the Darcy velocity, *v*, is written as

$$v = -K\nabla H,$$

where K (m/y) is the hydraulic conductivity and ∇H is the hydraulic gradient. The hydraulic conductivity of the fracture is assumed to depend on the viscosity of the fluid according to

$$K = K_w \frac{\eta_w}{\eta},$$

where η (Pa s) is the viscosity of the fluid and the subscript *w* indicates when the fluid is water.

TR-10-64 presents the above equation in terms of the transmissivity of the fracture in equation (TR-10-64, eq. 2-1) and defines the following relationship for the relative viscosity of the fluid (TR-10-64, eq. 2-19):

$$\frac{\eta}{\eta_w} = 1 + 1.022\phi_{cov} + 1.358\phi_{cov}^3.$$

Here ϕ_{cov} (-) is the co-volume fraction of the fluid (the volume equal to a sphere in which a coin-like smectite particle can rotate freely). The co-volume fraction is defined as

$$\phi_{cov} = \frac{2}{3}\frac{\left(D_p + 2m\kappa^{-1}\right)^3}{D_p^2\delta_p}\phi$$

where ϕ (-) is the volume fraction of the smectite in the fluid, δ_p (m) is the smectite particle thickness, and m is a fitting parameter (TR-09-25, Section 5.3), which is taken to be 1. D_p is not defined in TR-10-64, but TR-09-35 (Section 5.3) defines it to be the diameter of the cylindrical particles. In TR-09-35, Equation 5-7, the Debye length κ^{-1} (m) is given by

$$\kappa^{-1} = \sqrt{\frac{\varepsilon_0\varepsilon_r RT}{2IF^2}}$$

where I is the ionic strength of the fluid, F is the Faraday constant (9.6485 C/mol), ε_0 (F/m) is the permittivity in a vacuum and ε_r (-) is the relative permittivity. R is the gas constant (8.3145 J/K/mol) and T is the absolute temperature in Kelvin. The parameter values used in the model are given later in Table 1.

In the modelling in TR-10-64 the fluid solutes are assumed to be dominated by sodium and chloride ions, allowing the ionic strength in the formula for the Debye length to be expressed purely in terms of the sodium ion concentration. The reciprocal of the Debye length is then stated to be (TR-10-64, eq 2-12)

$$\kappa = \sqrt{\frac{2F^2cz^2}{\varepsilon_0\varepsilon_r RT}}$$

where z is the valence of the sodium ions (1) and c (mol/m^3) is the concentration of sodium.

It is noted that neither TR-10-64 nor TR-09-35 appear to state the value (or functional form) assumed for ε_r. In this modelling the relative permittivity of water was used assumed (see Table 1).

The values of η/η_w that are computed in the model are plotted in Figure 2 as a function of the smectite volume fraction. The range of the computed relative viscosity agrees well with the range of relative viscosities that are calculated by SKB for various sodium ion concentrations in TR-10-64, Figure 2-1 (a copy of which is shown in Figure 3). The values calculated here arise for the range of time-dependent sodium ion concentrations reported at the model output times, whereas in TR-10-64, Figure 2-1 the sodium ion concentrations are fixed, hence the curve plotted in in Figure 2 is not expected to lie perfectly on any of the individual curves in TR-10-64, Figure 2-1 (but is expected to lie between the curves corresponding to the bounding 0.1mM and 10mM concentrations occurring in the model, shown by the blue and red curves in Figure 3). Thus the plot lends confidence that the ratio η/η_w computed in the independent model is consistent with the formulation in TR-10-64.

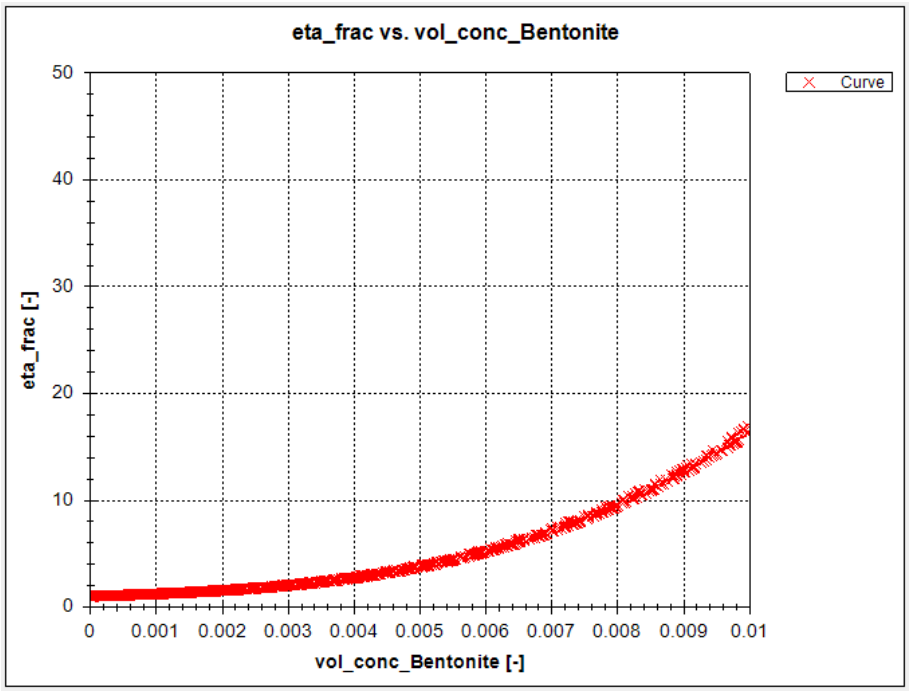

Figure 2 Plot of relative viscosity (η/η_w) as a function of the smectite volume fraction (ϕ) (with varying sodium concentrations). The curve is bounded by the similar curves with fixed sodium ion concentrations of 0.1 mM and 10 mM in TR-10-64, Figure 2-1 (which is copied in Figure 3).

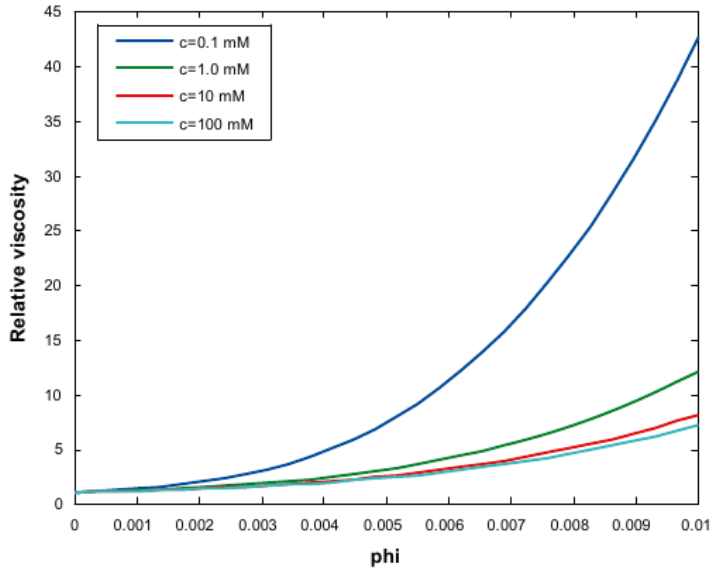

Figure 3 Relative viscosity as a function of the smectite volume fraction ϕ for different sodium ion concentrations (copy of TR-10-64, Figure 2-1)

Diffusion of Sodium Ions

The advection-diffusion equation is used to model the transport of sodium ions in the fluid. The advection-diffusion equation is given by

$$\frac{\partial c}{\partial t} = -v\nabla c + \nabla \cdot (D\nabla c)$$

where c is the concentration of sodium ions (mol/m^3), D (m^2/s) is the effective diffusion coefficient, and t is time. D is a scalar but varies with the bentonite volume fraction in the fluid as:

$$\frac{D}{D_0} = (1-\phi)^{1.6},$$

where the value of D_0 is taken to be 2x10^{-9} m^2/s (TR-10-64).

Smectite Expansion

In the calculations described in TR-10-64 gravity forces on the smectite expansion were found to be negligible. The same assumption is made here, therefore the equation describing the mass balance of smectite in the system is written as

$$\frac{\partial \phi}{\partial t} = -v\nabla\phi + \nabla \cdot (\frac{\chi}{f}\nabla\phi)$$

where χ (J) is the sum of the energy of the particles. The ratio of χ to f can be considered as diffusivity, where $f = f_{fr}/(1-\phi)$ considers that the smectite is moving into the fracture and the equivalent volume of water is moving in the opposite direction (TR-10-64). f_{fr} (kg/s) is the friction coefficient of the fluid and is defined as

$$f_{fr} = 6\pi\eta_w r_{eq} + V_p k_0 \tau^2 a_p^2 \eta_w \frac{\phi}{(1-\phi)^2}$$

where r_{eq}(m) is the equivalent radius of the non-spherical smectite particles, $\kappa_0\tau^2$ (-) is Kozeny's constant, V_p(m^3) is the volume of the particles and a_p(m^2/m^3) is the specific surface area per unit volume of the particles, both assuming coin-shaped particles.

The function χ is given by

$$\chi = k_B T + (h+\delta_p)^2 \left(\frac{\partial F_A}{\partial h} - \frac{\partial F_R}{\partial h}\right)$$

where k_B (J/K) is the Boltzmann constant, T (K) is the absolute temperature, h (m) is the separation between flat particles and δ_p (m) is the particle thickness. F_A (N) and F_R (N) denote the van der Waals attractive and repulsive forces. When the bentonite volume fraction is zero, the diffusivity reduces to the standard Einstein-Stokes equation:

$$\frac{\chi}{f} = \frac{k_B T}{6\pi\eta_w r_{eq}}.$$

Explicitly, the derivative terms in the formula for χ are given by

$$\frac{\partial F_A}{\partial h} = -\frac{A_H S_P}{2\pi}\left[\frac{1}{h^4} - \frac{2}{(h+\delta_p)^2} + \frac{1}{(h+2\delta_p)^4}\right],$$

where A_H(J) is the Hamaker constant and S_p(m^2) is the particle surface area, and

$$\frac{\partial F_R}{\partial h} = -4\kappa cRTS_P \tanh y^m \left[\cosh y_\infty^m \sinh\left(\frac{y_\infty^m}{2}\right) + \frac{1}{\kappa h}\sinh y_\infty^h + \frac{2}{(\kappa h)^2}\sinh\left(\frac{y_\infty^h}{2}\right)\right]$$

where

$$y^m = \sinh^{-1}\left[2\sinh y_\infty^m + \frac{4}{\kappa h}\sinh\left(\frac{y_\infty^h}{2}\right)\right],$$

$$y_\infty^m = 4\tanh^{-1}\left[\tanh\left(\frac{y_\infty^0}{2}\right)\exp\left(-\frac{\kappa h}{2}\right)\right],$$

and

$$y_\infty^h = 4\tanh^{-1}\left[\tanh\left(\frac{y_\infty^0}{2}\right)\exp(-\kappa h)\right].$$

Finally,

$$y_\infty^0 = 2\sinh^{-1}\left(\frac{s^0}{2}\right),$$

where s^0 is a dimensionless surface charge density given by

$$s^0 = \frac{zF\sigma^0}{\varepsilon_0\varepsilon_r\kappa RT}$$

where σ^0 (C/m^2) is the specific charge on the particle surface.

The above formulae are presented assuming that h, the separation between the particles, is a constant, consistent with the presentation in TR-10-64. However a precise value for this parameter is not reported in TR-10-64. In TR-09-35, h is expressed as a function of the smectite volume fraction ϕ, given by

$$h(\phi) = \delta_p\left(\frac{\phi_{max}}{\phi} - 1\right),$$

where ϕ_{max} is the maximum possible volume fraction of smectite in the fluid, which is necessarily less than 1. However, no value for ϕ_{max} is reported in TR-09-35, which is necessary to use this formulation.

Therefore for the majority of this modelling, h is treated as a constant, as it is presented in TR-10-64. However results from alternative cases are presented where the $h = h(\phi)$ formulation is used.

The approach taken to determining an appropriate value for h was to fit the model to the results of TR-10-64 for the 31.5 m/y flow field. A value of 2.85×10^{-8} m was obtained. The sensitivity of the resulting bentonite erosion rates to this choice was

then analysed in an attempt to evaluate the consequences of this uncertainty in the modelling. The value of 2.85×10^{-8} m is well within the range of particle separations presented TR-09-35 Sections 3 and 4, where experimental evidence and theory for the structure of bentonite stacks is discussed.

Parameter Values

The parameter values used in the model are given in Table 1. Values for several of the input parameter values were not specified in TR-10-64. Where possible, missing values have been obtained from TR-09-35 and Liu et al. (2009), Where values could not be found in these references, presumed reasonable values have been assumed (it is indicated in Table 1where this is the case). To summarise, the data that could not be found in any of the references are

- The relative permittivity value (or function) ε_r; and
- Either the constant value of h assumed in TR-10-64 or, if the functional form $h = h(\phi)$ was used, the maximum possible volume fraction of smectite in the fluid, ϕ_{max}.

Table 1: Parameter values used in modelling. Values that could not be found in TR-10-64 or the main references are highlighted with shading.

Parameter	Description	Value	Source / Comments
$\boldsymbol{\eta_w}$	Viscosity of water (Pa s)	8.9e-4 Pa s	CRC Handbook, assuming temperature of 25 °C
$\boldsymbol{\delta_p}$	Smectite particle thickness (m)	1e-9 m	Liu et al. (2009).
S_p	Smectite particle surface area (m^2)	9.0e-14 m^2	Liu et al. (2009).
D_p *(or d_p)*	Not defined in TR-10-64, have assumed they mean particle diameter	0.3e-6 m	TR-09-35, (p78)
F	Faraday constant (C/mol)	9.6485e4 C/mol	CRC Handbook
$\boldsymbol{\varepsilon_0}$	Permittivity in a vacuum (F/m)	8.8542e-12 F/m	CRC Handbook
$\boldsymbol{\varepsilon_r}$	Relative permittivity	80	No value/function given in TR-10-64 or TR-09-35, so assumed value for water at 25 °C from CRC Handbook.
k_B	Boltzmann constant (J/K)	1.3806e-23 J/K	CRC Handbook
R	Gas constant (J/K/mol)	8.3145 J/K/mol	CRC Handbook
T	Absolute temperature (K)	298.15 K	Assumed 25 °C
r_{eq}	Equivalent radius of particles (m)	0.15e-6 m	Diameter of particles given as 0.3microns in TR-09-35
$k_0\tau^2$	Kozeny's constant	5.0	Liu et al. (2009)
V_p	Volume of the	$\boldsymbol{\pi r_{eq}^2 \delta_p}$	Assumes a coin, equation (6-29)

	particles (m^3)		in TR-09-35
a_p	Specific surface area per unit volume of particles (m^2/m^3)	$\frac{2(r_{eq}+\delta_p)}{r_{eq}\delta_p}$	Assumes a coin
z	Valence	1	Liu et al. (2009)
A_H	Hamaker constant (J)	$2.5k_BT$	Liu et al. (2009)
h	Separation between flat particles	2.85e-8 m, or set as $\boldsymbol{h}(\boldsymbol{\phi})$	No value/function given in TR-10-64. A range of values are quoted in TR-09-35 Sections 3 and 4 (experimental evidence / theory for the structure of bentonite stack). The chosen value gives a reasonable fit to the results quoted in TR-10-64 while being in the range of values discussed in TR-09-35.
$\boldsymbol{\phi}_{\max}$	Maximum volume fraction in $\boldsymbol{h}(\boldsymbol{\phi})$ formula (see $\boldsymbol{h}$ above)	0.9	Not mentioned in TR-10-64 and no value given in TR-09-35
$\boldsymbol{\sigma^0}$	Specific charge on particle surface (C/m^2)	-0.131 C/m^2	Liu et al. (2009)

Boundary and Initial Conditions

Following TR-10-64 the smectite volume fraction at the deposition hole boundary is fixed at $\phi = 0.4$. The sodium ion concentration in the pore water at this boundary is fixed at $c = 10$ mM. There is no flow of water across this boundary.

The sodium ion concentration on the external boundaries is fixed at $c = 0.1$ mM and the smectite volume fraction is set to zero on these boundaries. Purely advective (zero concentration gradient) conditions are assumed on the outflowing boundaries.

The initial sodium concentration in the fracture is set to be $c = 0.1$ mM, and the initial smectite volume fraction in the fracture is set to zero.

Results

Fixed h case

A steady state situation is achieved in the model when the loss of bentonite due to the erosion at the tip of the bentonite penetrating the fracture is balanced by the introduction of 'fresh' bentonite at the deposition hole boundary. At this point the rate that bentonite passing across the deposition hole boundary is equal to the rate

that it is lost due to erosion. Thus the erosion rate is evaluated in the model by determining this steady state flux of bentonite across the deposition hole boundary.

The steady state situation in the current model is shown in Figure 4 for the case of the 31.5 m/y flow rate. The extent of the penetration of bentonite gel into the fracture does not match that shown in the corresponding figure of TR-10-64 (Figure 5-2 – reproduced here as Figure 5), where the depth of penetration of bentonite is greater. However the corresponding plume of sodium ions emanating from the deposition hole, shown in Figure 6 does provides a reasonable match to the extent of the gel penetration in Figure 5-2 of TR-10-64. Figure 7 shows the steady-state hydraulic conductivity in the fracture for a water velocity of 31.5 m/yr.

Given that a different penetration distance is obtained for the simulation it might be expected that the model presented here would give quite different values for the bentonite erosion rate than that predicted in TR-10-64. However as Figure 8 shows, the current model is in good agreement with the erosion rates presented in TR-10-64 for all flow rates. The precise rates of bentonite release computed in the current model are compared with those from TR-10-64 in Table 2.

As noted in the previous section, the approach taken in the current model was to fit the value of the erosion rate to that reported in TR-10-64 for the 31.5 m/y case, so the agreement at this data point is not surprising. However the agreement over the range of groundwater velocities might not necessarily be expected when taking this approach. The agreement between the erosion rates despite the differences in the extents of the plumes would suggest that there may be a misunderstanding between the quantities plotted in Figure 4 and TR-10-64 (Figure 5-2 - reproduced here as Figure 5), or that the erosion rate is somehow insensitive to the precise penetration depth.

The results begin to diverge at slower flow rates. This is most likely a consequence of the representation of h, the bentonite particle separation, as a constant in the current model (due to the difficulties associated with obtaining data for this parameter as discussed in the previous section). This assumes that the model in TR-10-64 used the $h(\phi)$ form, although this is not stated in TR-10-64.

It is noted that TR-10-64 did not carry out simulations for the two smallest velocities (shown as hollow triangles); the smectite release for these velocities was determined in TR-10-64 by linear extrapolation of the data at the larger velocities. The values quoted for the QPAC calculations for these two velocities are from direct simulations.

The results would therefore seem to confirm that the power law relationship that SKB derive for the erosion rate is valid, at least for flow rates > 0.1 m/y. However the modelling here has not confirmed the precise parameterisation of the power law, since it was required to fit one of the data points (at 31.5 m/y) in order to obtain the agreement.

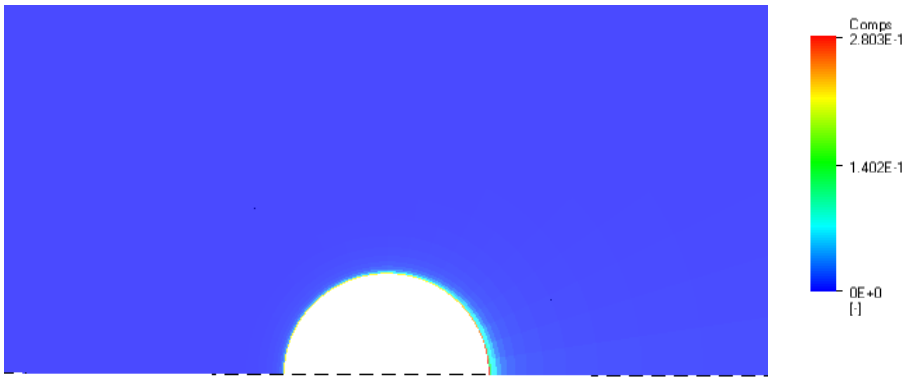

Figure 4: Smectite volume fraction distribution for a water velocity of 31.5m/y. (The limits on the axis are [-5,5]x[0,5] m.)

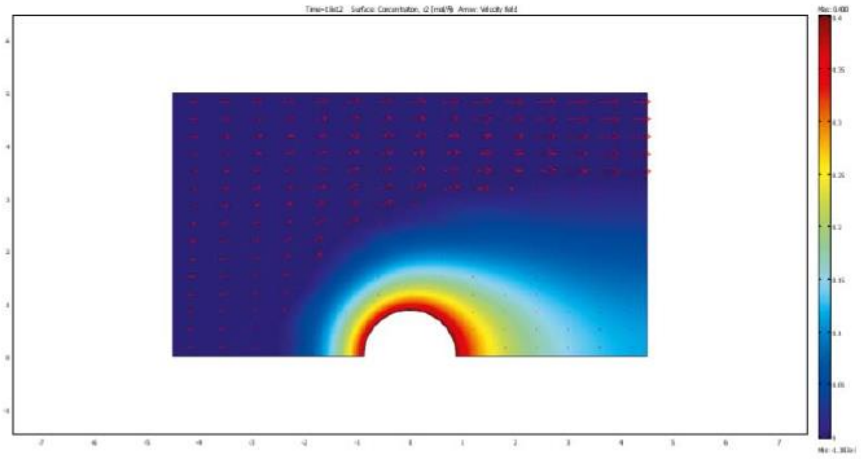

Figure 5 Smectite volume fraction distribution and velocity field (as arrows) for a water velocity of 31.5m/y from TR-10-64 (Figure 5-2).

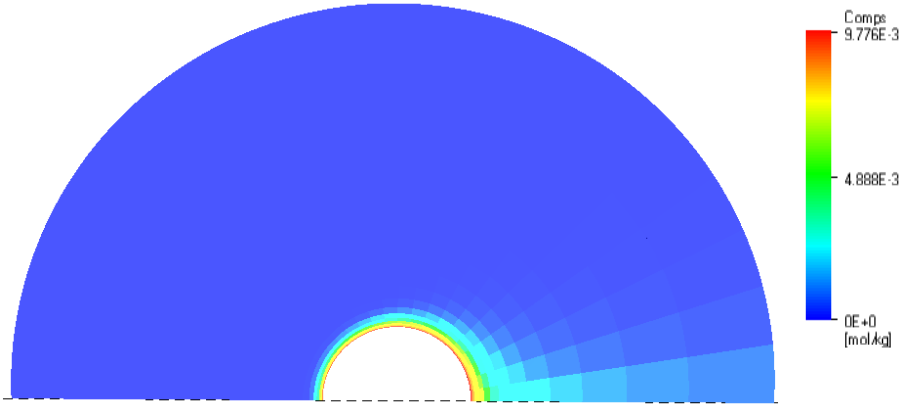

Figure 6: Distribution of sodium in the fracture for a water velocity of 31.5m/y. (The limits on the axis are $r < 5$ m.)

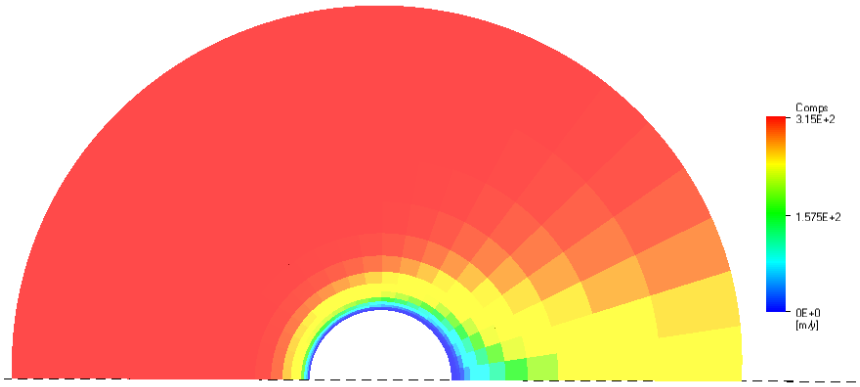

Figure 7: Hydraulic conductivity in the fracture for a water velocity of 31.5 m/y

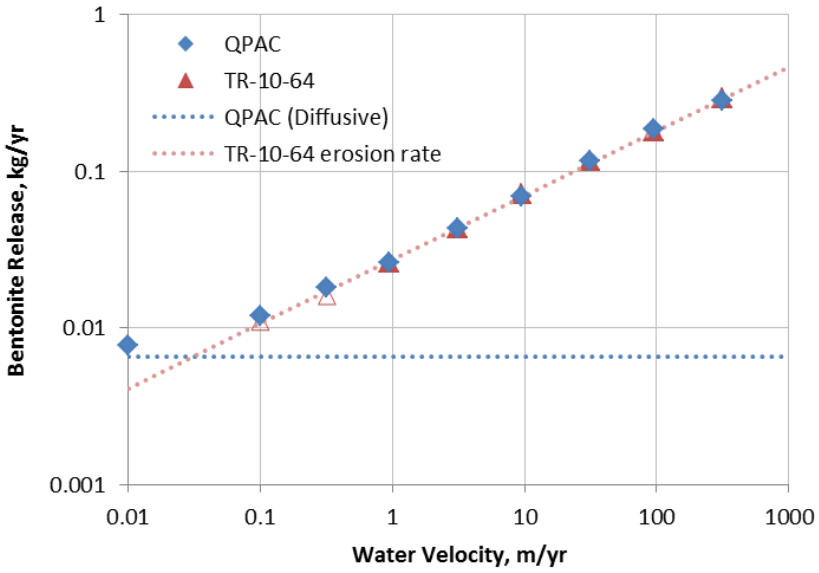

Figure 8: Smectite release for different water velocities; comparison of the results calculated using QPAC and those quoted in TR-10-64. The values shown as hollow triangles were obtained in the modelling in TR-10-64 by extrapolation. The curve labelled "QPAC (Diffusive)" results from setting a zero flow velocity in the model.

Table 2: The smectite release for different water velocities; comparison of the results calculated using QPAC and those quoted in TR-10-64

Water velocity (m/yr)	Smectite release (kg/yr) QPAC	TR-10-64
0	0.0066	Not reported
0.10	0.012	0.011 (extrapolated)
0.32	0.018	0.016 (extrapolated)
0.95	0.026	0.026
3.15	0.043	0.043
9.45	0.069	0.071
31.50	0.117	0.117
94.50	0.184	0.180
315.0	0.280	0.292

Also shown in Figure 8 is the flux of bentonite across the deposition hole boundary that arises when setting the flow rate to zero, which is labelled as "QPAC (Diffusive)". This corresponds to a purely diffusive release of bentonite into the fracture and so might not be considered a genuine erosion rate, but is the limiting bentonite flux out of the deposition hole in the current model for slow flow rates.

This result contrasts with the extrapolated results for slow flow rates in TR-10-64, which are shown here as hollow triangles and which suggest that the flux of bentonite from the deposition hole tends to zero as the flow rate in the fracture tends to zero. Since the diffusivity χ/f_{fr} in the model does not tend to zero with the flow rate (it tends to the standard Einstein-Stokes diffusivity), it is not expected that the true limit of the erosion rate will be zero in the SKB model as groundwater velocities tend to zero. It may therefore be the case that the interpolated erosion rate adopted by SKB may tend to underestimate rates of erosion for very slow flows, although more work would be required to confirm this.

The calculated smectite release is sensitive to the value used for *h*, the particle separation. As noted earlier, we have taken *h* to be a constant value, consistent with the way that it is presented in TR-10-64, although TR-09-35 represents *h* as a function of the smectite volume concentration (but does not report the necessary parameter values to use the function).

In the current model, a value of h =2.85e-8 m was found to provide a good fit to the results in TR-10-64 for the water velocity of 31.5 m/y (and subsequently was found to fit the range of erosion rates for different flow velocities- Figure 8). Figure 9 shows the dependence of the smectite release on the value chosen for *h*, when the water velocity is fixed at 31.5 m/yr. The calculated release varies from 1.6 kg/y to 0.1 kg/y as *h* varies from 1e-9 m to 3e-8 m. When *h* is less than 1e-8 m the calculated bentonite release increases rapidly as *h* decreases.

The calculated smectite release is also dependent on the assumed relative permittivity (ε_r), which was also not reported in TR-10-64 and so a value of 80 was assumed in the current model (the relative permittivity of water at 25 °C). Sensitivity of the bentonite release to this parameter is shown in Figure 10 when a flow rate of 31.5 m/y is assumed with a constant particle separation of *h* = 2.85e-8 m.

The sensitivity of the model to the exterior sodium concentration was also assessed. Reducing the external concentration by two orders of magnitude (to 0.001 mM) resulted in an almost identical amount of erosion as the base case.

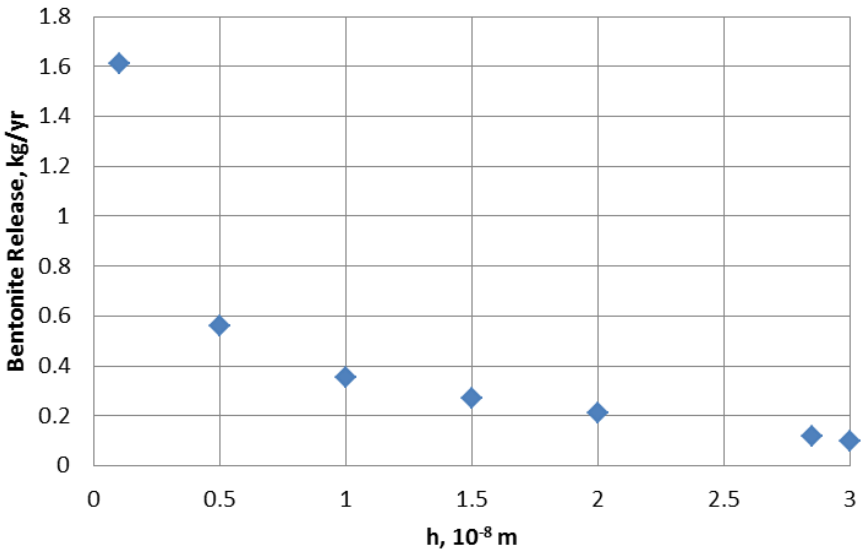

Figure 9: The dependence of the bentonite release on *h* (distance between particles) for a water velocity of 31.5 m/y

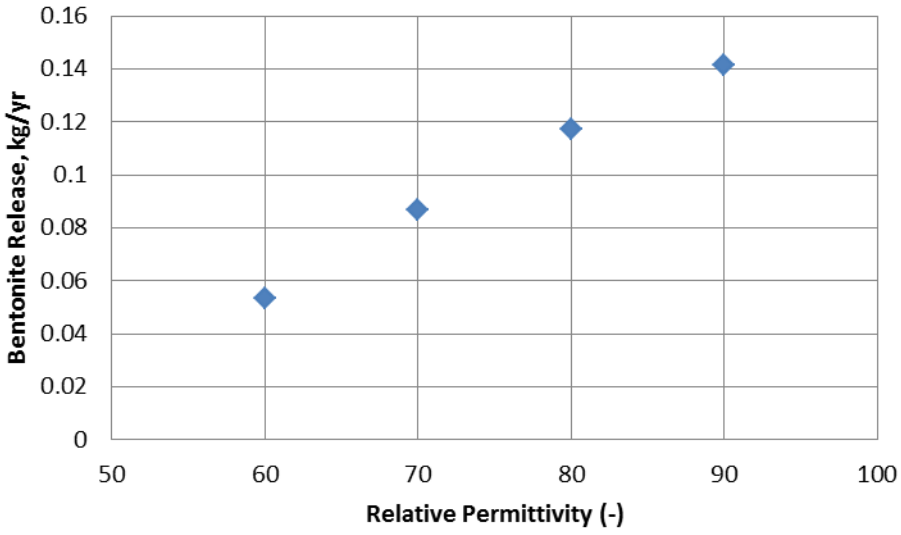

Figure 10: The dependence of the bentonite release on the relative permittivity (ε_r) for a water velocity of 31.5 m/y and *h* = 2.85e-8 m.

As noted above, the bentonite 'plume' in the fracture is smaller in the independent model than in SKB's model in TR-10-64 (as can be seen in Figure 4 and Figure 5). It might be expected that increasing the diffusion coefficient would lead to a larger plume and so the model was modified to introduce an arbitrary scaling to the

diffusion coefficient (χ/f) for the bentonite. shows the effect on the erosion rate of scaling the diffusivity for a water velocity of 31.5m/y when the 'best fit' h = 2.85e-8 m value is used, while Figure 12 shows the corresponding effect on the plume when the diffusivity is scaled by a factor of 25. Clearly the scaling has little effect on the plume size, but the erosion rate increases (very approximately linearly) with the square root of the diffusivity scaling factor.

These results suggest that the increased transport of bentonite due to the arbitrary increase in the diffusion simply leads to a more rapid rate at which bentonite is introduced to the fracture that is immediately balanced by the erosive removal by advection in the groundwater. To reduce the rate of erosion, the rate of advection would therefore need to be decreased local to the deposition hole as the bentonite fraction in the fracture increases. This is represented in the model in the increase in viscosity as the bentonite volume fraction increases in the fluid, but the magnitude of this factor was already shown to be in broad agreement with the corresponding values used by SKB in Figure 2.

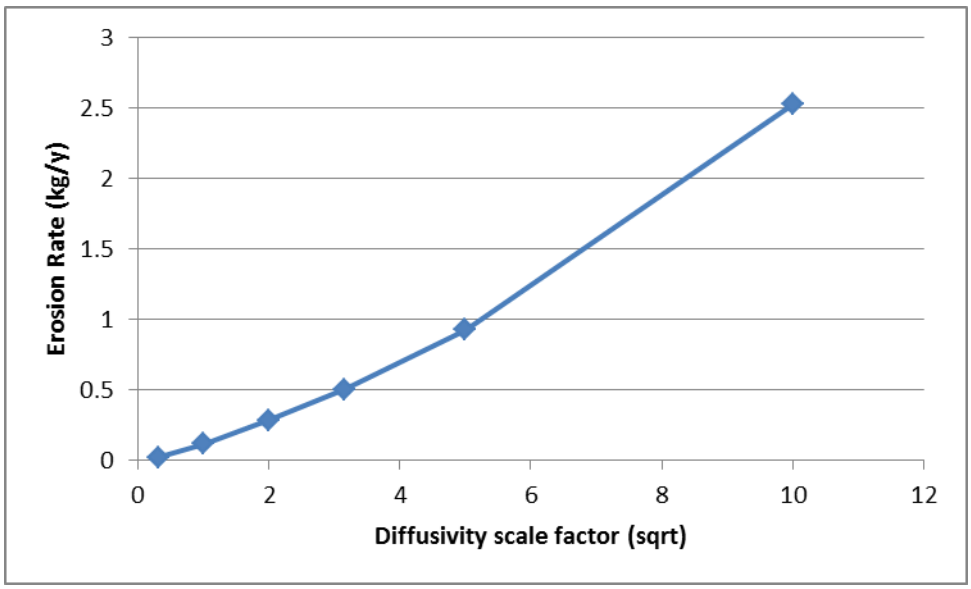

Figure 11 Effect on erosion rate of arbitrarily scaling the diffusivity (χ/f) for bentonite for a water velocity of 31.5m/y. (Note X-axis is the square root of the scaling factor)

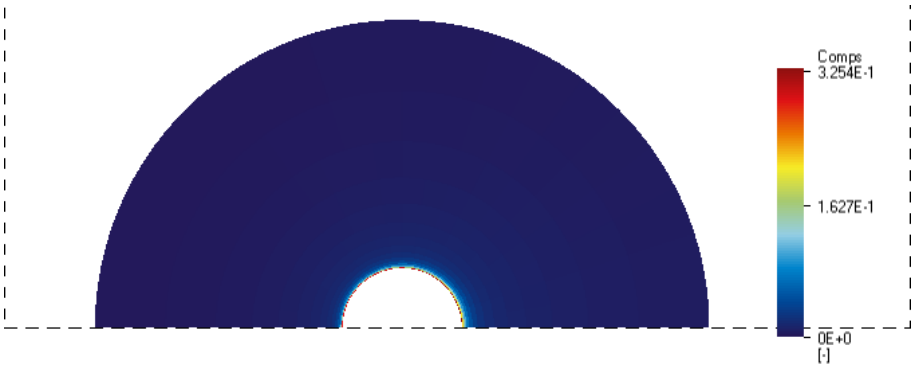

Figure 12 Smectite volume fraction distribution for a water velocity of 31.5m/y when the diffusivity (χ/f) is arbitrarily scaled by a factor of 25. (The limits on the axis are r<5 m.)

$h = h(\phi)$ case

When the $h = h(\phi)$ form is used for the particle separation parameter, the value of the $\phi_{\max}$ parameter is required to complete the parameterisation. As noted earlier, a value for this parameter could not be found in TR-09-35 (the form itself is not mentioned in TR-10-64). A representative value of $\phi_{\max} = 0.9$ has been used. It is expected that results should be relatively insensitive to this choice since, by maximum principles, the value of ϕ in the model is not expected to exceed 0.4 due to the choice of boundary conditions that are used.

The values of the diffusivity χ/f_{fr} that arise in the model are plotted as a function of ϕ in Figure 13. The reason for the sparsity of the plot is that for the chosen output times in the model there are no output data points with values of ϕ in the range [0.04,0.2]. The computed values can be compared with the plots of χ/f_{fr} for constant values of the sodium ion concentration in TR-09-35, Figure 8-4, which is copied in Figure 14.

From these graphs it would seem that the values of the diffusivity computed in the current model with $h = h(\phi)$ are a factor of approximately 20 times too large. If all other factors in the models were equal, this difference would tend to imply that the current model should exhibit a faster rate of penetration of the gel into the fracture than the corresponding model in the SKB reports and, presumably, a faster rate of release of bentonite. However this is not the case and in fact for the 31.5 m/y flow rate, the bentonite release rate is 0.0117 kg/y, compared to 0.117 kg/y in the corresponding simulation in TR-10-64. The factor of 10 difference between these rates of release possibly suggests that the models may differ by a factor of 10 error in one of the other parameters in the model, but this is not consistent with the factor of 20 difference in the χ/f_{fr} values.

Figure 15 shows the erosion rates computed with the $h = h(\phi)$ version of the independent model superimposed in the erosion rates reported by SKB in TR-10-64 and TR-09-35 (which were shown in Section 2, Figure 1). The independent model provides a good fit to the erosion rates shown in TR-09-35, Figure 9-6, although as was discussed in Section 2, these results differ from those reported in TR-10-64 by around an order of magnitude, but no discussion of this difference was found in TR-10-64 (and also differ from those that are reported in TR-09-35, Table 9-2).

Further attempts have been made to identify the source of any other differences in the models that might explain the differences, but these have been unsuccessful. More details of the precise formulation used in the modelling in TR-10-64 are needed in order to identify the differences.

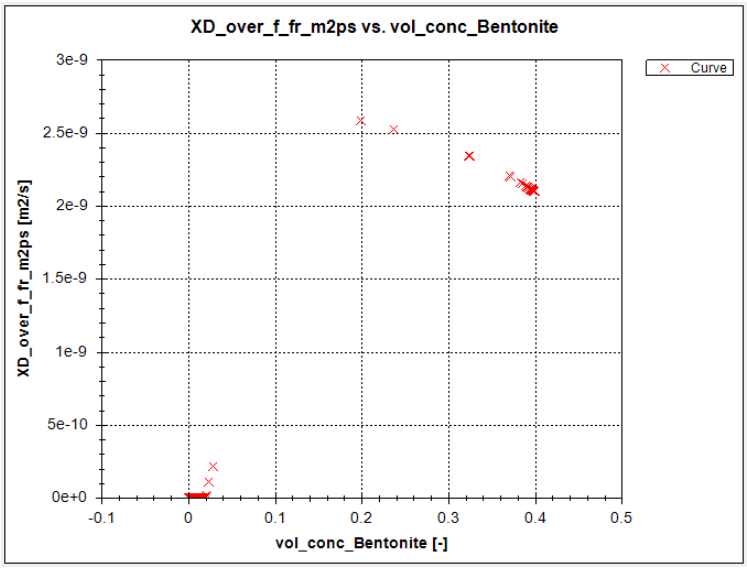

Figure 13 Values of χ/f_{fr} that arise in the model when the smectite particle separation $h = h(\phi)$ is used, with $\phi_{max} = 0.9$.

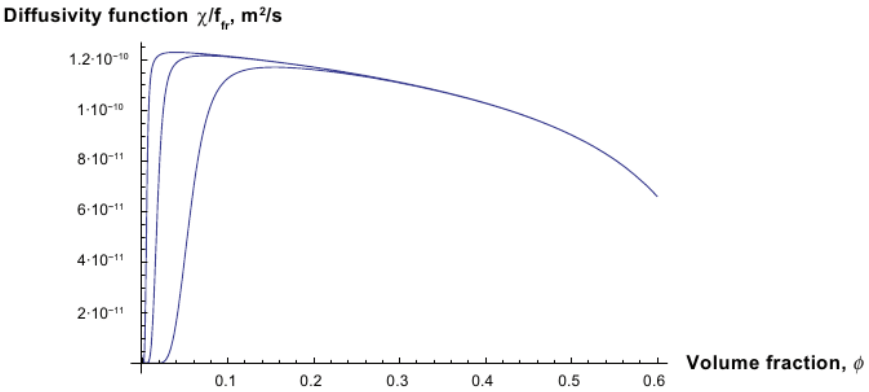

Figure 14 Values of χ/f_{fr} for particle diameter 175 nm and thickness 1 nm for sodium ion concentrations of 10, 1, 0.1 mM (left to right). (copy of TR-09-35, Figure 8-4)

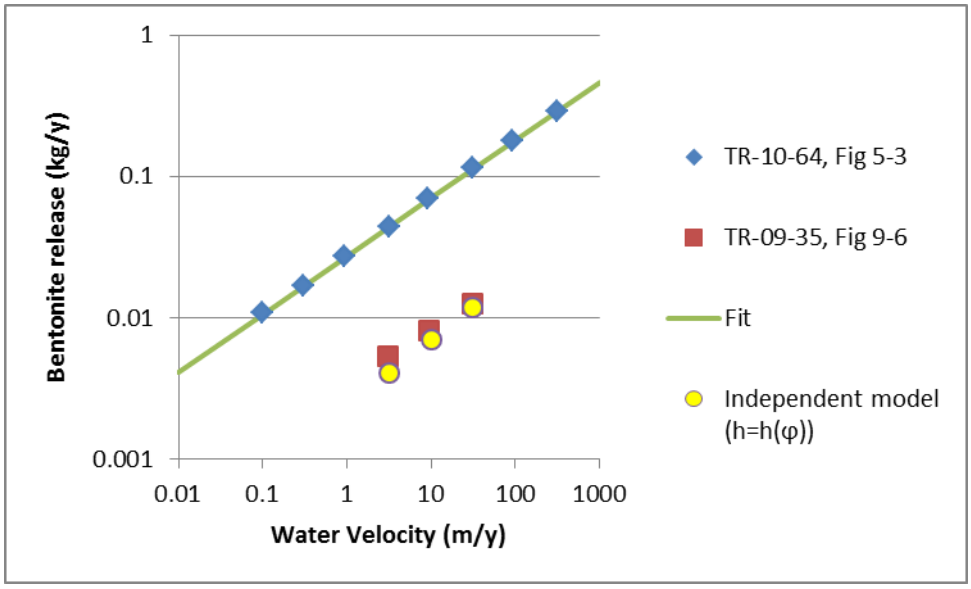

Figure 15 Erosion rates predicted by models in TR-10-64 and TR-09-35, and the corresponding erosion rates computed by the independent model when the $h = h(\phi)$ form is used (yellow circles).

Summary

An attempt has been made to reproduce the detailed erosion model documented in TR-10-64, which is the basis for the simplified erosion model used in the deposition hole erosion calculations, and subsequent canister corrosion calculations, in TR-10-66.

It was found that TR-10-64 and the supporting documents (mostly TR-09-35) do not appear to list the full set of input parameters that are needed to describe the model. In particular, the representation of the particle separation parameter h in the model is not clear. In TR-10-64 the presentation of the model suggests that h is a (constant) input parameter to the model, whereas in TR-09-35 it would appear that this parameter is derived from the bentonite volume fraction ϕ, but the additional parameter $\phi_{\max}$ that is needed to parameterise the $h = h(\phi)$ model is not given.

Despite the missing input data, it was possible to achieve a good match to the bentonite erosion model as a function of the groundwater velocity in the fracture by fitting a constant value of h to SKB's result in TR-10-64 for a flow rate of 31.5 m/y. This fitted model was then found to also provide a very good match to SKB's erosion rates at a range of flow rates.

The fitted model highlighted a possible inconsistency in SKB's simplified fit to the erosion rate at low flow rates; the lowest flow rate results in TR-10-64 were obtained by extrapolation rather than by direct modelling. The independent modelling suggests that (according to the detailed model) the erosion rate would not tend to zero as the flow rate tended to zero.

It is noted that the 'plume' of bentonite entering the fracture did not provide a good match in the models despite the good agreement in the erosion rates that are calculated by the model.

A version of the independent model was run using the $h = h(\phi)$ form for the particle separation by taking a nominal value for the missing $\phi_{\max}$ input value. The 'diffusivity' χ/f that arises in the model was found to be around 20 times larger than the corresponding diffusivity reported in TR-09-35, but the erosion rates calculated by the model were almost exactly 0.1 times the erosion rates calculated by SKB in TR-10-64 (the basis for the simplified erosion rate). However the results did agree very well with data that is graphed in TR-09-35, Figure 9-6 (but differs from the data that is tabulated in TR-09-35, Table 9-2, which appears to be an inconsistency in the report).

Thus there is a seeming inconsistency between the model developed here and SKB's model described in TR-10-64 that it has not been possible to resolve using the available documentation in the primary references TR-10-64 and TR-09-35.

SKB derived the power law relationship

$$R_{Erosion} = A_{ero}\delta v^{0.41} \qquad \text{(TR-10-66, Eqn. 4-20)}$$

(where δ is the fracture aperture, v is the water velocity and the constant $A_{ero} = 27.2$ when the velocity is given in m/y and the buffer erosion rate is given in kg/y) from the modelling presented in TR-10-64 for use in their probabilistic erosion/corrosion calculations. It is noted that this form of the power law relationship can be reproduced in the independent model (with h constant), although its precise parameterisation can only be reproduced by fitting one of the data values. To be precise, the power (0.41) is reproduced in the current model but the constant $A_{ero} = 27.2$ is only obtained through fitting the independent model to one of the outputs of SKB's model.

References

SKB Reports

TR-10-64: Moreno L, Neretnieks I, Lui L, 2010. Modelling of erosion of bentonite gel by gel/sol flow. SKB TR-10-64, Svensk Kärnbränslehantering AB.

TR-09-35: Neretnieks I, Liu L, Moreno L, 2009. Mechanisms and models for bentonite erosion. SKB TR-09-35, Svensk Kärnbränslehantering AB.

Other* Reports *and Papers

Liu L, Moreno L, and Neretnieks I (2009). A Dynamic Force Balance Model for Colloidal Expansion and Its DLVO-Based Application. Langmuir, 25, pp 679-687.

Quintessa Limited (2013). QPAC: Quintessa's General-Purpose Modelling Software. QRS-QPAC-11.

Appendix E: Further Checking of SR-Site Erosion and Failure Timescales

Introduction

Results for the 'canister failure due to corrosion scenario' are presented in TR-11-01 and TR-10-50. TR-11-01 gives details of the number of eroded locations in the semi-correlated, fully-correlated and uncorrelated DFN scenarios, while TR-10-50 gives details of locations that fail due to erosion. Independent analysis that has been undertaken to attempt to verify these results is presented in the following sections.

Comparison of mean numbers of advective positions at 10^5 and 10^6 y (TR-11-01, Figure 12-4)

Mean numbers of advective positions at 10^5 and 10^6 y have been calculated for the semi-correlated, correlated and uncorrelated DFN scenarios for comparison with the results presented by SKB in TR-11-01, Figure 12-4.

Ten realisations of the semi-correlated DFN and three realisations of each of the correlated and uncorrelated DFN were provided for use in the independent modelling (Appendix A). Ten realisations of the semi-correlated DFN were also used in the SKB analysis. However, Section 13.5.3 of TR-11-01 states that 5 realisations were used in the SKB analysis for each of the correlated and uncorrelated DFN scenarios. Therefore we do not expect a perfect match with the results presented by SKB for the correlated and uncorrelated DFN scenarios, but nevertheless the results would be expected to be similar.

The mean numbers of advective positions at 10^5 and 10^6 y calculated in the SKB analysis and independent analysis for each of the DFN scenarios are shown in Table 1.

Perfect agreement is seen between the SKB and independent analysis for the semi-correlated DFN scenario (to the precision reported by SKB).

As noted above, a perfect match is not seen for the correlated and uncorrelated DFN scenarios since a different number of realisations was used in the SKB and

independent analyses. However the results are close with the mean number of advective positions at 10^5 y in the independent analysis being 1.66 and 1 in the uncorrelated and fully-correlated cases respectively, compared to 1.2 in both cases in the SKB analysis. At 10^6 y the corresponding numbers from the independent analysis are 283.66 and 67.33 for the uncorrelated and fully-correlated cases respectively compared to 280 and 68 in the SKB analysis.

The results from the uncorrelated and fully-correlated cases lend confidence that the 3 realisations used in the independent analysis are consistent with (and possibly a subset of) the 5 cases used in the SKB analysis.

Table 1 Mean numbers of advective positions at 10^5 and 10^6 y calculated in the SKB and independent analysis for each of the three DFN scenarios

	SKB analysis – Mean number of advective positions		Independent analysis – Mean number of advective positions	
	At 10^5 y	At 10^6 y	At 10^5 y	At 10^6 y
Uncorrelated	1.2	280	1.66	283.66
Semi-correlated	0.6	19	0.6	18.5
Fully-correlated	1.2	68	1	67.33

Lists of all of the eroded locations in each of the DFN realisations that were used in the independent analysis are provided in the following spreadsheets, which accompany this report:

- ErosionSummary_Uncorrelated_x3.xlsx (851 locations)
- ErosionSummary_Semicorrelated_x10.xlsx (185 locations)
- ErosionSummary_Fullycorrelated_x3.xlsx (202 locations)

Comparison of failed locations from the ten realisations of the semi-correlated DFN (TR-10-50, Table 4-3)

Table 2 shows the calculated times for canister failure up to 10^6 y in the ten realisations of the semi-correlated DFN model calculated by SKB (taken from TR-10-50, Table 4-3) and calculated in the independent analysis. The calculations are shown side-by-side and are ordered by failure time.

The independent analysis assumes that all locations have the maximum sulphide concentration of [HS-] = 1.2e-4 mol/kg. It does not appear to be stated in TR-10-50 whether the SKB analysis makes the same assumption, however the level of agreement between the analyses, which is described further below, suggests that SKB also assumed a maximal sulphide concentration, rather than being sampled from the distribution of concentrations.

The SKB analysis results in 56 failed locations across the ten realisations, whereas the independent analysis results in 27 failed locations.

All of the 27 failed locations in the independent analysis are found to match with a subset of the results calculated by SKB to within 0.05% relative agreement in failure time. In each of these cases the flow rate, q (m^3/y), is found to agree exactly to the 3 s.f. reported by SKB, which lends confidence that the calculations implemented in the independent analysis faithfully repeat those performed by SKB[8].

The 6 locations in the ten realisations that were found to be eroded within the first 10^5 y, leads to a mean number of advective locations of 0.6, which agrees with the result presented by SKB in TR-11-01, Figure 12-4 (see previous section).

It is noted that the matching results between the analyses contain a range of cases for which Q_{eq} is given by both sides of the limit specified in equation (2-8). This suggests that the calculation of q_{lim} and Q_{eq} is correctly implemented in the independent analysis scripts and that calculation of these quantities cannot therefore be the reason for any differences. Also the matching results include cases from all of the realisations of the semi-correlated DFN except r9, suggesting that at least 9 of the realisations that were used in the independent analysis are identical to those used by SKB.

The question that naturally arises from the results is why there are 29 failed locations that appear in the SKB analysis that do not appear in the independent analysis.

[8] It is noted that the erroneous form for the V_{zone}parameter (Section 2.8) is implemented in the independent analysis in this section, in contrast to the analysis in Section 2.

Table 2 Calculated times for canister failure in the ten realisations of the semi-correlated DFN model ordered by failure time. Left-hand block: SKB analysis from TR-10-50, Table 4-3; Central block: Independent analysis (Column # provides the realisation number); Right-hand block: Relative difference in calculated times for canister failure. Shading: Green indicates identification of matching SKB and independent calculation result; Red shows results for locations where erosion occurs before 10^5 y.

TR-10-50 Table 4-3				Independent Analysis									Check
Time of failure (y)	Rock transport resistance, F (yr/m)	Advective travel time, t_w (yr)	Advective flow, q (m3/yr)	#	DFN hole ID	Qeq (m3/y)	q_eb > q_lim	q_eb (m3/y)	Erosion time (y)	Sulphide conc. (mol/kg)	Corrosion time (y)	Failure time (y)	Failure time rel. diff. (%)
114,485	53,660	6	0.733	r12	396	0.360363	1	0.732725	70,464	0.00012	44,032	114,497	0.010
122,557	564,900	61	0.557	r7	400	0.314052	1	0.5565	72,041	0.00012	50,526	122,567	0.008
132,155	14,510	23	0.267	r8	6485	0.217482	1	0.266875	59,191	0.00012	72,961	132,152	0.002
157,452	26,260	7	0.358	r12	395	0.251969	1	0.358225	94,491	0.00012	62,975	157,466	0.009
157,805	642,100	78	0.316	r7	401	0.236803	1	0.3164	90,808	0.00012	67,008	157,816	0.007
179,621	87,820	14	0.251	r3	2026	0.21104	1	0.2513	104,447	0.00012	75,188	179,635	0.008
201,037	89,910	17	0.144	r1	1978	0.143973	0	0.143973	90,919	0.00012	110,213	201,132	0.047
230,828	818,600	38	0.148	r1	411	0.14826	0	0.14826	123,909	0.00012	107,026	230,935	0.046
305,884	33,970	16	0.082	r1	6875	0.081778	0	0.081778	111,999	0.00012	194,035	306,034	0.049
313,807	33,140,000	2,501	0.079	r3	400	0.079328	0	0.079328	113,934	0.00012	200,027	313,961	0.049
361,884	2,184,000	124	0.083	r12	4762	0.083055	0	0.083055	171,005	0.00012	191,050	362,055	0.047
377,494	38,170	14	0.095	r7	6647	0.09492	0	0.09492	210,499	0.00012	167,169	377,668	0.046
391,981	24,220,000	2,021	0.06	r3	399	0.060008	0	0.060008	127,747	0.00012	264,428	392,175	0.050
402,471	157,900	19	0.086	r7	6561	0.086328	0	0.086328	218,850	0.00012	183,808	402,657	0.046
442,257	155,100	19	0.075	r7	6559	0.075233	0	0.075233	231,548	0.00012	210,915	442,463	0.047
471,801	163,400	29	0.067	r5	4719	0.067253	0	0.067253	236,081	0.00012	235,942	472,022	0.047
480,309	25,290,000	2,070	0.047	r3	398	0.046795	0	0.046795	141,460	0.00012	339,089	480,549	0.050
504,166	53,660	6	0.733					(no match)					
521,967	24,830,000	1,994	0.042	r3	401	0.042333	0	0.042333	147,394	0.00012	374,834	522,228	0.050
526,759	116,600	241	0.05	r6	3048	0.050033	0	0.050033	209,866	0.00012	317,147	527,014	0.048

TR-10-50 Table 4-3				Independent Analysis									Check
Time of failure (y)	Rock transport resistance, F (yr/m)	Advective travel time, t_w (yr)	Advective flow, q (m3/yr)	#	DFN hole ID	Qeq (m3/y)	q_eb > q_lim	q_eb (m3/y)	Erosion time (y)	Sulphide conc. (mol/kg)	Corrosion time (y)	Failure time (y)	Failure time rel. diff. (%)
531,274	53,660	6	0.733					(no match)					
569,225	53,660	6	0.733					(no match)					
569,701	564,900	61	0.557					(no match)					
595,478	53,660	6	0.733					(no match)					
600,806	564,900	61	0.557					(no match)					
612,248	471,800	31	0.048	r7	6646	0.047618	0	0.047618	279,308	0.00012	333,232	612,539	0.048
612,252	53,660	6	0.733					(no match)					
644,354	564,900	61	0.557					(no match)					
652,328	211,100	20	0.044	r7	6560	0.04368	0	0.04368	289,368	0.00012	363,271	652,639	0.048
674,477	564,900	61	0.557					(no match)					
693,725	564,900	61	0.557					(no match)					
705,692	1,710,000	99	0.033	r8	399	0.033303	0	0.033303	229,570	0.00012	476,471	706,041	0.049
714,768	26,260	7	0.358					(no match)					
750,814	642,100	78	0.316					(no match)					
753,537	26,260	7	0.358					(no match)					
777,848	14,510	23	0.267					(no match)					
792,067	642,100	78	0.316					(no match)					
803,247	11,330	20	0.035	r10	4938	0.035123	0	0.035123	351,850	0.00012	451,781	803,631	0.048
807,815	26,260	7	0.358					(no match)					
822,765	14,510	23	0.267					(no match)					
845,022	87,820	14	0.251					(no match)					
845,360	26,260	7	0.358					(no match)					
849,820	642,100	78	0.316					(no match)					

TR-10-50 Table 4-3				Independent Analysis									Check
Time of failure (y)	Rock transport resistance, F (yr/m)	Advective travel time, t_w (yr)	Advective flow, q (m3/yr)	#	DFN hole ID	Qeq (m3/y)	q_eb > q_lim	q_eb (m3/y)	Erosion time (y)	Sulphide conc. (mol/kg)	Corrosion time (y)	Failure time (y)	Failure time rel. diff. (%)
869,351	26,260	7	0.358					(no match)					
885,650	14,510	23	0.267					(no match)					
889,770	642,100	78	0.316					(no match)					
891,310	87,820	14	0.251					(no match)					
893,681	53,660	6	0.733					(no match)					
901,874	9,083,000	601	0.026	r1	401	0.02555	0	0.02555	281,278	0.00012	621,044	902,322	0.050
915,297	642,100	78	0.316					(no match)					
918,487	2,008,000	135	0.024	r8	400	0.02415	0	0.02415	261,900	0.00012	657,046	918,946	0.050
929,149	14,510	23	0.267					(no match)					
941,008	61,400	18	0.032	r4	5283	0.032253	0	0.032253	449,470	0.00012	491,983	941,453	0.047
956,114	87,820	14	0.251					(no match)					
956,944	14,510	23	0.267					(no match)					
978,463	3,845,000	91	0.033	r6	6461	0.03346	0	0.03346	504,692	0.00012	474,228	978,920	0.047
												Max % diff:	**0.050**

Investigations that did not reveal a possible reason for the different calculated number of failed locations

Initial investigation of the differences in the number of failed locations calculated in the independent and SKB analysis focussed on features of the model that could have been implemented inconsistently in the separate analyses. Ultimately this investigation did not reveal a possible cause for the difference. A record of the investigation is repeated here for completeness, since some of the results are possibly interesting in their own right.

One potential cause of the difference is the implementation of the deposition hole rejection criteria. Table 3 shows the calculated times for canister failure up to 300,000 y from the independent analysis when the T/L rejection criteria (TR-11-01, Section 5.2.3) are not applied. The transmissivity / fracture length (T/L) rejection criteria causes deposition holes with intersecting fractures of length greater than 250 m whose transmissivity is greater than 10^{-6} m^2/s to be rejected. Its omission is likely to lead to fewer additional failed locations than if the FPC or EFPC rejection criteria were omitted. Not applying the T/L rejection criteria in the analysis leads to 8 additional failed locations. All of the additional failed locations fail within 125,000 y (7 occur within 100,000 y) and all of which are eroded in less than 40,000 y. None of these new results match with any calculated by SKB. 5 of the new locations that are introduced are from realisation r9, which was the only realisation that did not provide a matching result in the original analysis (see above). Thus a potentially different implementation of the T/L rejection criteria in the SKB and independent analyses would not appear to explain the difference between the analyses.

(NB. When the T/L criteria are not included, the mean number of locations becoming advective in the first 10^5 y rises from 0.6 to 1.4.)

A separate analysis was run on all of the 31 DFN model outputs that were supplied (Appendix A), which includes other DFN models than the semi-correlated, fully-correlated and uncorrelated cases considered in TR-11-01, Figure 12-4 and TR-10-50, Table 4-3. This analysis was performed in order to check whether any other DFN outputs were mistakenly included in the SKB analysis of the semi-correlated DFN model in TR-10-50, Table 4-3 (i.e. whether the SKB semi-correlated analysis included contributions from non-semi-correlated cases). The calculations were run with all of the deposition hole rejection criteria (FPC, EFPC and T/L) disabled in case this was the cause of the disagreement. This naturally leads to a greater number of locations that would experience complete erosion and corrosion, with 2848 locations being identified in total across all 31 realisations.

The 2848 locations identified were analysed to see if any of these agreed with the first non-matching SKB result from the original analysis, which is the location identified as failing at 504,166 y. 19 cases were found to fail in the range 500,000 to 510,000, which would be expected to contain the independent analysis result corresponding to the SKB result at 504,166 y if it were present, given that less than 0.05% disagreement in failure times was seen in the original analysis. However, none of the independent results provided a match to the corresponding q_{eb} reported by SKB of 0.733 m^3/y, whereas a perfect match (to 3 d.p.) to the q_{eb} values was found in the original analysis. Moreover, only one of the 2848 results has a

$q_{eb} = 0.733$ m^3/y to 3d.p.. This is location #396 from semi-correlated case r12 ($q_{eb} = 0.732725$m^3/y), which is already listed as a failing case from the original analysis (Table 2 – it is the first case).

Thus it can be concluded that the additional failed locations in the SKB analysis of the semi-correlated DFN case in TR-10-50, Table 4-3 do not arise as a consequence of the inclusion of the additional sets of DFN results that were available in the independent analysis, or as a result of the erroneous implementation of the deposition hole rejection criteria in the independent analysis.

Table 3 Calculated times for canister failure up to 300,000 y when the T/L criteria are not included, for the ten realisations of the semi-correlated DFN model ordered by failure time. Left-hand block: SKB analysis from TR-10-50, Table 4-3; Central block: Independent analysis (Column # provides the realisation number); Right-hand block: Relative difference in calculated times for canister failure. Shading: Green indicates identification of matching SKB and independent calculation result; Red shows results for locations where erosion occurs before 10^5 y; Blue shows the 8 additional erosion cases before 100,000 y that arise when the T/L criteria is not included (other than these additional rows, the table is identical to Table 2.

TR-10-50 Table 4-3				Independent Analysis									Check
Time of failure (y)	Rock transport resistance, F (yr/m)	Advective travel time, t_w (yr)	Advective flow, q (m3/yr)	#	DFN hole ID	Qeq (m3/y)	q_eb > q_lim	q_eb (m3/y)	Erosion time (y)	Sulphide conc. (mol/kg)	Corrosion time (y)	Failure time (y)	Failure time rel. diff. (%)
				r9	3304	0.543498	1	1.6667	17,115	0.00012	29,195	46,311	
				r12	2140	0.480917	1	1.304975	15,677	0.00012	32,995	48,671	
				r12	2138	0.432354	1	1.054725	17,107	0.00012	36,701	53,807	
				r12	2139	0.432354	1	1.054725	17,107	0.00012	36,701	53,807	
				r9	5584	0.41008	1	0.94885	21,562	0.00012	38,694	60,256	
				r9	5601	0.402715	1	0.915075	21,885	0.00012	39,402	61,287	
				r9	5600	0.351386	1	0.696675	24,474	0.00012	45,157	69,631	
114,485	53,660	6	0.733	r12	396	0.360363	1	0.732725	70,464	0.00012	44,032	114,497	0.010
				r9	5583	0.193242	1	0.2107	39,961	0.00012	82,113	122,074	
122,557	564,900	61	0.557	r7	400	0.314052	1	0.5565	72,041	0.00012	50,526	122,567	0.008
132,155	14,510	23	0.267	r8	6485	0.217482	1	0.266875	59,191	0.00012	72,961	132,152	0.002
157,452	26,260	7	0.358	r12	395	0.251969	1	0.358225	94,491	0.00012	62,975	157,466	0.009
157,805	642,100	78	0.316	r7	401	0.236803	1	0.3164	90,808	0.00012	67,008	157,816	0.007
179,621	87,820	14	0.251	r3	2026	0.21104	1	0.2513	104,447	0.00012	75,188	179,635	0.008
201,037	89,910	17	0.144	r1	1978	0.143973	0	0.143973	90,919	0.00012	110,213	201,132	0.047
230,828	818,600	38	0.148	r1	411	0.14826	0	0.14826	123,909	0.00012	107,026	230,935	0.046
							…						
(Table then continues identically to Table 2***)***													

Investigations that reveal a possible reason for the different calculated number of failed locations

Inspection of the SKB results that were found to not match with any in the independent analysis suggests that identical copies of some of the realisation locations that do match with the independent analysis appear multiple times in the table with different failure times. For example, the location with the earliest failure time (114,485 y), for which a perfect match with the independent analysis is obtained, has the 'parameter set' F=53,660 y/m, t_w=6 y and q=0.733 m^3/y. This same set of F, t_w and q parameters appears in 6 other rows, with failure times of 504,166, 531,274, 569,225, 595,478, 612,252 and 893,681 y, which do not match with the independent analysis.

The collection of location parameter sets that appear multiple times in the SKB failure analysis are listed in Table 4. There are 6 such parameter sets, which lead to an additional 29 failure instances. Thus these cases account for all of the additional failure cases in the SKB analysis that did not appear in the independent analysis. The 6 parameter sets correspond to the first 6 failed locations identified in the failure analysis (i.e. the first 6 rows in Table 2).

It is not clear why these 6 parameter sets appear multiple times in the SKB analysis. It would appear unlikely that exactly the same flow rate would arise in different sampled realisations so many times. For example, the analysis described above, where the calculations were repeated with all rejection criteria disabled, showed that only one location in one of the 31 DFN realisations provided a case where q=0.733 m^3/y (the value of q in the first of the 6 parameter sets). Therefore, the most likely explanation would seem to be that the same locations in the same realisations have been considered multiple times in the SKB analysis, with different failure times resulting each time. The only quantities in the analysis that could lead to different failure times for the same flow conditions are if a different fracture aperture was assumed (leading to a different time scale for erosion) or if a different sulphide concentration was assumed (leading to a different time scale for corrosion), since all of the other parameters in the analysis are constant across all cases. It is suspected that the difference most likely arises due to the inclusion of cases with different groundwater sulphide concentrations in SKB's analysis, since only the maximum sulphide concentration considered by SKB (0.00012 mol/kg) was considered in the independent analysis. However, since neither of these quantities is reported in TR-10-50 Table 4-3, it is difficult to determine if this is the cause of the 'repeats' or if they are caused by some other explanation.

Table 4 The six location 'parameter sets' that appear multiple times in the SKB failure analysis

Location parameters			# Matches with independent analysis	# Additional occurrences in SKB analysis	Realisation and location in independent analysis
F (y/m)	t_w (y)	q (m^3/y)			
53,660	6	0.733	1	6	r12, 396
564,900	61	0.557	1	5	r7, 400
14,510	23	0.267	1	5	r8, 6485
26,260	7	0.358	1	5	r12, 395
642,100	78	0.316	1	5	r7, 401
87,820	14	0.251	1	3	r3, 2026
				29	

Summary of failed locations from all realisations of the semi-correlated, uncorrelated and fully-correlated DFN scenarios in the independent analysis

The complete list of all 27 corrosive failure locations for the 10 realisations of the semi-correlated DFN model in the independent calculations, which were compared with the corresponding SKB results in the previous section, are listed in Table 5.

The similar results for the 71 corrosive failure locations from the 3 realisations of the fully-correlated DFN and 73 failed locations from the 3 realisations of the uncorrelated DFN are provided in Table 6 and Table 7 respectively. Corresponding tables were not presented by SKB for these cases, so it is not possible to perform a direct comparison.

Table 5 The 27 corrosive failure locations from the 10 realisations of the semi-correlated DFN, ordered by failure time. (Also shown in Table 2, where the results are compared with those presented by SKB)

Realisation	DFN hole ID	Qeq (m3/y)	q_eb > q_lim	q_eb (m3/y)	Erosion time (y)	Sulphide (mol/kg)	Corrosion time (y)	Failure time (y)
r12	396	0.360363	1	0.732725	70,464.32	0.00012	44,032.49	114,496.82
r7	400	0.314052	1	0.5565	72,041.46	0.00012	50,525.56	122,567.02
r8	6485	0.217482	1	0.266875	59,190.99	0.00012	72,960.84	132,151.83
r12	395	0.251969	1	0.358225	94,491.16	0.00012	62,974.66	157,465.82
r7	401	0.236803	1	0.3164	90,808.45	0.00012	67,007.82	157,816.27
r3	2026	0.21104	1	0.2513	104,446.70	0.00012	75,187.82	179,634.52
r1	1978	0.143973	0	0.143973	90,919.30	0.00012	110,213.19	201,132.49
r1	411	0.14826	0	0.14826	123,909.14	0.00012	107,025.96	230,935.11
r1	6875	0.081778	0	0.081778	111,999.27	0.00012	194,034.66	306,033.93
r3	400	0.079328	0	0.079328	113,933.61	0.00012	200,027.34	313,960.95
r12	4762	0.083055	0	0.083055	171,005.07	0.00012	191,050.14	362,055.21
r7	6647	0.09492	0	0.09492	210,499.17	0.00012	167,168.87	377,668.04
r3	399	0.060008	0	0.060008	127,747.18	0.00012	264,428.10	392,175.28
r7	6561	0.086328	0	0.086328	218,849.68	0.00012	183,807.81	402,657.49
r7	6559	0.075233	0	0.075233	231,547.88	0.00012	210,915.09	442,462.97
r5	4719	0.067253	0	0.067253	236,080.62	0.00012	235,941.70	472,022.32
r3	398	0.046795	0	0.046795	141,460.06	0.00012	339,088.99	480,549.04
r3	401	0.042333	0	0.042333	147,393.83	0.00012	374,834.21	522,228.03
r6	3048	0.050033	0	0.050033	209,866.27	0.00012	317,147.24	527,013.51
r7	6646	0.047618	0	0.047618	279,307.61	0.00012	333,231.88	612,539.49
r7	6560	0.04368	0	0.04368	289,368.46	0.00012	363,270.81	652,639.27
r8	399	0.033303	0	0.033303	229,570.26	0.00012	476,470.81	706,041.07
r10	4938	0.035123	0	0.035123	351,850.39	0.00012	451,780.74	803,631.13
r1	401	0.02555	0	0.02555	281,278.22	0.00012	621,043.80	902,322.02
r8	400	0.02415	0	0.02415	261,899.76	0.00012	657,046.34	918,946.10
r4	5283	0.032253	0	0.032253	449,470.33	0.00012	491,982.61	941,452.94
r6	6461	0.03346	0	0.03346	504,691.99	0.00012	474,228.01	978,920.00

Table 6 The 71 corrosive failure locations from the 3 realisations of the fully-correlated DFN, ordered by failure time. Corresponding results are not directly presented by SKB, so cannot be compared.

Realisation	DFN hole ID	Qeq (m3/y)	q_eb > q_lim	q_eb (m3/y)	Erosion time (y)	Sulphide (mol/kg)	Corrosion time (y)	Failure time (y)
r5	6477	0.333079	1	0.625975	52,063.92	0.00012	47,639.29	99,703.21
r2	42	0.325878	1	0.5992	73,560.54	0.00012	48,692.03	122,252.56
r5	6476	0.228335	1	0.294175	70,957.27	0.00012	69,492.97	140,450.24
r2	163	0.215476	1	0.261975	103,267.29	0.00012	73,640.01	176,907.30
r2	162	0.149118	0	0.149118	130,107.58	0.00012	106,410.51	236,518.09
r4	3623	0.14819	0	0.14819	153,740.63	0.00012	107,076.52	260,817.14
r4	3651	0.109585	0	0.109585	120,280.79	0.00012	144,797.82	265,078.61
r2	164	0.111773	0	0.111773	146,430.65	0.00012	141,963.98	288,394.63
r5	1663	0.11305	0	0.11305	151,387.52	0.00012	140,359.74	291,747.26
r5	1719	0.1365	0	0.1365	182,406.11	0.00012	116,246.66	298,652.77
r5	1720	0.132598	0	0.132598	184,588.35	0.00012	119,667.94	304,256.28
r5	639	0.078225	0	0.078225	125,757.46	0.00012	202,846.52	328,603.98
r4	3626	0.101815	0	0.101815	179,317.04	0.00012	155,848.05	335,165.09
r4	3624	0.101185	0	0.101185	179,773.96	0.00012	156,818.39	336,592.35
r4	3627	0.100223	0	0.100223	180,479.82	0.00012	158,324.42	338,804.24
r4	4926	0.092418	0	0.092418	171,139.48	0.00012	171,695.50	342,834.98
r2	48	0.150203	0	0.150203	244,618.73	0.00012	105,641.84	350,260.58
r4	3653	0.068163	0	0.068163	146,130.40	0.00012	232,791.77	378,922.18
r4	3277	0.10115	0	0.10115	229,867.46	0.00012	156,872.66	386,740.12
r5	746	0.061828	0	0.061828	138,490.81	0.00012	256,644.20	395,135.01
r4	4597	0.06328	0	0.06328	149,445.49	0.00012	250,753.30	400,198.80
r5	1690	0.069738	0	0.069738	184,548.19	0.00012	227,534.24	412,082.43
r4	3628	0.073518	0	0.073518	204,929.37	0.00012	215,835.27	420,764.63
r2	165	0.062528	0	0.062528	185,806.20	0.00012	253,771.05	439,577.25
r2	166	0.058415	0	0.058415	191,062.01	0.00012	271,636.89	462,698.90
r4	1719	0.077735	0	0.077735	259,182.69	0.00012	204,125.16	463,307.85
r5	802	0.0504	0	0.0504	150,594.44	0.00012	314,834.71	465,429.14
r4	3781	0.06377	0	0.06377	217,235.93	0.00012	248,826.55	466,062.48

Realisation	DFN hole ID	Qeq (m3/y)	q_eb > q_lim	q_eb (m3/y)	Erosion time (y)	Sulphide (mol/kg)	Corrosion time (y)	Failure time (y)
r2	6828	0.077158	0	0.077158	269,876.86	0.00012	205,652.97	475,529.83
r4	4925	0.180633	1	0.1841	389,433.92	0.00012	87,844.96	477,278.88
r4	4847	0.052045	0	0.052045	179,908.45	0.00012	304,883.64	484,792.09
r4	3361	0.07014	0	0.07014	267,096.10	0.00012	226,228.53	493,324.64
r5	1689	0.053778	0	0.053778	205,298.02	0.00012	295,061.49	500,359.50
r2	49	0.08008	0	0.08008	316,579.28	0.00012	198,147.72	514,727.00
r5	6472	0.058923	0	0.058923	264,708.26	0.00012	269,297.28	534,005.55
r5	584	0.111528	0	0.111528	397,312.35	0.00012	142,275.84	539,588.19
r5	6152	0.058853	0	0.058853	284,979.43	0.00012	269,617.59	554,597.02
r4	1898	0.05712	0	0.05712	281,248.55	0.00012	277,795.33	559,043.88
r4	3783	0.049123	0	0.049123	241,768.33	0.00012	323,022.43	564,790.75
r4	3782	0.048563	0	0.048563	242,907.53	0.00012	326,747.37	569,654.89
r4	5480	0.051608	0	0.051608	263,610.26	0.00012	307,468.28	571,078.54
r4	5481	0.12467	0	0.12467	454,352.45	0.00012	127,277.37	581,629.82
r4	3193	0.054075	0	0.054075	297,156.30	0.00012	293,438.17	590,594.47
r5	1691	0.043138	0	0.043138	224,719.35	0.00012	367,839.33	592,558.68
r4	1897	0.050663	0	0.050663	295,428.19	0.00012	313,203.44	608,631.63
r4	5426	0.04599	0	0.04599	276,364.70	0.00012	345,024.33	621,389.03
r4	4551	0.041475	0	0.041475	241,936.95	0.00012	382,583.95	624,520.90
r4	615	0.04151	0	0.04151	278,512.99	0.00012	382,261.36	660,774.35
r4	616	0.041423	0	0.041423	278,754.05	0.00012	383,068.84	661,822.90
r4	5424	0.041685	0	0.041685	287,728.48	0.00012	380,656.57	668,385.05
r4	3652	0.032848	0	0.032848	197,118.91	0.00012	483,070.83	680,189.74
r4	1720	0.043295	0	0.043295	329,472.62	0.00012	366,501.19	695,973.81
r4	3667	0.048178	0	0.048178	368,952.66	0.00012	329,358.50	698,311.16
r5	2698	0.034913	0	0.034913	262,300.34	0.00012	454,498.22	716,798.56
r5	2699	0.034913	0	0.034913	262,300.34	0.00012	454,498.22	716,798.56
r4	377	0.036435	0	0.036435	302,050.65	0.00012	435,506.22	737,556.87
r4	3625	0.101728	0	0.101728	582,972.60	0.00012	155,982.10	738,954.70
r4	3780	0.06832	0	0.06832	517,030.15	0.00012	232,255.11	749,285.26

Realisation	DFN hole ID	Qeq (m3/y)	q_eb > q_lim	q_eb (m3/y)	Erosion time (y)	Sulphide (mol/kg)	Corrosion time (y)	Failure time (y)
r5	2700	0.032428	0	0.032428	270,362.54	0.00012	489,327.55	759,690.09
r4	3779	0.06251	0	0.06251	536,217.76	0.00012	253,842.09	790,059.86
r4	498	0.027755	0	0.027755	220,740.69	0.00012	571,704.89	792,445.58
r4	4432	0.030223	0	0.030223	275,460.40	0.00012	525,028.34	800,488.74
r4	4553	0.030118	0	0.030118	275,853.74	0.00012	526,858.77	802,712.51
r2	6829	0.035525	0	0.035525	370,912.71	0.00012	446,662.04	817,574.75
r5	5387	0.03591	0	0.03591	399,778.46	0.00012	441,873.27	841,651.73
r4	4552	0.025778	0	0.025778	294,026.11	0.00012	615,562.76	909,588.88
r4	4927	0.075705	0	0.075705	700,287.15	0.00012	209,598.69	909,885.85
r4	2023	0.025095	0	0.025095	288,158.23	0.00012	632,304.01	920,462.24
r4	4430	0.024238	0	0.024238	301,546.73	0.00012	654,674.33	956,221.06
r5	6687	0.027458	0	0.027458	379,702.84	0.00012	577,899.27	957,602.11
r4	3854	0.023573	0	0.023573	326,691.68	0.00012	673,143.24	999,834.93

Table 7 The 73 corrosive failure locations from the 3 realisations of the uncorrelated DFN, ordered by failure time. Corresponding results are not directly presented by SKB, so cannot be compared.

Realisation	DFN hole ID	Qeq (m3/y)	q_eb > q_lim	q_eb (m3/y)	Erosion time (y)	Sulphide (mol/kg)	Corrosion time (y)	Failure time (y)
r3	5827	0.336968	1	0.640675	50,728.06	0.00012	47,089.59	97,817.64
r2	76	0.286419	1	0.462875	62,886.02	0.00012	55,400.27	118,286.29
r3	3972	0.25775	1	0.37485	61,058.59	0.00012	61,562.32	122,620.91
r3	344	0.207857	1	0.243775	68,837.03	0.00012	76,339.48	145,176.50
r3	3973	0.166985	0	0.166985	85,061.02	0.00012	95,024.52	180,085.54
r3	342	0.205606	1	0.238525	125,771.48	0.00012	77,175.03	202,946.51
r3	58	0.195555	1	0.215775	123,111.35	0.00012	81,141.53	204,252.88
r2	5229	0.1666	0	0.1666	207,139.88	0.00012	95,244.11	302,383.99
r3	4596	0.075968	0	0.075968	124,090.55	0.00012	208,874.44	332,964.99
r3	165	0.104965	0	0.104965	189,345.76	0.00012	151,171.05	340,516.81
r2	432	0.09394	0	0.09394	201,891.73	0.00012	168,912.81	370,804.54
r5	379	0.080605	0	0.080605	190,833.80	0.00012	196,857.13	387,690.93
r2	1365	0.059885	0	0.059885	150,716.74	0.00012	264,969.01	415,685.75
r2	729	0.062913	0	0.062913	197,793.03	0.00012	252,218.07	450,011.10
r5	818	0.06048	0	0.06048	188,901.49	0.00012	262,362.25	451,263.74
r2	617	0.050733	0	0.050733	142,349.26	0.00012	312,771.28	455,120.55
r2	619	0.06916	0	0.06916	232,601.15	0.00012	229,434.20	462,035.35
r5	1539	0.04704	0	0.04704	128,967.44	0.00012	337,322.90	466,290.34
r2	5230	0.200876	1	0.227675	395,223.21	0.00012	78,992.54	474,215.75
r5	6186	0.05061	0	0.05061	165,215.40	0.00012	313,528.34	478,743.73
r5	819	0.052885	0	0.052885	199,585.91	0.00012	300,041.02	499,626.93
r3	1232	0.050785	0	0.050785	187,454.20	0.00012	312,447.95	499,902.15
r5	5143	0.04333	0	0.04333	158,629.62	0.00012	366,205.15	524,834.77
r3	4233	0.053778	0	0.053778	238,618.37	0.00012	295,061.49	533,679.86
r3	3881	0.039708	0	0.039708	143,682.78	0.00012	399,613.91	543,296.69
r5	2013	0.042088	0	0.042088	189,569.08	0.00012	377,016.20	566,585.28
r2	278	0.183359	1	0.1897	527,082.36	0.00012	86,538.64	613,621.01
r2	5619	0.039043	0	0.039043	207,577.03	0.00012	406,420.42	613,997.45

Realisation	DFN hole ID	Qeq (m3/y)	q_eb > q_lim	q_eb (m3/y)	Erosion time (y)	Sulphide (mol/kg)	Corrosion time (y)	Failure time (y)
r5	4138	0.032918	0	0.032918	152,737.66	0.00012	482,043.57	634,781.23
r2	5935	0.038483	0	0.038483	229,694.59	0.00012	412,334.68	642,029.27
r2	2096	0.041808	0	0.041808	269,923.28	0.00012	379,541.21	649,464.49
r5	1102	0.03465	0	0.03465	191,750.89	0.00012	457,941.39	649,692.28
r3	6547	0.036943	0	0.036943	226,466.77	0.00012	429,523.43	655,990.20
r2	2207	0.034405	0	0.034405	196,000.73	0.00012	461,202.42	657,203.14
r5	817	0.03689	0	0.03689	231,346.89	0.00012	430,134.70	661,481.59
r2	2307	0.041685	0	0.041685	290,816.80	0.00012	380,656.57	671,473.37
r3	6558	0.050418	0	0.050418	364,561.89	0.00012	314,725.43	679,287.31
r2	728	0.035735	0	0.035735	249,416.21	0.00012	444,037.19	693,453.41
r3	371	0.033233	0	0.033233	219,841.61	0.00012	477,474.43	697,316.04
r3	392	0.031588	0	0.031588	222,648.63	0.00012	502,340.14	724,988.77
r5	4793	0.033495	0	0.033495	269,891.29	0.00012	473,732.47	743,623.76
r5	111	0.028333	0	0.028333	186,191.00	0.00012	560,051.85	746,242.85
r5	621	0.031343	0	0.031343	253,463.28	0.00012	506,266.86	759,730.15
r3	3691	0.031255	0	0.031255	254,008.07	0.00012	507,684.18	761,692.25
r5	2009	0.038885	0	0.038885	354,298.48	0.00012	408,066.58	762,365.06
r3	5423	0.02793	0	0.02793	198,355.69	0.00012	568,122.78	766,478.47
r2	6003	0.02681	0	0.02681	185,675.07	0.00012	591,856.36	777,531.44
r2	670	0.03038	0	0.03038	266,582.82	0.00012	522,306.42	788,889.24
r3	3902	0.057943	0	0.057943	517,799.05	0.00012	273,851.99	791,651.05
r3	3437	0.02499	0	0.02499	164,628.78	0.00012	634,960.75	799,589.52
r5	2008	0.03612	0	0.03612	365,176.97	0.00012	439,304.24	804,481.21
r2	3561	0.02485	0	0.02485	184,599.60	0.00012	638,537.99	823,137.59
r2	730	0.028578	0	0.028578	273,352.59	0.00012	555,250.43	828,603.02
r2	3989	0.02667	0	0.02667	241,482.43	0.00012	594,963.22	836,445.66
r3	1240	0.02996	0	0.02996	318,828.47	0.00012	529,628.48	848,456.95
r5	6433	0.0294	0	0.0294	314,259.95	0.00012	539,716.64	853,976.59
r3	408	0.023765	0	0.023765	196,176.18	0.00012	667,690.69	863,866.87
r5	2157	0.026303	0	0.026303	263,870.92	0.00012	603,276.08	867,147.00

Realisation	DFN hole ID	Qeq (m3/y)	q_eb > q_lim	q_eb (m3/y)	Erosion time (y)	Sulphide (mol/kg)	Corrosion time (y)	Failure time (y)
r3	3713	0.02408	0	0.02408	223,728.98	0.00012	658,956.36	882,685.34
r5	807	0.029838	0	0.029838	361,960.67	0.00012	531,802.90	893,763.57
r3	4610	0.024378	0	0.024378	246,214.56	0.00012	650,914.54	897,129.09
r2	4346	0.022943	0	0.022943	209,331.13	0.00012	691,627.73	900,958.86
r3	1615	0.023485	0	0.023485	229,693.68	0.00012	675,651.23	905,344.91
r5	3277	0.024098	0	0.024098	247,779.92	0.00012	658,477.81	906,257.73
r5	3857	0.04809	0	0.04809	584,082.42	0.00012	329,957.77	914,040.19
r3	1652	0.025953	0	0.025953	311,705.90	0.00012	611,411.97	923,117.87
r5	319	0.03115	0	0.03115	422,324.06	0.00012	509,395.48	931,719.54
r3	4896	0.022698	0	0.022698	234,968.33	0.00012	699,093.25	934,061.58
r3	377	0.022628	0	0.022628	251,743.56	0.00012	701,255.96	952,999.52
r5	4553	0.03633	0	0.03633	516,268.05	0.00012	436,764.91	953,032.96
r3	5285	0.023258	0	0.023258	274,797.96	0.00012	682,260.31	957,058.27
r2	813	0.035543	0	0.035543	532,850.53	0.00012	446,442.12	979,292.65
r5	6679	0.020195	0	0.020195	201,537.15	0.00012	785,722.66	987,259.81

Summary

A good agreement with the mean numbers of advective positions at 10^5 and 10^6 y shown in TR-11-01, Figure 12-4 was obtained in the independent analysis. A precise match was obtained for the semi-correlated DFN model results, based on 10 realisations of the DFN. A perfect match could not be obtained for the fully-correlated and uncorrelated cases because only 3 realisations of the DFN were available for the independent analysis for each of these cases, whereas in the SKB analysis 5 realisations were used in each case. However the mean numbers of advective positions that were calculated from the 3 realisations appear consistent with those calculated by SKB over 5 realisations. Spreadsheets containing details of the advective positions across all realisations have been supplied with this report.

Across the 10 realisations of the semi-correlated DFN, 27 locations were identified in the independent analysis that would be expected to experience failure by corrosion within 10^6 y. The 27 locations were found to match with those identified by SKB in TR-10-50 Table 4-3, but SKB's analysis identified a further 29 locations that were also expected to fail. I.e. the independent analysis results appear to correspond to a subset of the results calculated by SKB.

Upon inspection, the 29 additional failed locations identified by SKB in TR-10-50 Table 4-3 appear to be 'repeats' of the first (earliest) 6 locations identified in the independent analysis, with the same 'parameter set' F, t_w and q given for the location, but with different times of failure. Inspection of the SKB DFN files for one of the parameter sets (the first) suggests that the set appears only once within the suite of 10 realisations, therefore it is understood that only a single unique time of failure should be computed for the parameter set, corresponding to the unique location for which the parameter set appears. It is therefore not clear from the description given in TR-10-50 why these 6 parameter sets appear multiple times in the SKB analysis with different failure times. It is suspected that the difference may arise due to the inclusion of cases with different groundwater sulphide concentrations, since only the maximum sulphide concentration considered by SKB (0.00012 mol/kg) was considered in the independent analysis. However, since the sulphide concentration is not reported in TR-10-50 Table 4-3 this cannot be confirmed.

Questions for SKB

- Please confirm whether the ten realisations of the semi-correlated DFN model used in the analysis were r1, r3-10, r12.
- Please confirm which 5 realisations were used in the analysis for each of the fully-correlated and uncorrelated scenarios. (Only 3 were available for the independent analysis.)
- Why do the same 'parameter sets' for the semi-correlated DFN (which appear to correspond to unique locations within a unique realisation of the semi-correlated DFN) appear multiple times in TR-10-50 Table 4-3? I.e. have multiple failure times been calculated for the same locations, and if so

why? (Is it due to alternative sulphide concentrations being assumed at each location?)

References

SKB Reports

TR-11-01: Long-term safety for the final repository for spent nuclear fuel at Forsmark: Main report of the SR-Site project. SKB TR-11-01, Svensk Kärnbränslehantering AB.

TR-10-66: Corrosion calculations report for the safety assessment SR-Site. SKB TR-10-66, Svensk Kärnbränslehantering AB.

TR-10-50: Radionuclide transport report for the safety assessment SR-Site. SKB TR-10-66, Svensk Kärnbränslehantering AB.

SKB (2011). "Documentation of the code for erosion and corrosion calculations in SR-Site", Public Memo 1396663 version 1.0.

2015:49

The Swedish Radiation Safety Authority has a comprehensive responsibility to ensure that society is safe from the effects of radiation. The Authority works to achieve radiation safety in a number of areas: nuclear power, medical care as well as commercial products and services. The Authority also works to achieve protection from natural radiation and to increase the level of radiation safety internationally.

The Swedish Radiation Safety Authority works proactively and preventively to protect people and the environment from the harmful effects of radiation, now and in the future. The Authority issues regulations and supervises compliance, while also supporting research, providing training and information, and issuing advice. Often, activities involving radiation require licences issued by the Authority. The Swedish Radiation Safety Authority maintains emergency preparedness around the clock with the aim of limiting the aftermath of radiation accidents and the unintentional spreading of radioactive substances. The Authority participates in international co-operation in order to promote radiation safety and finances projects aiming to raise the level of radiation safety in certain Eastern European countries.

The Authority reports to the Ministry of the Environment and has around 300 employees with competencies in the fields of engineering, natural and behavioural sciences, law, economics and communications. We have received quality, environmental and working environment certification.

Strålsäkerhetsmyndigheten
Swedish Radiation Safety Authority

SE-171 16 Stockholm
Solna strandväg 96

Tel: +46 8 799 40 00
Fax: +46 8 799 40 10

E-mail: registrator@ssm.se
Web: stralsakerhetsmyndigheten.se